Department of Applied Mechanics

Ultimate strength tests of corroded web-core and corrugated-core sandwich beams

Jasmin Jelovica, Jani Romanoff, Sören Ehlers, Heikki Remes

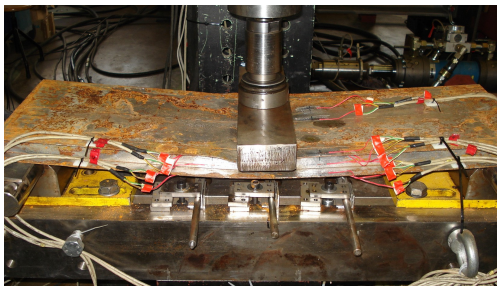

Aalto University | SCIENCE + TECHNOLOGY | RESEARCH REPORT

Jelovica et al. Ultimate strength tests of corroded web-core and corrugated-core sandwich beams Aalto University

Aalto University publication series
SCIENCE + **TECHNOLOGY** 28/2011

Ultimate strength tests of corroded web-core and corrugated-core sandwich beams

Jasmin Jelovica, Jani Romanoff, Sören Ehlers, Heikki Remes

Aalto University
School of Engineering
Department of Applied Mechanics
Marine Technology

Aalto University publication series
SCIENCE + **TECHNOLOGY** 28/2011

ISBN 978-952-60-4434-7 (pdf)
ISSN-L 1799-4896
ISSN 1799-490X (pdf)

Unigrafia Oy
Helsinki 2011

Finland

Author
Jasmin Jelovica, Jani Romanoff, Sören Ehlers, Heikki Remes

Name of the publication
Ultimate strength tests of corroded web-core and corrugated-core sandwich beams

Publisher School of Engineering

Unit Department of Applied Mechanics

Series Aalto University publication series SCIENCE + TECHNOLOGY 28/2011

Field of research Marine Technology

Abstract

This report describes the ultimate strength experiments on web-core and corrugated-core sandwich beams. The beams were tested in three-point bending. Each of the beam types was divided in three groups of specimens based on the extent of corrosion: (i) uncorroded, corroded for duration of (ii) one and (iii) two years. The beams were submerged in the Baltic Sea. The experiments outlined the reduction in ultimate strength by 14.5% and 17% for the unprotected one- and two-year corroded web-core beams, respectively. In case of the corrugated-core beams, the reduction was 10% and 16% in the same respect. The corresponding average thickness reduction of beam's top and bottom face-plates was 5.5% and 11.0% in case of web-core beams and 10.5% and 16% in case of corrugated-core beams. Furthermore, the experiments showed that the corrosion protection via coating, filling the core with the polyurethane (PU) foam and using the corrosion inhibitor is effective in preventing the corrosion for the studied time span.

The stress-strain behaviour of the beam's plates was determined with standard tensile tests. Before testing, the thickness of the specimens was measured to reveal the extent of corrosion. The average thickness reduction per exposed surface was 0.1 mm after the first year and 0.07 mm after the second year in the sea. The stress-strain curves from corroded tensile specimens were untypical. The ductility was reduced and the material started to strain harden immediately after the onset of yielding. Yield and ultimate strength were, however, unchanged.

Keywords steel sandwich panel, web-core, corrugated-core, ultimate strength, corrosion, stress-strain

ISBN (printed) **ISBN (pdf)** 978-952-60-4434-7

ISSN-L 1799-4896 **ISSN (printed)** 1799-4896 **ISSN (pdf)** 1799-490X

Location of publisher Espoo **Location of printing** Helsinki **Year** 2011

Pages 133

Table of contents

1 INTRODUCTION

Steel sandwich panels have potential to satisfy increasing demand for lighter, safer and eco-friendly structures. They posses high stiffness to weight ratio compared with conventional structures. These panels are formed of various core types enclosed by flat face plates. One of the ways to produce the steel sandwich panels is by using laser-welding to join the core- and the face-plates. Small thickness of the plates demands low heat input that can be achieved in such way. Laser weld is typically smaller than the thickness of the plates; see Roland and Reinert [1]. An option to improve panel properties exists in filling the void space in the core; see Romanoff and Kujala 2001, Kolsters 2008. Marine sector utilizes these structures in various ways, for example as superstructures, bulkheads, decks, hoistable ramps.

Few issues have to be understood better in order to enable higher use of these panels for ship structures. One of them is the influence of corrosion on the strength. Corrosion is a significant problem in a humid marine environment, especially for sandwich panels where the number of exposed steel surfaces is higher than for a conventional stiffened plate. This causes faster thickness reduction and raises the question of the remaining strength of such structure during exploitation.

Therefore, the ultimate strength tests were performed on the sandwich beams. The web-core and corrugated-core sandwich beams were considered. Corrosion was achieved by submerging the beams in the Baltic Sea in duration of one and two years which provided two sets of specimens. Few different types of corrosion protection schemes were used on them. Additionally, beams without corrosion were tested for comparison. Experiments with material specimens cut from the sandwich beams after ultimate strength testing are also reported here.

The experiments were conducted in the Laboratory of Mechanics of Materials of Aalto University during second half of 2010 and beginning of 2011.

2 DESCRIPTION OF SANDWICH BEAMS

2.1 Specimen planning

The design of the test specimens involved material and scantling selection in the way that within two years notable reduction on ultimate strength can be achieved. This was done assuming the plate thickness reduction of 0.1 mm per year per exposed surface. This requirement indicates that the plate thickness should be as small as possible, for one and two year exposure times. However, due to the fact that the production-induced initial deformations are considerable on thin plates it was decided that the minimum thickness to be used is 2 mm. In absence of any other limiting factor, this plate thickness was selected to fabricate corrugated core beams. On the other hand, the production process required the use of 4 mm web plates for the web core beams while 2.5 mm

was used for the face plates. The submerged beams could be at maximum 1000 mm in length which meant that in order to secure proper collapse mode in testing the height should be minimum. Therefore, the core height was selected to be 40 mm, which is still relevant for practical applications. For the corrugated core beam, the angle between corrugation and face plates was selected to be 60 degrees and the corrugation flange 20 mm due to production issues. The total width of the beam was selected to be 360 mm for the corrugated-core beam and 300mm for the web-core beam. The correct failure mode (by buckling) was verified using Finite Element Method (FEM) simulations prior to the testing.

2.2 Production

The production process is different for the corrugated-core and the web-core sandwich beams. Meyer Werft in Germany produced the web-core beams. They were cut in required dimensions from the sandwich panel that was welded on the panel line. First, the web-plates were positioned on the jig, where the web-plate spacing was fixed to 120 mm. A face sheet was placed on top of the web-plates. The laser-beam travels from one end of the panel to the other, while penetrating the face sheet and melting part of the web-plate. As a result, a laser stake weld is obtained. After the web-plates have been welded, the panel is turned. The second face sheet is placed again on top of the web-plates and the welding procedure is repeated.

Corrugated-core sandwich beams were produced by Kennotech in Finland. For these beams, prepared pieces of the core are put on the face sheet and spaced 120 mm. The laser-welding is carried out here from inside of the beam, meaning that the laser beam melts firstly the part of the core plate and then the face sheet. The need to turn the panel around is avoided in this way and the second steel sheet can be positioned on top of the core. The second round of welding commences now from outside first melting the face plate and penetrating to the core. The corrugated-core sandwich beams were assembled and welded from the components already cut to the final size.

2.3 Preparation

The sandwich beams were submerged in the sea to simulate the worst case scenario for the corrosion development in the marine environment. Before doing so, the beams were protected with paint that was applied from outside and/or inside of the specimens. The paint that was used was Tikkurila Oy Temacoat RM40, applied on the surfaces with a hand roller. Furthermore, the commercial inhibitor of corrosion was used inside of the beams which were later filled with foam. The corrosion inhibitor was Cortec VpCI-645. The foam was Edulan 1746.2 polyurethane (PU) foam with density of about 40 kg/m^3. Similar corrosion protection scheme involved mixing the foam with the inhibitor and filling the core with the mixture; see Figure 2-1. Certain specimens were filled with pure foam. All the beams filled with the foam received outside

painting. These corrosion protection schemes are listed in Table 2-1. The specimen preparation was performed in the Laboratory of Corrosion and Material Chemistry at Aalto University.

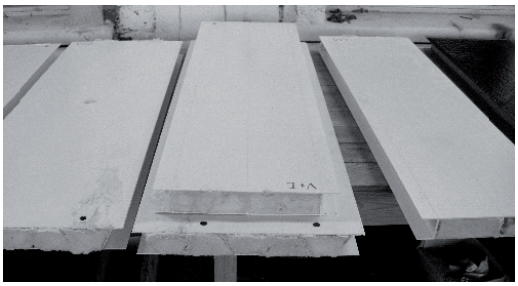

Figure 2-1. The sandwich beams after applying the paint from the outside and foam mixed with inhibitor from the inside as a corrosion protection.

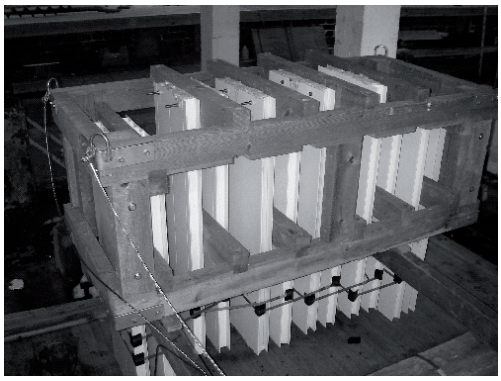

Figure 2-2. The sandwich beams attached to the wooden rack to be submerged into the sea.

The specimens were submerged in the Baltic Sea for one and two years. They were placed two meters below the sea level on a wooden rack (see Figure 2-2) positioned vertically to maximize the water flow around and inside the specimens due to wave motions.

Plate thickness reduction due to corrosion was measured on the unprotected beams with micrometer after the ultimate strength experiments on the parts of the beams that were only elastically loaded in tests. The reduced thicknesses are presented in Chapter 2.5. Furthermore, experiments with the material specimens were conducted to obtain the stress-strain properties of the uncorroded and corroded material. These are shown in Chapter 2.6 and Appendix B.

2.4 Sandwich beam nomenclature

Sandwich beams are specified as ‘XAbY’. ‘X’ is the duration of beam exposure to the sea water, i.e. the corrosion duration, either 1, 2 or 0 years for uncorroded beams. ‘A’ is the type of the sandwich core, either web core (W) or corrugated core (C). ‘b’ denotes the empty core (e) or core

filled with PU foam (f). The last marking, 'Y', is a numerator that presents the different types of beam corrosion protection. Additionally, a number in a bracket is added to the end of the notation for the corroded beams in case there are several specimens with the same nominal characteristics. Table 2-1 shows the nomenclature of the beams with their short description.

Table 2-1 Sandwich beam nomenclature with short description.

	Web-core	Corrugated-core	Exterior condition	Interior condition
Uncorroded	0We1	0Ce1	Untreated	Untreated
	0We2	0Ce2	Untreated	Untreated
	-	0Ce3	Untreated	Untreated
	-	0Ce4	Untreated	Untreated
	-	0Ce5	Untreated	Untreated
	-	0Ce6	Untreated	Untreated
	-	0Ce7	Untreated	Untreated
	0Wf1	0Cf1	Untreated	Foam
	0Wf2	0Cf2	Untreated	Foam
One-year corroded	1We1	1Ce1	Untreated	Untreated
	-	1Ce2	Paint	Untreated
	1We2	1Ce3(1) 1Ce3(2)	Paint	Paint
	1Wf1	1Cf1	Paint	Foam
	1Wf2	1Cf2	Paint	Inhibitor mixed with foam
	1Wf3	1Cf3	Paint	Inhibitor on surfaces only and filled with foam
	1We3	-	Carbon fibre laminate	Untreated
Two- year corroded	2We1	2Ce1(1) 2Ce1(2)	Untreated	Untreated
	-	2Ce2	Paint	Untreated
	2We2(1) 2We2(2)	2Ce3(1) 2Ce3(2)	Paint	Paint
	2Wf1	2Cf1	Paint	Foam
	2Wf2	2Cf2	Paint	Inhibitor mixed with foam
	2Wf3	2Cf3	Paint	Inhibitor on surfaces only and filled with foam
	2We3	-	Carbon fibre laminate	Untreated

2.5 Dimensions

The cross-section of the web-core and the corrugated-core beams is shown in Figure 2-3. Production process of the steel plates and later the beams causes imperfections, hence none of the dimensions can be considered exact. However, after the preliminary measuring, it was observed that the length, breadth and the angles were very accurate. Thicknesses of the plates, on the other hand, were differing, especially for the corroded specimens.

2.5.1 Thickness measurements

The thickness was measured on both uncorroded and corroded beams with a micrometer. The measured corroded beams were those without corrosion protection. Thus, six beams were examined:

Web-core:	(1)	uncorroded	(0We1)
	(2)	corroded for one year	(1We1)
	(3)	corroded for two years	(2We1)
Corrugated-core:	(4)	uncorroded	(0Ce1)
	(5)	corroded for one year	(1Ce1)
	(6)	corroded for two years	(2Ce1(1))

The measurements were made on the tensile specimens (see dimensions in Figure 2-4) that were cut from the beams after the ultimate strength experiments for the purpose of determining the stress-strain curves of the material. They were cut from the beam locations shown in Appendix A. Nine measurements were taken along each uncorroded specimen to have a sufficient data for statistical analysis. This relative large amount of data (considering that the plate thickness should be constant) was taken to reduce the error from hand measuring, thus a mean value and a standard deviation are presented in Table 2-2.

The corroded specimens were cleaned with a wire brush before measuring the thicknesses. They were exposed to the 5% HCl solution for about 15 min while removing the rust. The thickness of the corroded specimens had a large variation. The imperfections of the surface were significant relative to the average plate thickness. This is visible from the standard deviation in Table 2-2 which is in average 17 times larger for the two-year corroded specimens than for the uncorroded specimens. Locations of the thickness measurements in the corroded specimens are shown in Figure 2-4. Figure 2-5 shows the exemplary surface roughness due to corrosion in one tensile specimen.

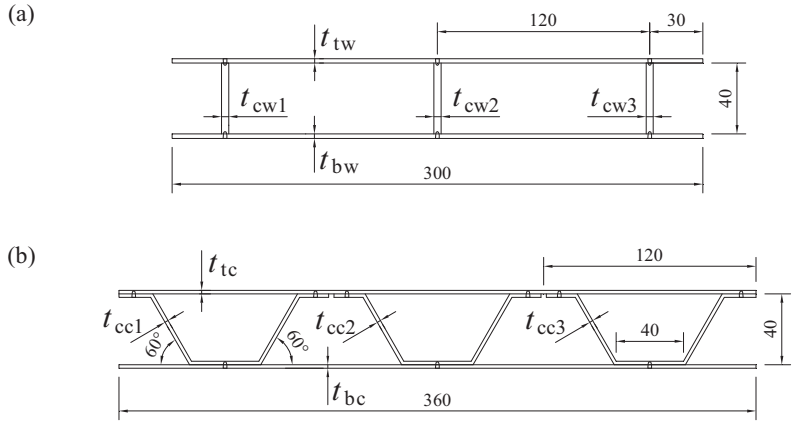

Figure 2-3. The cross-section dimensions for (a) web-core sandwich beam and (b) corrugated-core sandwich beam.

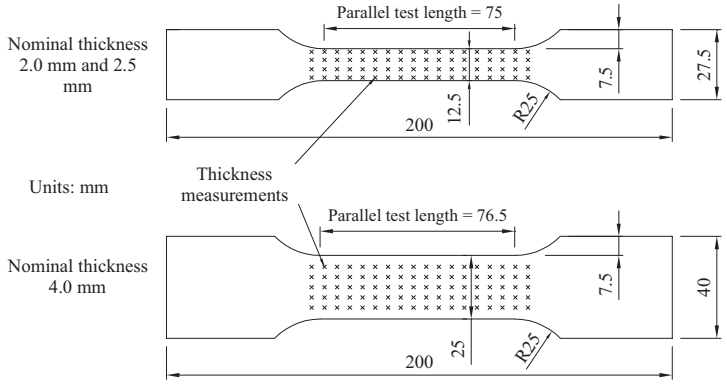

Figure 2-4. Dimensions of the tensile specimens.

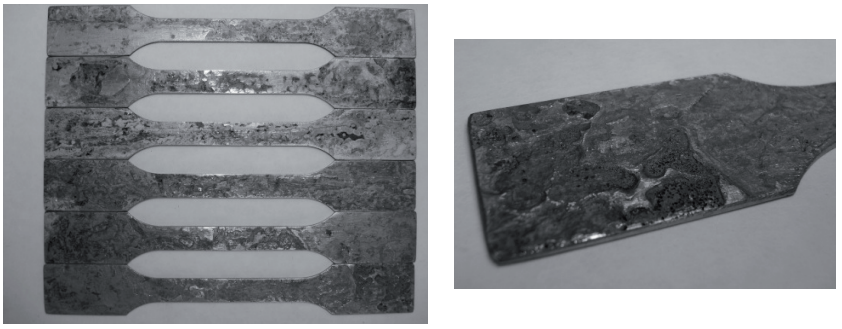

Figure 2-5. The exemplary surface roughness due to corrosion on tensile specimens.

Table 2-2. The measured thicknesses.

		Nominal thickness [mm]	Measured thickness [mm]					
			Uncorroded		1 year corrosion		2 year corrosion	
			μ	σ	μ	σ	μ	σ
Web-core beam	t_{tw}	2.5	2.494	0.005	2.337	0.090	2.120	0.146
	t_{cw1}	4	3.954	0.003	3.665	0.036	3.566	0.080
	t_{cw2}	4	3.975	0.004	3.750	0.074	3.557	0.101
	t_{cw3}	4	3.951	0.003	3.670	0.055	3.516	0.104
	t_{bw}	2.5	2.480	0.008	2.327	0.103	2.232	0.140
Corrugated-core beam	t_{tc}	2	1.965	0.008	1.751	0.084	1.660	0.132
	t_{cc1}	2	1.980	0.012	1.760	0.071	1.687	0.148
	t_{cc2}	2	1.954	0.007	1.796	0.068	1.734	0.095
	t_{cc3}	2	1.963	0.007	1.745	0.060	1.651	0.119
	t_{bc}	2	1.972	0.012	1.774	0.092	1.642	0.147

The corrosion-based thickness reduction is presented in Figure 2-6 for the separate plates and in Figure 2-7 for the two beam types in general. Despite the difference in thinning between the material used in the web-core and the corrugated-core beams, it can be averaged to 0.1 mm per exposed surface after one year. For the two-year specimens, the rate is reduced to 0.06 mm. Comparing the two core types, the relative thickness reduction was higher on the initially thinner corrugated-core beam plates; see Figure 2-6(b). The thickness reduction of the face plates (that have highest influence on the response) is 5.5% and 11.0% for the one- and two-years corroded web-core beams. Corresponding reduction in case of the corrugated-core beam is 10.5% and 16.1%.

(a) (b)

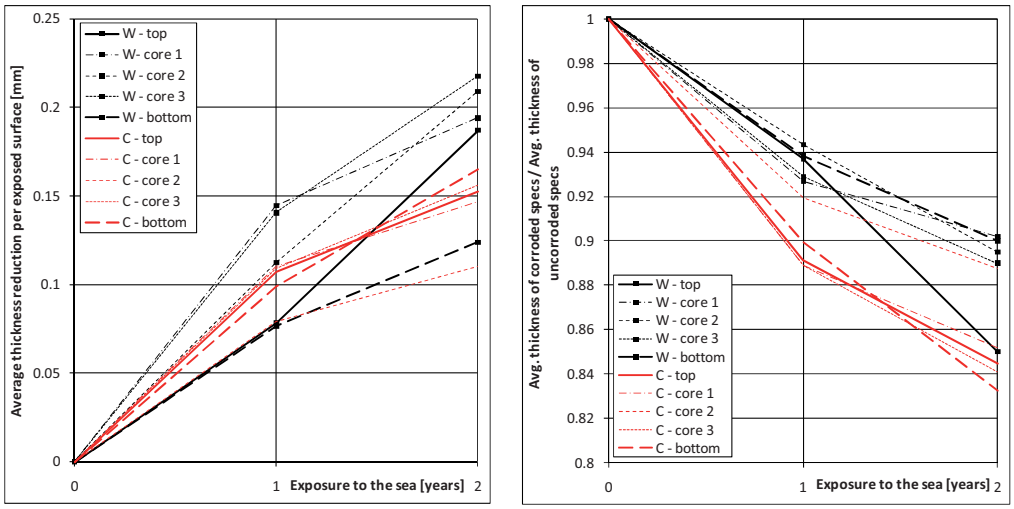

Figure 2-6. (a) Average thickness reduction of plates per exposed surface; (b) Relative thickness reduction compared to the uncorroded plates. W – web-core beam, C – corrugated-core beam.

(a) (b)

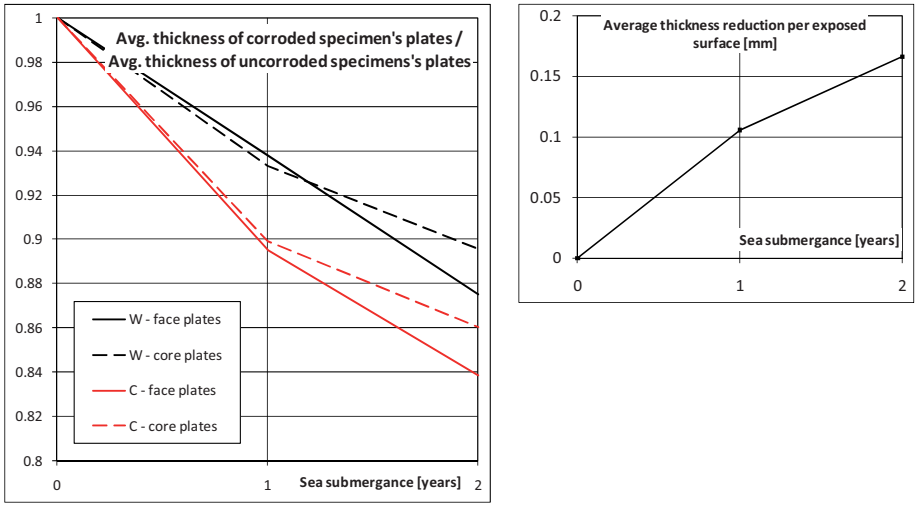

Figure 2-7. (a) Relative thickness reduction of face and core plates per exposed surface; (b) Average thickness reduction of plates per exposed surface. W – web-core beam, C – corrugated-core beam.

2.6 Material strength properties

The material stress-strain curves were determined by tensile testing on the tensile specimens shown in Figure 2-4. The specimens were cut from the sandwich beams after the ultimate strength experiments. They were cut from the locations that were only elastically deformed during experiments; see Appendix A. The stress levels were validated with FEM.

The tests were performed on the two machines: MTS Insight with 30 kN force capacity (see Figure 2-8) for the specimens of 2 mm and 2.5 mm nominal thickness; MTS Insight with 100 kN force capacity for the specimens of 4 mm nominal thickness. The original software from the machine manufacturer was used for the control of the strain rate and data acquisition.

The elongation speed of the experiments was 1.2 mm/min which is appropriate to capture the yield stress, strain flow and the strength accurately.

(a) (b)

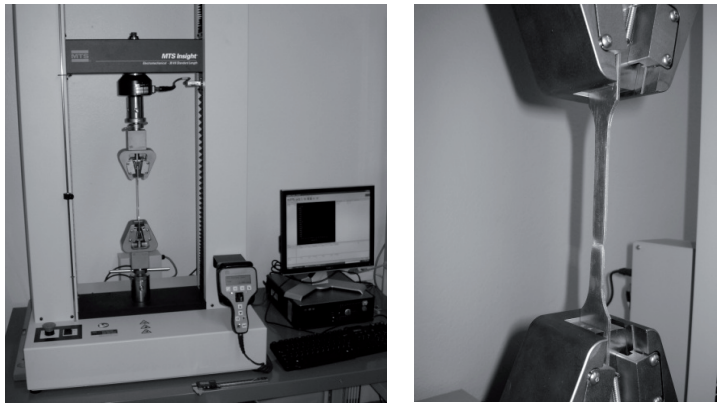

Figure 2-8. (a) The MTS Insight with 30 kN force capacity; (b) Test specimen after failure.

The tensile tests showed that the material behaviour differs whether the specimen originates from:

(a) Web-core or corrugated-core beam;
(b) Top face-plate, bottom face-plate or core plates and
(c) Uncorroded or corroded beam for one and two years.

Thus, for the web-core beams, nine typical curves from these categories are presented in Figure 2-9. The top face-plate and the bottom-face plate of the same beam, although nominally the same type of steel, differ within the tolerances of the steel producer. The core material does neither yield nor it strain hardens but instead reaches the ultimate strength and continues with reduction in stress until the point of fracture.

The increased corrosion rate reduced the fracture elongation for both the face-plates and core material, however, the ultimate strength remained the same. The same was reported by Almusallam 2001 for steel bars. Furthermore, the corroded face-plate specimens did not yield on the specimen level and instead started to strain harden. This can be attributed to several factors: (1) the surface roughness allowed the corroded specimens to propagate the fracture from one side of the specimen to the other much easier; exposure of the material to the hostile sea environment with numerous chemicals is known to cause (2) hydrogen and (3) chloride ions to penetrate into the material and deposit on the boundaries of the grains (see Domzalicki et al. 2007), which might cause their easier separation under load.

For the corrugated-core beams, the face and the core material had the same principle strength properties. However, the increased corrosion had the same effect on the steel specimens as for the web-core beams. The typical curves are presented in Figure 2-10.

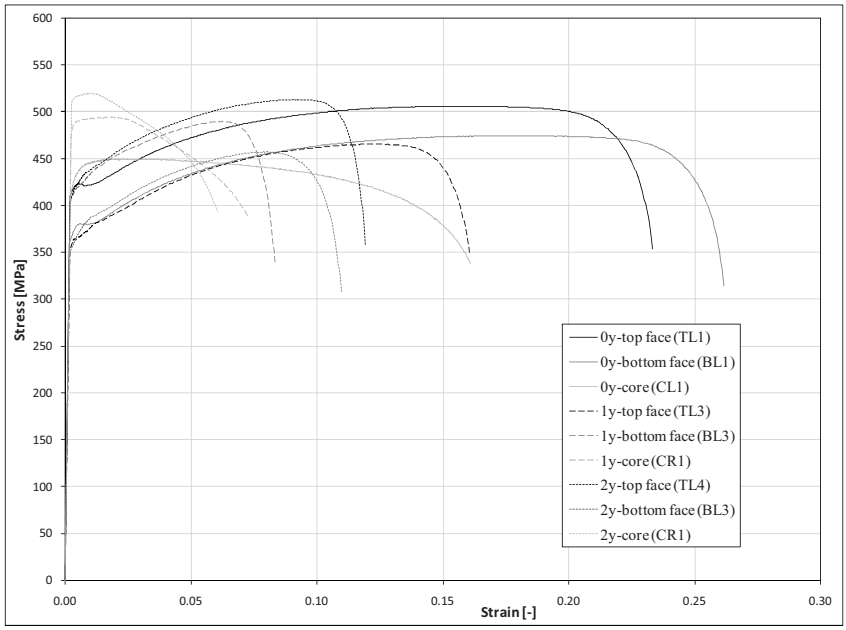

Figure 2-9. Example of the stress-strain curves for the web-core beams.

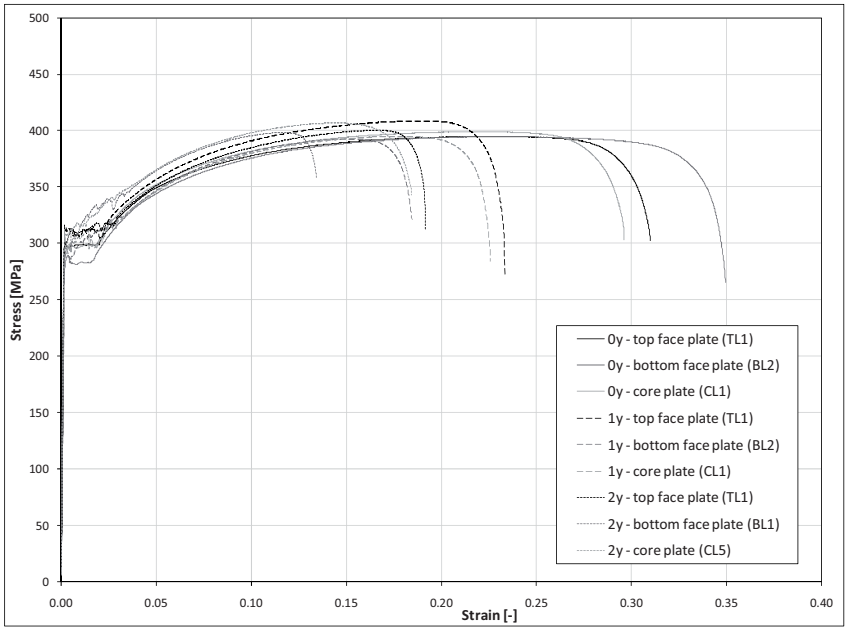

Figure 2-10. Example of the stress-strain curves for the corrugated-core beams.

3 ULTIMATE STRENGTH EXPERIMENTS

3.1 Experimental setup

The force-deflection behaviour of the sandwich beam specimens was numerically simulated prior to assembling the test system. The aim was to determine the ultimate force that the specimens can sustain in order to use the appropriate force cylinder for testing. The force transducer with 100 kN load capacity was found to be sufficient and the model HBM U2B was used. The supporting frame was assembled to be stiff enough well beyond this limit so that the origin of the force vector remains constant during the test. The distance between the force cylinder support and the sandwich beam was 2 m. Numerical investigation also unveiled the maximum deflection of interest. This allowed the use of appropriate size of the supports to the specimens. The test rig was sufficiently stiff not to deform during the test. The floor on which it was positioned could easily take the force magnitude of interest.

The cylindrical supports below the beam were 900 mm apart; see Figure 3-1. The allowed degrees of freedom for the supports were the rotation around and displacement along their axes. Furthermore, thin steel stripes were located between the beam and the supports to reduce the possible stress concentrations in the beam close to the contact area.

The force was imposed on the beam via steel block indenter on top of the beam in the beam mid-span; see Figure 3-1. The plain bearing between the indenter and the force cylinder allowed the indenter to rotate freely around the cylinder's spherical tip. Possible sliding of the indenter away from the beam mid-span during the test was not additionally prevented beside the action of the frictional forces.

The signal from the gauges, displacement sensors and the force cylinder were recorded with SignaSoft 6000 software package. It automatically interpreted the change in the voltage of the current in the sensors to actual strains, displacements and force level.

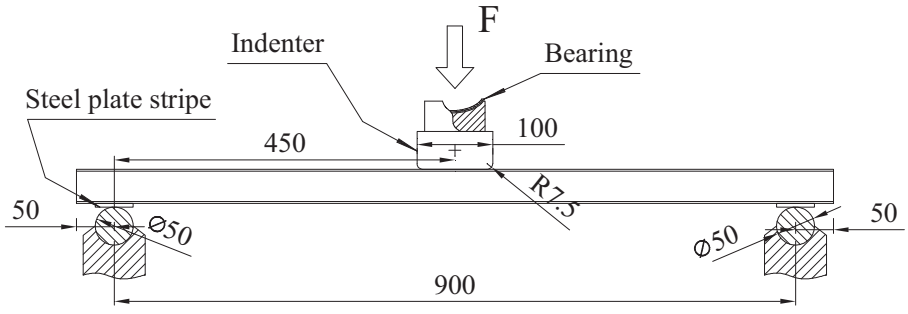

Figure 3-1. Position of the sandwich beam on the supports and the force direction.

3.1.1 Position of the strain gauges

12 strain gauges were placed on each beam on the positions depicted in Figure 3-2 for the web-core sandwich beams and in Figure 3-3 for the corrugated-core sandwich beams.

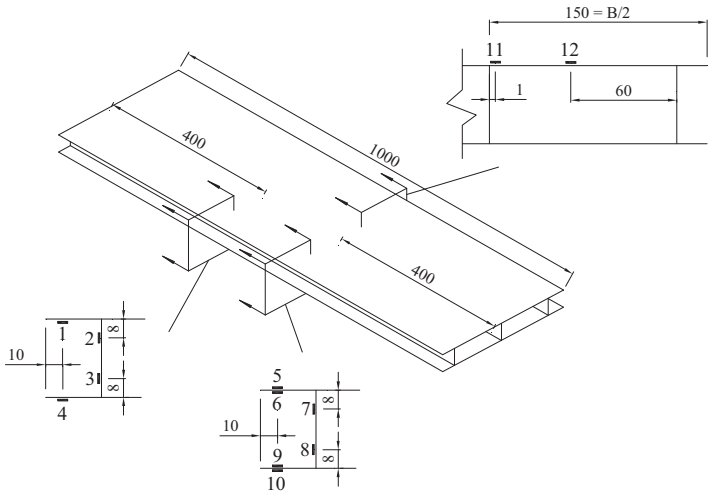

Figure 3-2. Position of the strain gauges on the web-core sandwich beam.

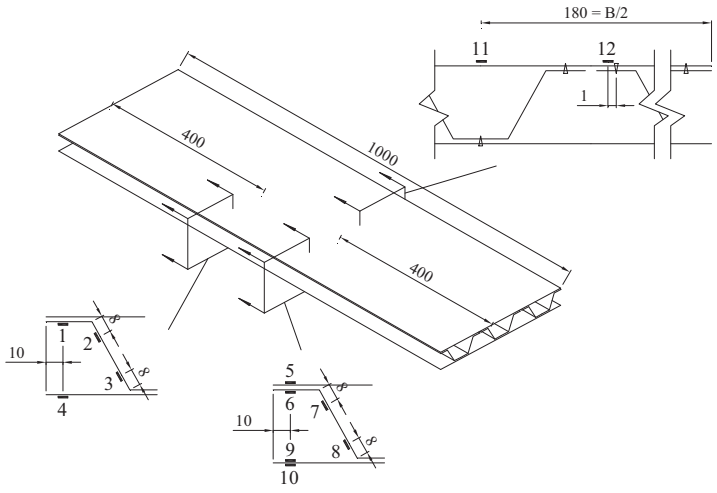

Figure 3-3. Position of the strain gauges on the corrugated-core sandwich beam.

Corrosion, dirt and grease were firstly removed from the place where the strain gauge was glued. Considerably wider area than the strain gauge size was grinded to remove the top layer of

rust. It was further polished by sandpaper with rough (#250) and, afterwards, fine (#600) granulation. The rougher granulation corresponds to the grain size of 10 μm and the finer to 4.2 μm. It was sufficient to use only the sandpaper for uncorroded beams. Afterwards, acetone was used to remove the rust powder and any possible oils and fats from the surface. After cleaning, the strain gauge bonding site was marked.

Five millimetre long Kyowa strain gauges, type KFG-5-120-C1-11L1M2R, were attached to the beam by Kyowa CC-33A glue, recommended for this gauge type. The temperature of the surfaces was the same when gluing the gauges and later conducting the experiments, around 22 °C. Adhesive was applied to the back side of the gauge and it was pressed down on the site for about one minute until the adhesive cured. In the end, the leadwire was attached to the beam using the same glue as for the gauges themselves. More accurate information on the strain gauge positioning and the site preparation is available from Kyowa Sensor System Solutions [2] which was followed here.

3.1.2 Position of the displacement sensors

Deflection of the bottom face plate was measured on the three positions shown in Figure 3-4 for the longitudinal direction and in Figure 3-5 for the transverse direction. The sensors HBM WA with maximum measuring range of 50 mm were placed below the beam through the holes in the test rig which caused their asymmetrical position along the beam. In the transverse direction, they were 10 mm away from the central laser weld to be able to freely slide when the bottom face plate deflects.

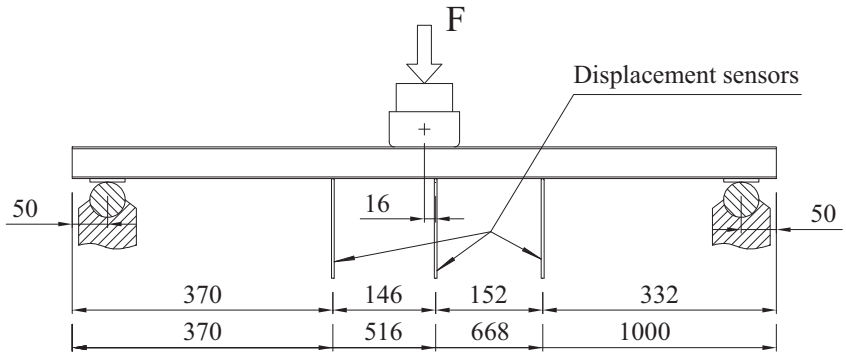

Figure 3-4. Longitudinal position of the displacement sensors relative to the sandwich beam.

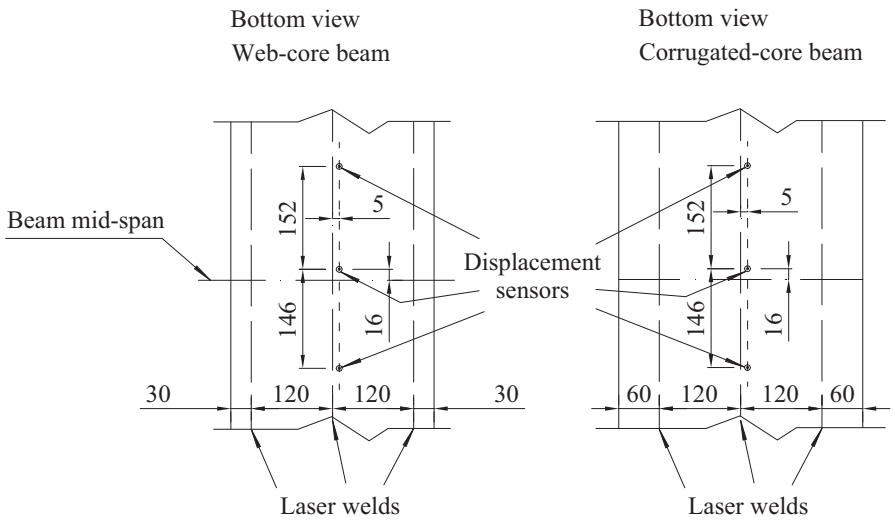

Figure 3-5. Transverse position of the displacement sensors relative to the sandwich beam.

3.2 Loading procedure

The experiments were displacement controlled. The displacement was increased and decreased manually in steps. At each step, the corresponding values of the strains, displacements and force were recorded twice. In order to obtain more information about the behaviour around the buckling and the ultimate strength, the number of recordings was increased to three after reaching the force level of 30 kN.

The loading procedure was as follows: initially, two loading cycles up to 8 kN were made to stabilise the force-deflection curve. The experiment was then continued until the deflection of the bottom face plate, measured with the central displacement sensor, reached 40 mm. Ultimate strength was obtained during that process. Afterwards, the sandwich beam was unloaded, followed by the final loading cycle to the same maximum deflection. The described loading procedure was followed in the same way for all specimens.

3.3 Stiffness and ultimate strength measurements

An example of the stiffness of the tested sandwich beams is presented in Figure 3-6 for the web-core specimens and in Figure 3-7 for the corrugated core specimens. Due to its geometric imperfections, the beam is not in full contact with the supports at the beginning of the experiment. This results in nonlinear initial response. Figure 3-6 shows that the stiffness for the unprotected web-core beams is linear above 5 kN. Furthermore, the corrosion decreases the stiffness of the beams by reducing the plate thicknesses. The same trend can be noticed for the corrugated-core beams, see Figure 3-7, although the one-year specimen had much lower stiffness.

This was caused by severe twist which the beam possessed, and it came into full contact at about 30kN. One corner of the specimen was elevated 10 mm above the support when the test started. At 15 kN, the distance was 4 mm. After 30 kN, the stiffness was about the same as the other unprotected corrugated-core beams. The stiffness of the tested specimens is presented in Appendix D.

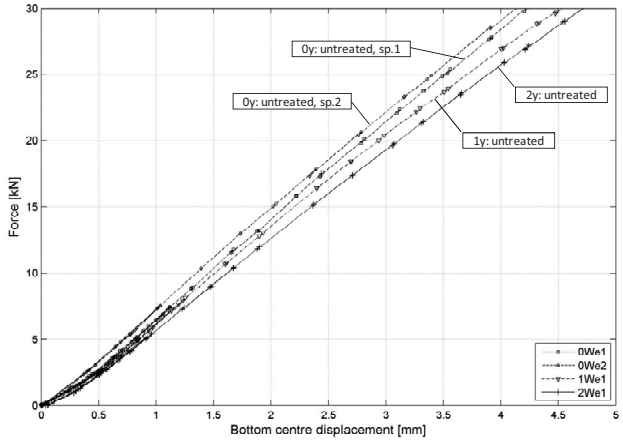

Figure 3-6. The stiffness of the web-core beams without the corrosion protection.

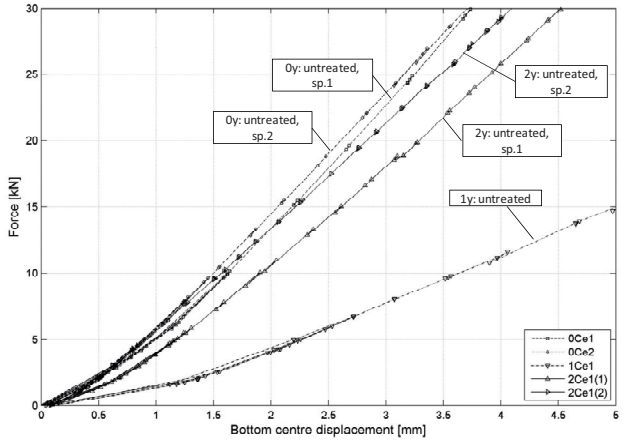

Figure 3-7. The stiffness of the corrugated-core beams without the corrosion protection.

The example of the force-displacement curves is presented in Figure 3-8 for the web-core specimens and in Figure 3-9 for the corrugated core specimens. The ultimate strength of the uncorroded web-core beam is 60.7 kN. The value decreases to 51.9 kN and 50.4 kN for the one-

and two-years of corrosion influence, respectively. Thus the reduction in strength follows the same trend as the reduction in plate thickness. For the corrugated-core beams, the ultimate strength is at 57 kN for the both uncorroded specimens. The one-year corroded beam reached 50 kN in the experiment. The ultimate strength of the two-year corroded specimens is 48 kN and 40 kN.

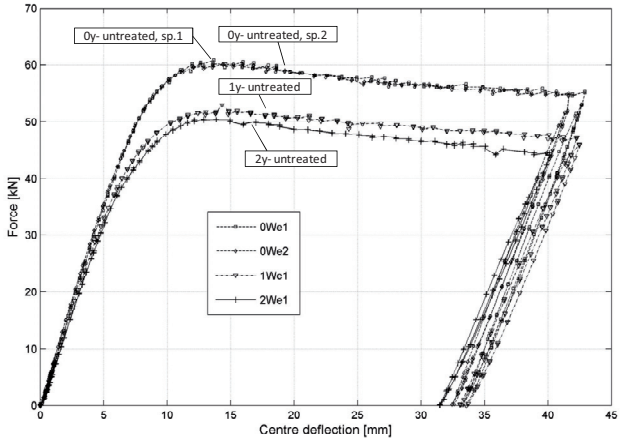

Figure 3-8. The force-displacement curve the web-core beams without the corrosion protection.

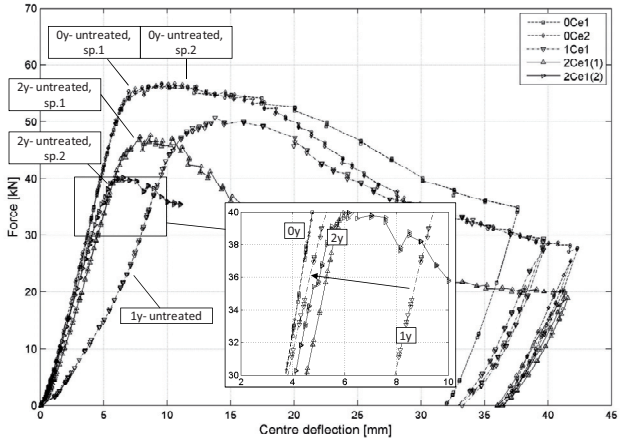

Figure 3-9. The force-displacement curve the corrugated-core beams without the corrosion protection.

The top face plate of each specimen buckled in the experiment. The deformation was either symmetrical with respect to the middle of the beam length or appearing on one side of the

indenter. After that point, the indenter was not in full contact with the beam. It was pressing the buckle peaks during the post-buckling and rotating around the contact line. The symmetrical buckling deformation is shown in Figure 3-10. Unsymmetrical buckling deformation was soon followed by formation of the plastic hinge; see Figure 3-11. The buckles were more extensive for the beams without the foam.

The buckles on the top face plate appeared on each specimen at about 90 % of the ultimate strength. This observation was made visually and it is thus very crude, but more accurate estimate can be made from the strains measured at gauges 11 and 12. All the strain measurements are presented in the Appendices C.

(a) (b)

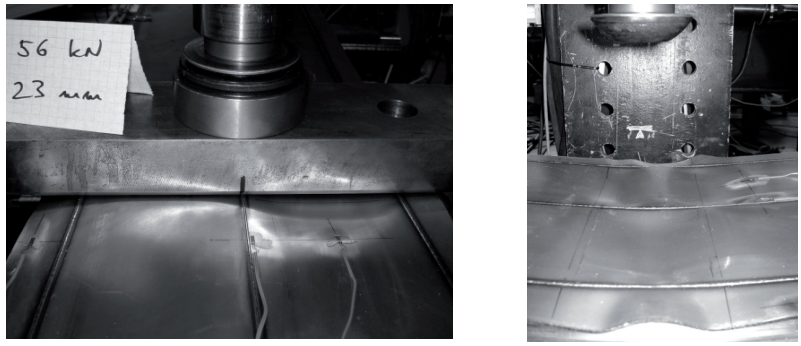

Figure 3-10. The buckling deformation of the face plate in the specimen 0We1 (a) during the experiment and (b) after the indenter was removed.

(a) (b)

Figure 3-11. The plastic hinge in the end of the experiment in the specimen 1Ce3(2) showing the angle (a) of the indenter {-5.1°} and (b) the face plate {-4.4°}.

4 SOURCES OF ERROR

4.1 Systematic error

The systematic errors can be divided into errors in determining the thickness of the plates and errors in performing the beam strength experiments.

The thickness was measured with digital micrometer. The systematic error can occur there since the micrometer is adjusted by hand to each measuring point. Multiple measurements of the same point in the uncorroded specimen revealed that the difference can be up to 5 μm. Thus the thickness of uncorroded plates is considered accurate. Although the same error applies the measurements of corroded specimens, the number of measured points in not sufficient to accurately describe the real surface profile which is quite complex. Digital scanning of the surface would be better in outlining the real situation but it was beyond the scope of this work.

The sources of systematic error in beam strength experiments are coming from the following deviations: longitudinal and transverse position of the gauge ±1 mm, angle of the gauge ±10º, longitudinal and transverse position of the beam on the supports ±1.5 mm, longitudinal and transverse position of the indenter on the top of the beam ±1 mm.

4.2 Random error

The part of the uncontrollable and unknown error is caused by the twist of some of the corroded beams. This means that if the beam would be put on the flat floor, one or two corners would be elevated from the ground. The reason for this kind of imperfection is not known, but it could arise from uneven thinning of the steel plates in the sea water. Also, initial residual stresses and strains could be fostered in such environment. The effect of this distortion is mirrored into the nonlinear beginning of the force-displacement curve, where the stiffness of the beam increases with the force. The most severe example of the initial nonlinearity in response is present for the beam 1Ce1which came into full contact with the supports at 30 kN. There the corner elevation was 16mm before the experiment. Other beams were deformed less, around 1mm. This value was not particularly measured for each beam since the relevant stiffness is anyway not obtained at the beginning of the experiment and the full contact is achieved soon enough.

The force-displacement curve of each specimen oscillates to certain extent from the average path. This is due to the problems with the test equipment. The piston of the force cylinder was constantly oscillating around the equilibrium state. The amplitudes were from about 0.2 mm to even 8 mm in most extreme cases. All efforts to remove the cause of this behaviour were unsuccessful. The most severe oscillations resulted in a sudden drop in force at the next recorded measurement. The example can be seen in Figure 3-9 for the specimen 2Ce1(2).

5 REFERENCES

[1] Roland F, Reinert T. *Laser welded sandwich beams for the ship building industry*. In lightweight construction – latest developments 2000; SW1:1-17.

[2] Romanoff, J., Kujala, P. *Optimum design for steel sandwich beams filled with polymeric foams*. Proc. FAST, Southampton, UK, 2001.

[3] Kolsters, H., Zenkert, D. *Buckling of laser-welded sandwich beams: ultimate strength and experiments*. J. Engineering for the Maritime Environment 2009; 224: 29-45.

[4] http://www.kyowa-ei.co.jp/english/products/gauges/index.htm; *How strain gauges work*, 26.1.2011

[5] Domzalicki, P., Lunarska, E., Birn J. *Effect of cathodic polarization and sulfate reducing bacteria on mechanical properties of different steels in synthetic sea water*. Materials and Corrosion, 58 (6), 2007.

[6] Almusallam, A.A. *Effect of degree of corrosion on the properties of reinforcing steel bars*. Construction and Building Materials, 15, 2001.

6 Appendix A – The cutting locations for the tensile specimens

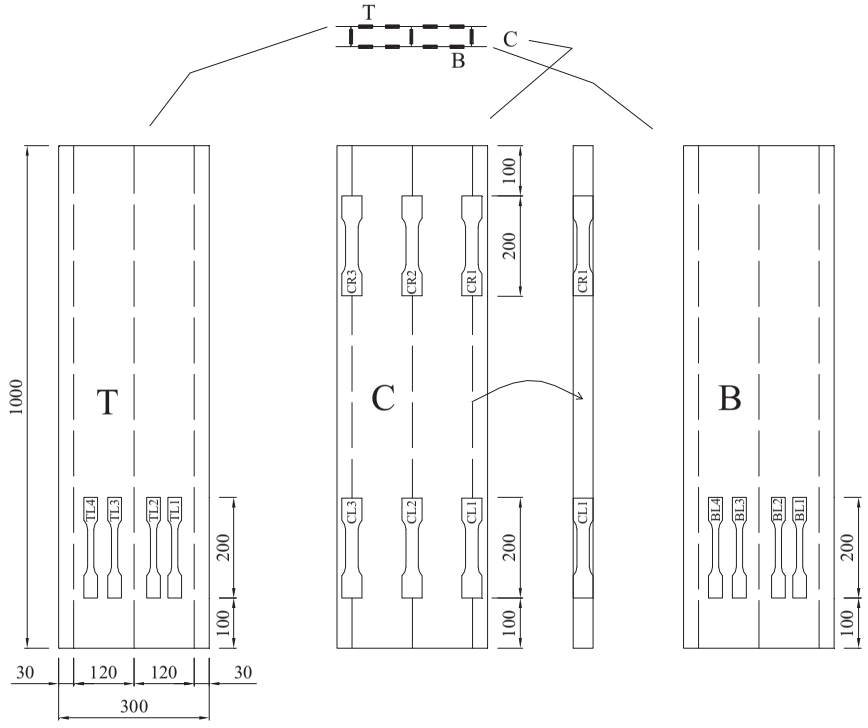

Figure 6-1. The cutting locations for the tensile specimens on the uncorroded web-core sandwich beam (0We1).

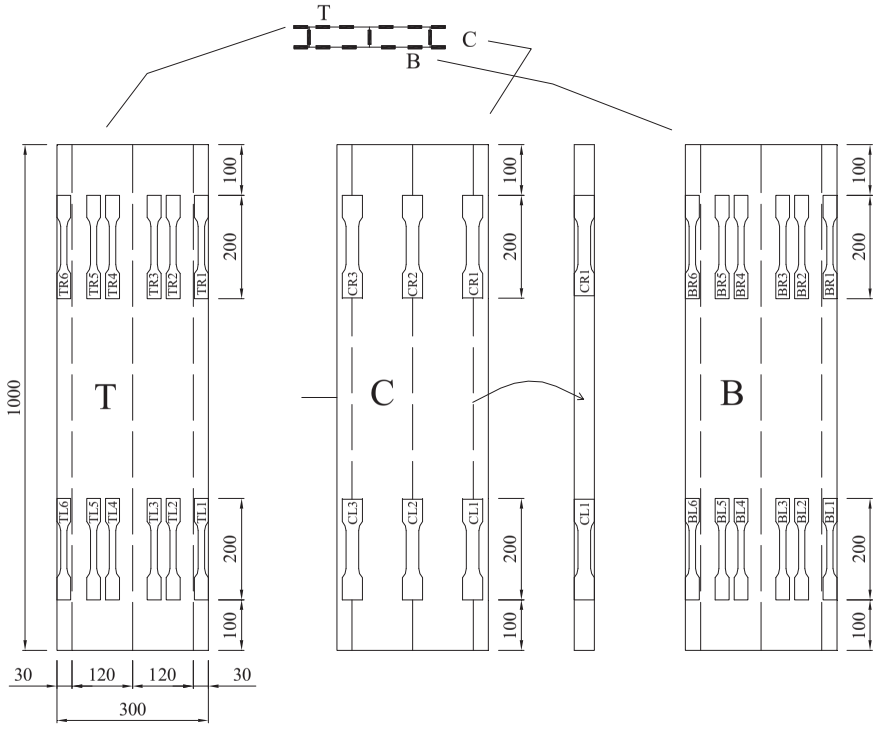

Figure 6-2. The cutting locations for the tensile specimens on the corroded web-core sandwich beams (1We1, 2We1).

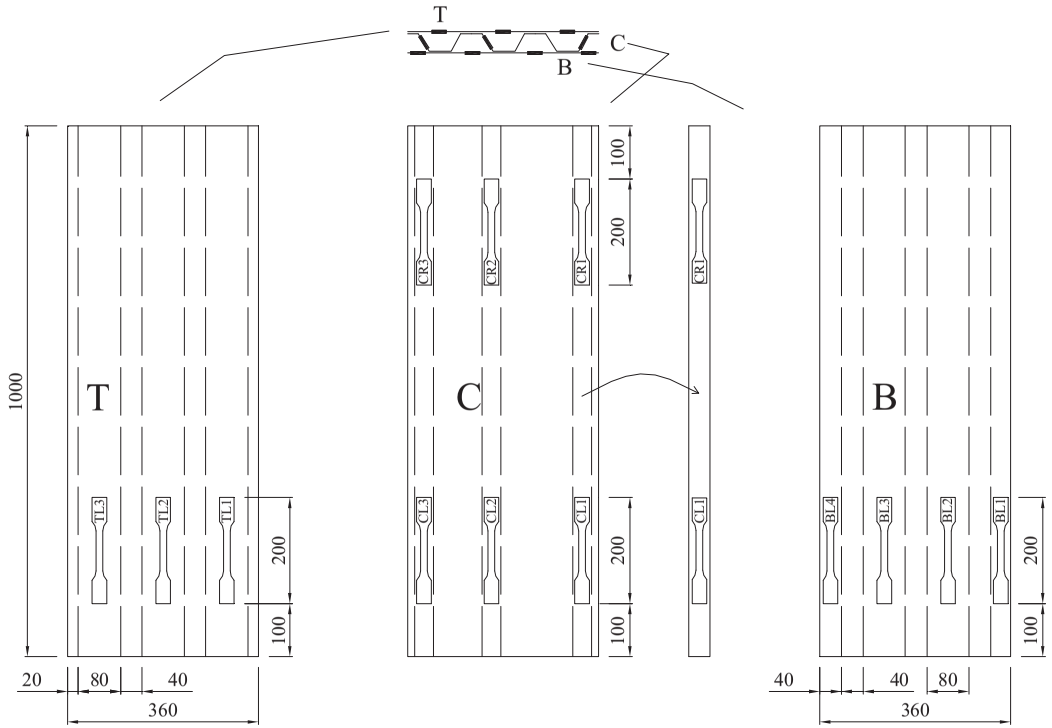

Figure 6-3. The cutting locations for the tensile specimens on the uncorroded corrugated-core sandwich beam (0Ce1).

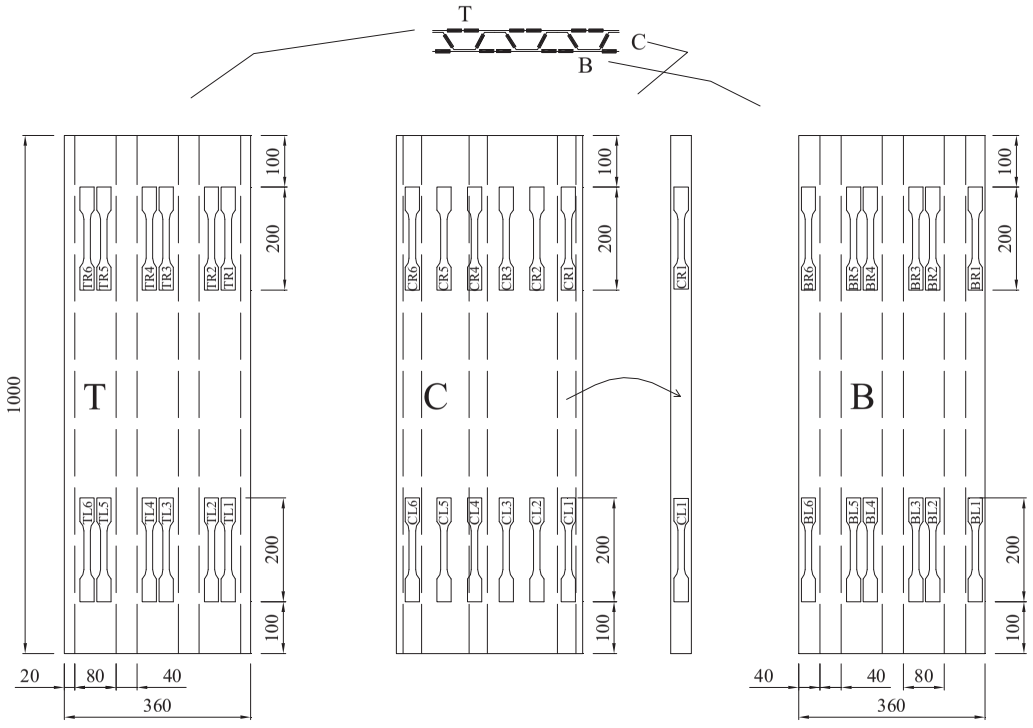

Figure 6-4. The cutting locations for the tensile specimens on the corroded corrugated-core sandwich beams (1Ce1, 2Ce1).

7 Appendix B – Stress-strain curves

The following tensile specimens were tested and are presented in continuation:

		Uncorroded (0We1)	One-year corroded (1We1)	Two-year corroded (2We1)
Web-core beam	Top face plate	TL1, TL2, TL3, TL4	TL3, TL4, TL5 TR3, TR4	TL3, TL4, TL5 TR3, TR4
	Core plate 1	CL1, CR1	CL1, CR1	CL1, CR1
	Core plate 1	CL2, CR2	CL2, CR2	CL2, CR2
	Core plate 1	CL3, CR3	CL3, CR3	CL3, CR3
	Bottom face plate	BL1, BL2, BL3, BL4	BL3, BL4, BL5 BR3, BR4	BL3, BL4, BL5 BR3, BR4

		Uncorroded (0Ce1)	One-year corroded (1Ce1)	Two-year corroded (2Ce1)
Corrugated-core beam	Top face plate	TL1, TL2, TL3	TL1, TL3, TL5	TL1, TL3, TL5
	Core plate 1	CL1, CR1	CL1, CR1	CL1, CR1
	Core plate 1	CL2, CR2	CL3, CR3	CL3, CR3
	Core plate 1	CL3, CR3	CL5, CR5	CL5, CR5
	Bottom face plate	BL2, BL3, BL4	BL2, BL4, BL6	BL1, BL3, BL5

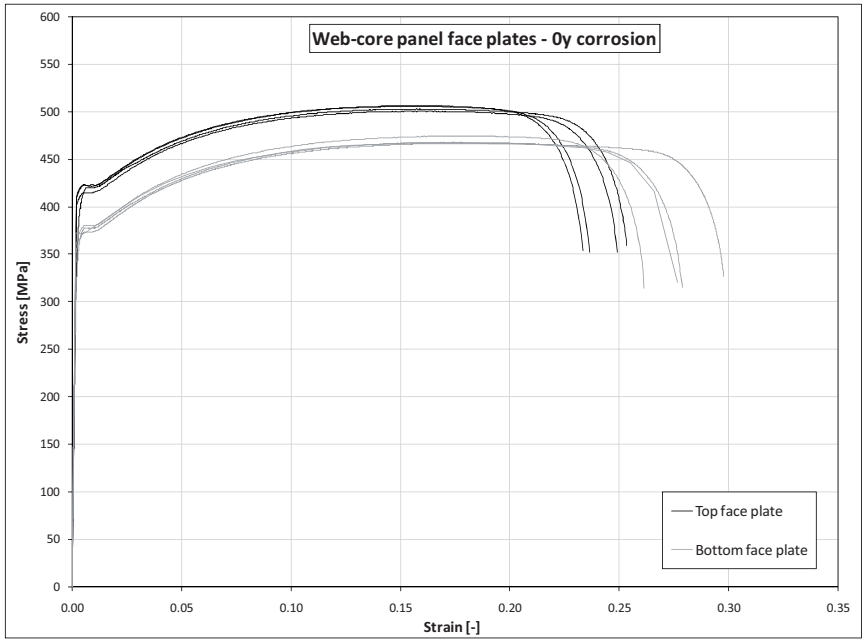

Figure 7-1. Uncorroded web-core beam: face plates.

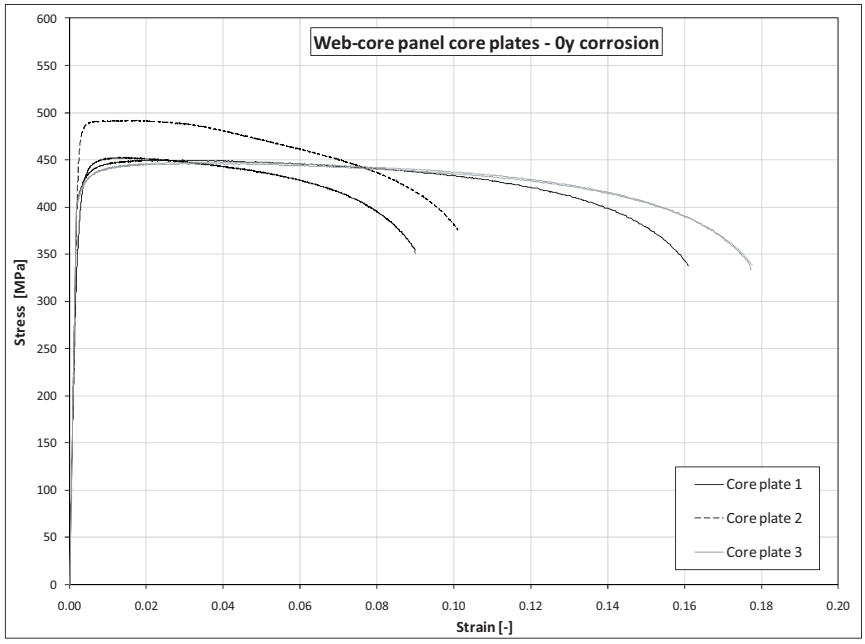

Figure 7-2. Uncorroded web-core beam: core plates.

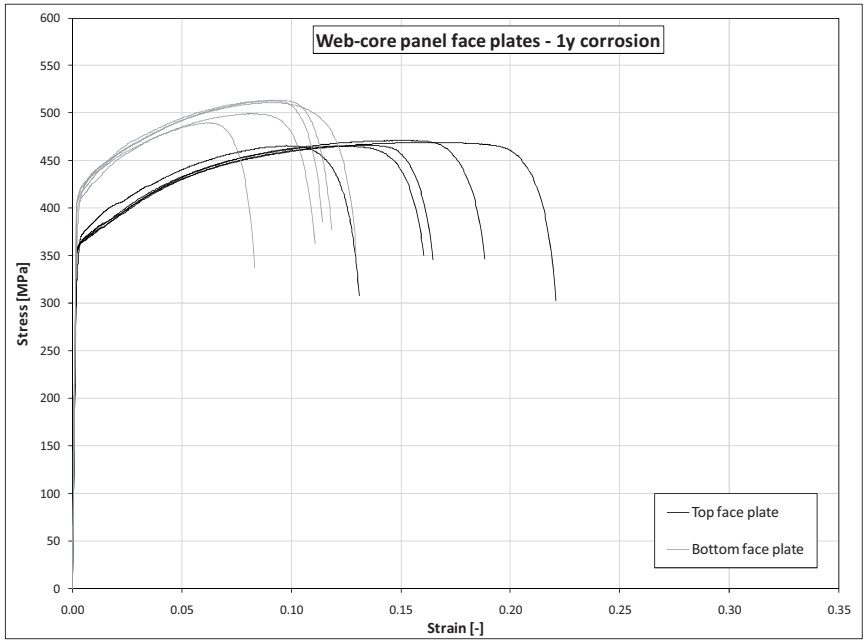

Figure 7-3. One-year corroded web-core beam: face plates.

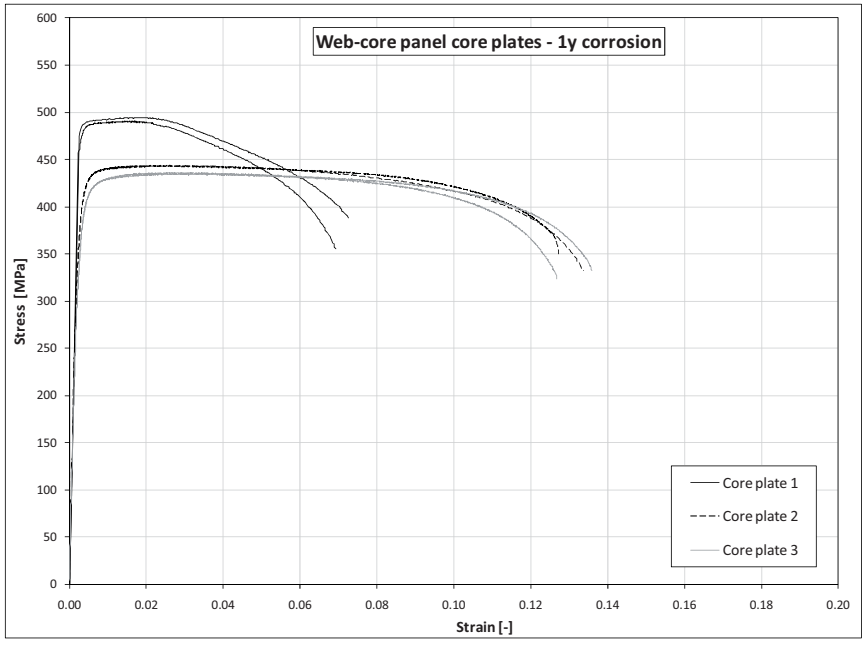

Figure 7-4. One-year corroded web-core beam: core plates.

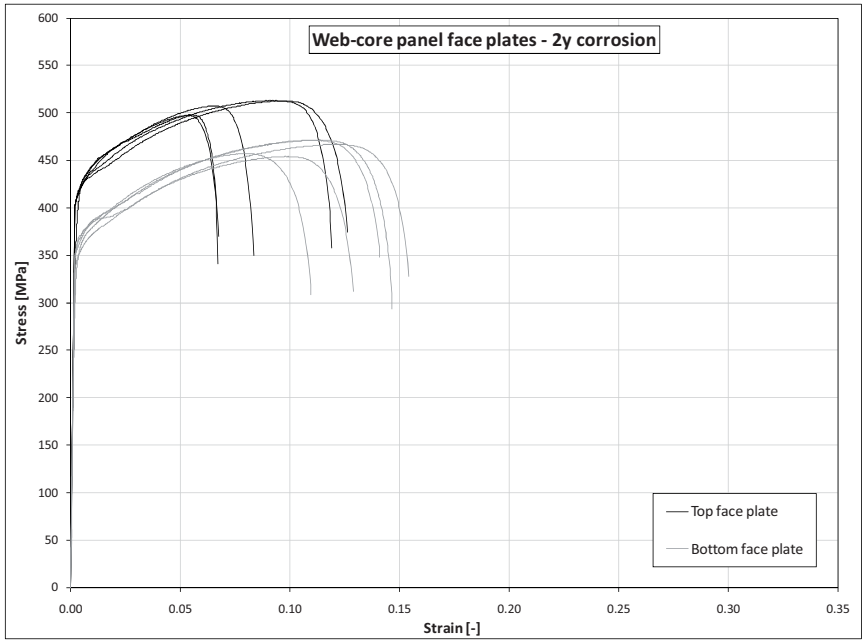

Figure 7-5. Two-year corroded web-core beam: face plates.

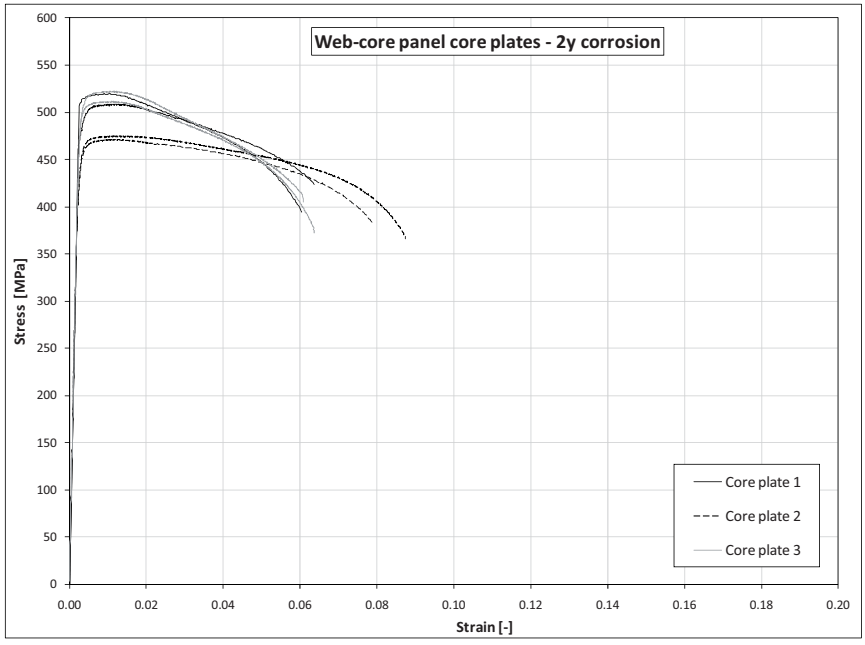

Figure 7-6. Two-year corroded web-core beam: core plates.

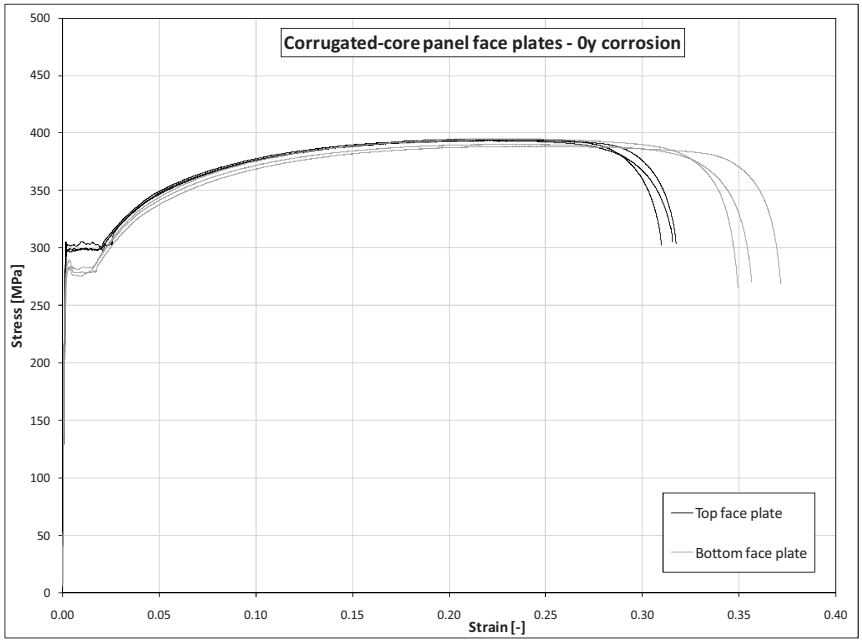

Figure 7-7. Uncorroded corrugated-core beam: face plates.

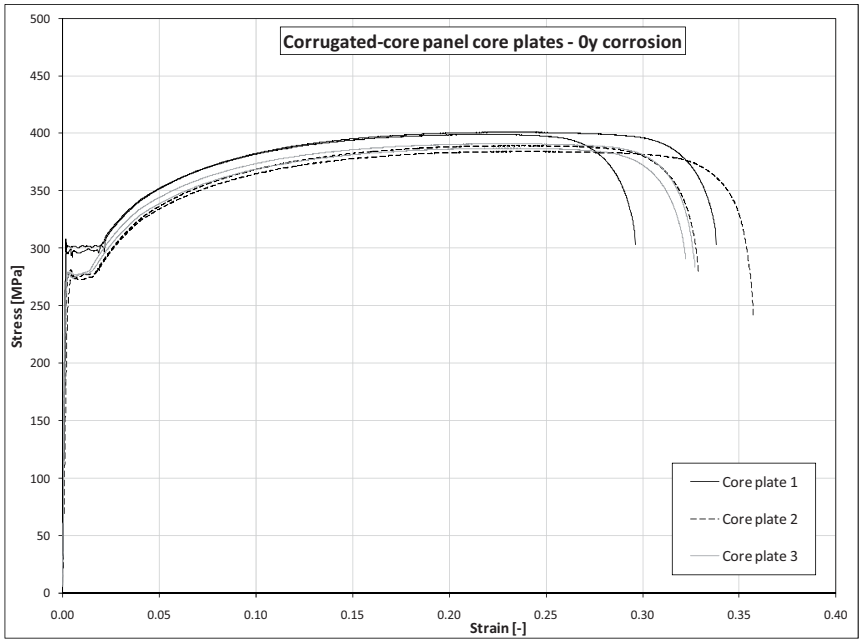

Figure 7-8. Uncorroded corrugated-core beam: core plates.

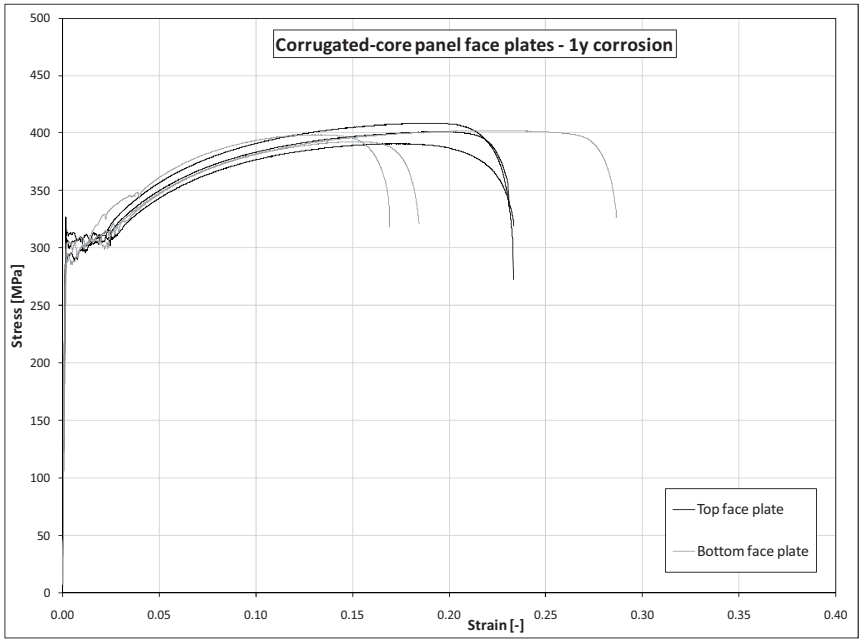

Figure 7-9. One-year corroded corrugated-core beam: face plates.

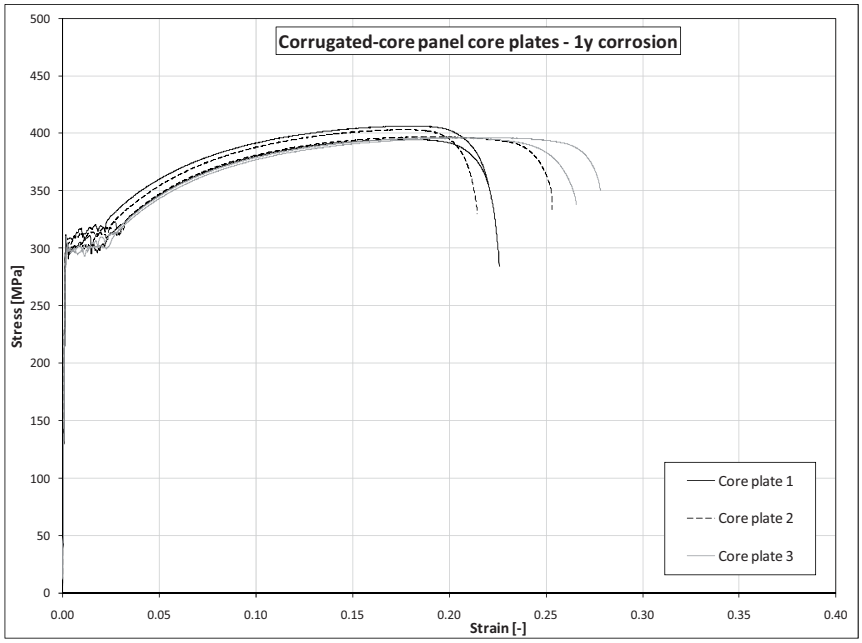

Figure 7-10. One-year corroded corrugated-core beam: core plates.

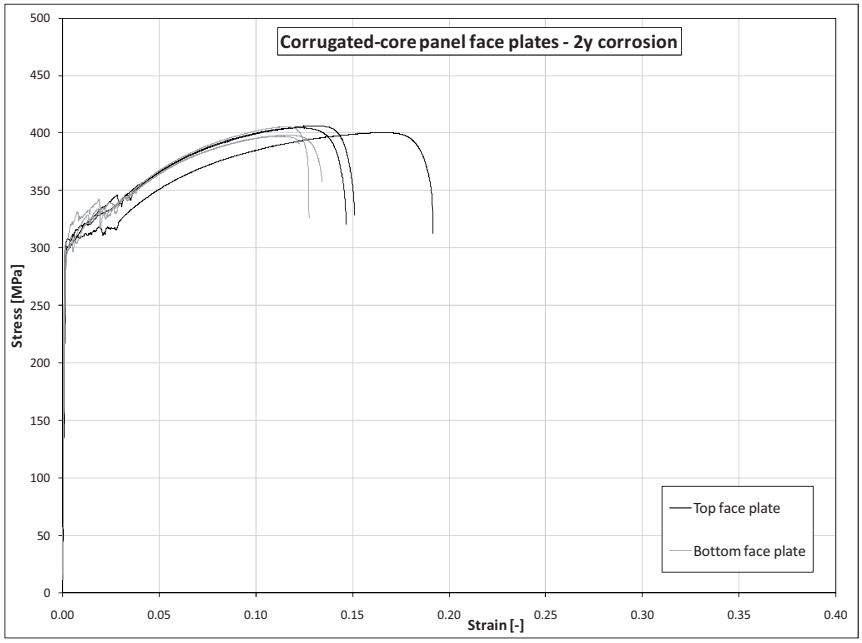

Figure 7-11. Two-year corroded corrugated-core beam: face plates.

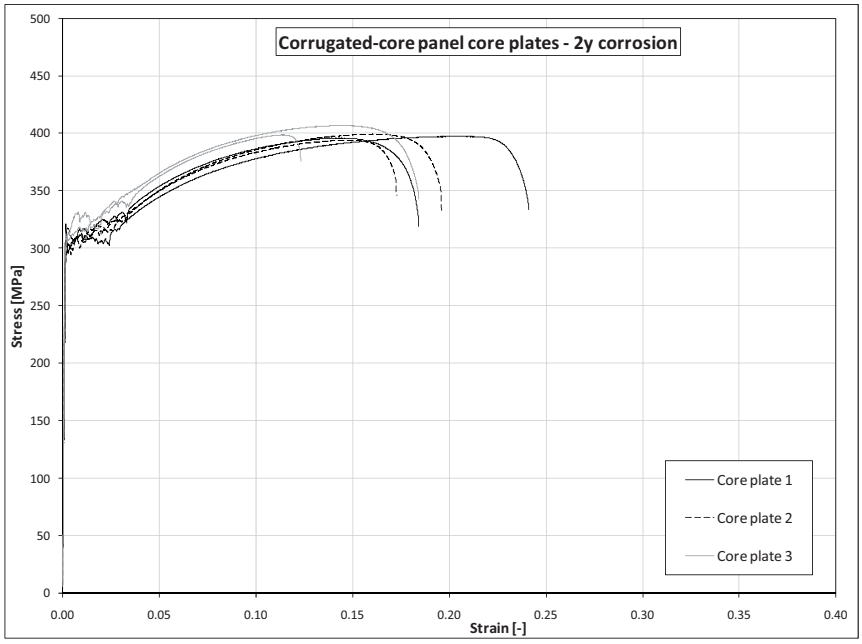

Figure 7-12. Two-year corroded corrugated-core beam: core plates.

8 Appendix C-W0 – Strain measurements from uncorroded web-core sandwich beams

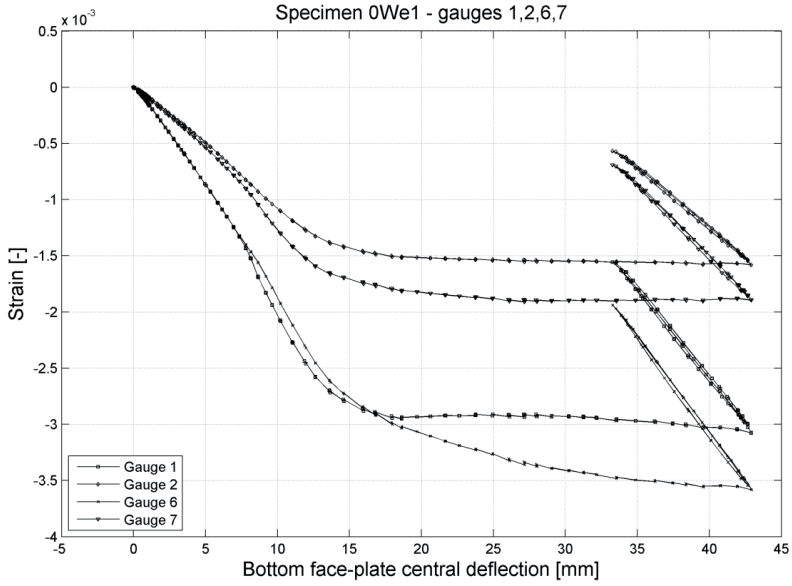

Figure 8-1. Strain measurements

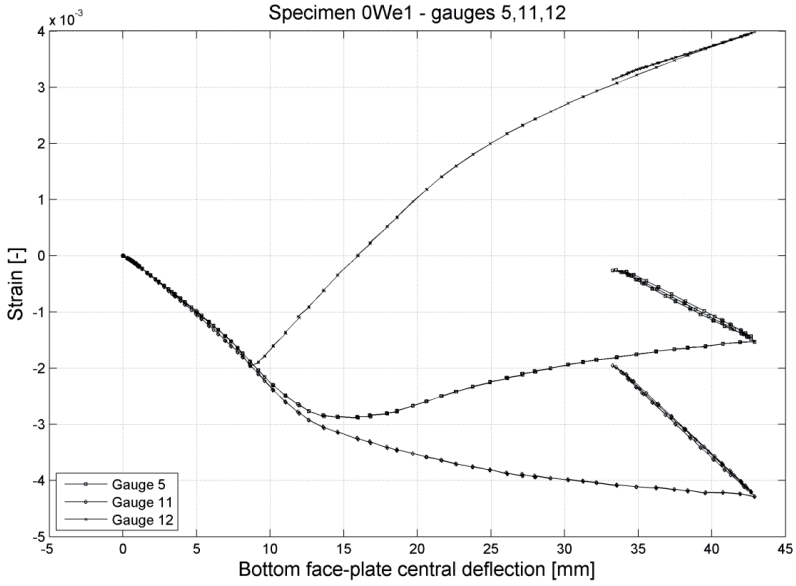

Figure 8-2. Strain measurements

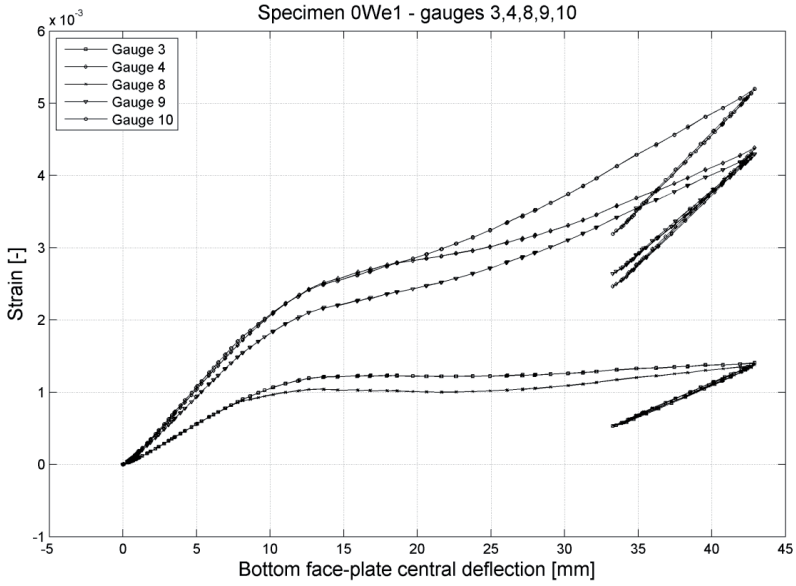

Figure 8-3. Strain measurements

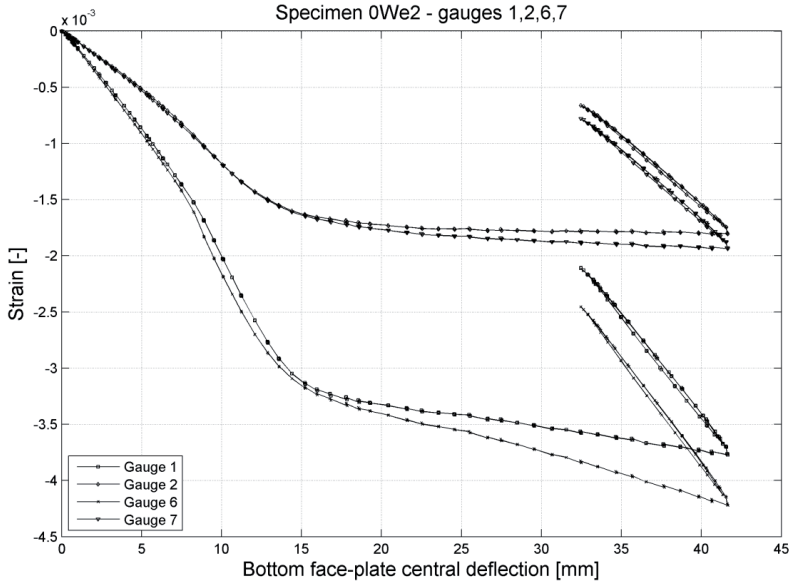

Figure 8-4. Strain measurements

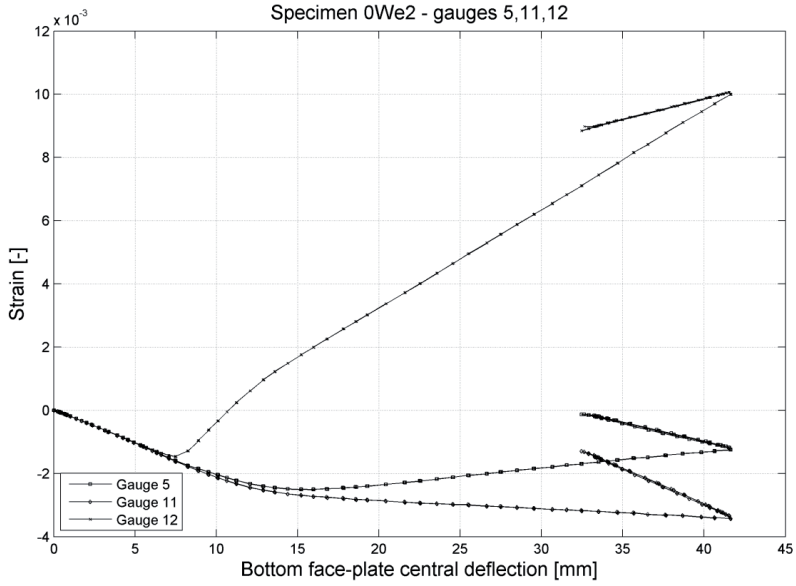

Figure 8-5. Strain measurements

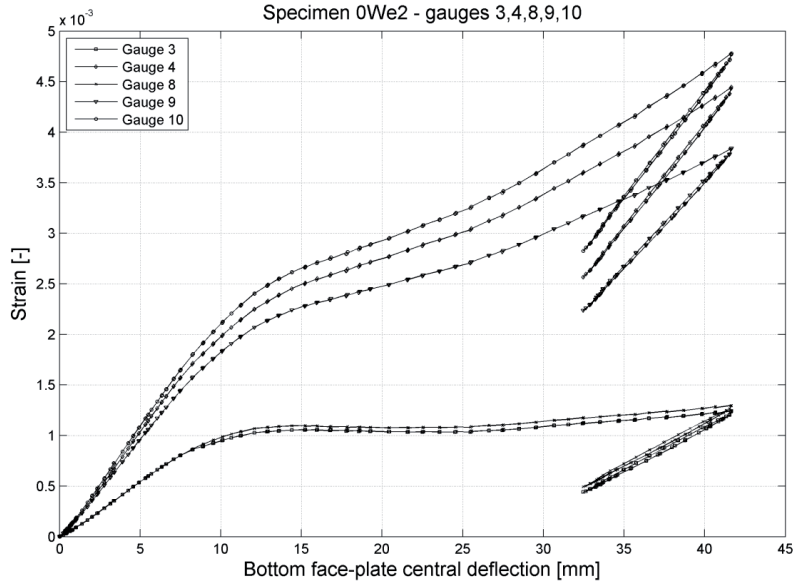

Figure 8-6. Strain measurements

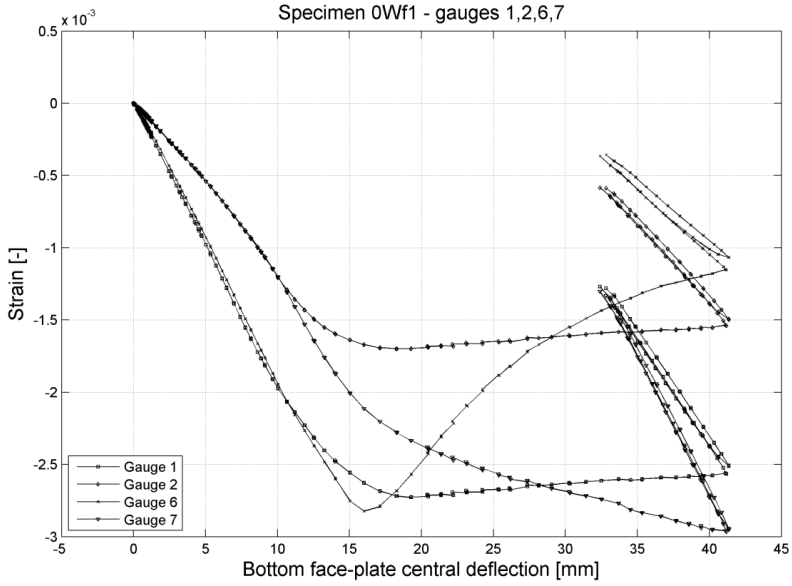

Figure 8-7. Strain measurements

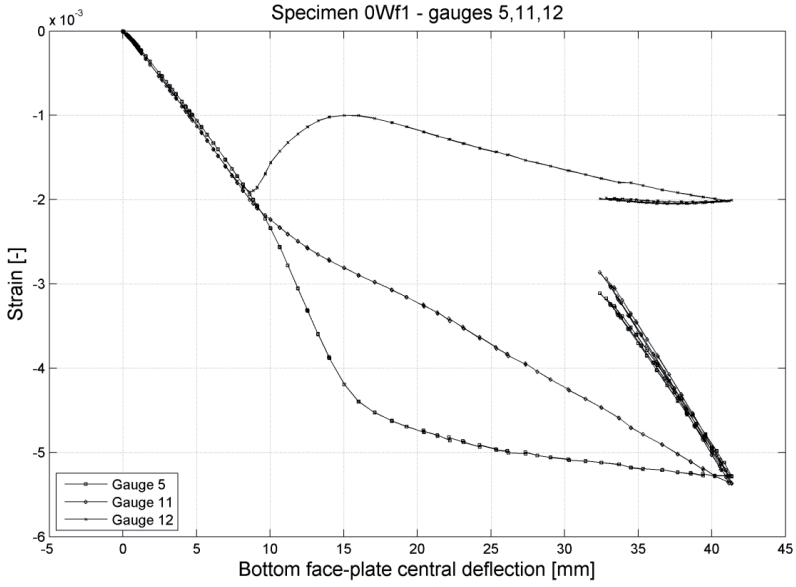

Figure 8-8. Strain measurements

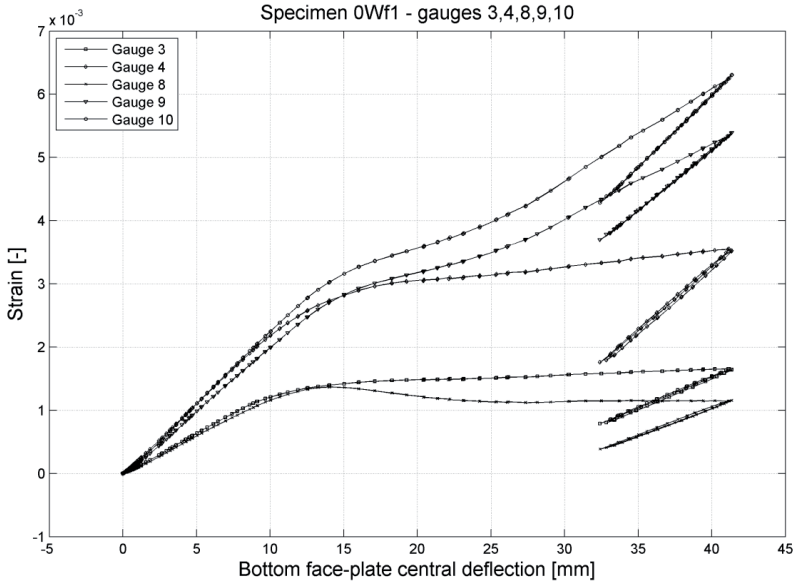

Figure 8-9. Strain measurements

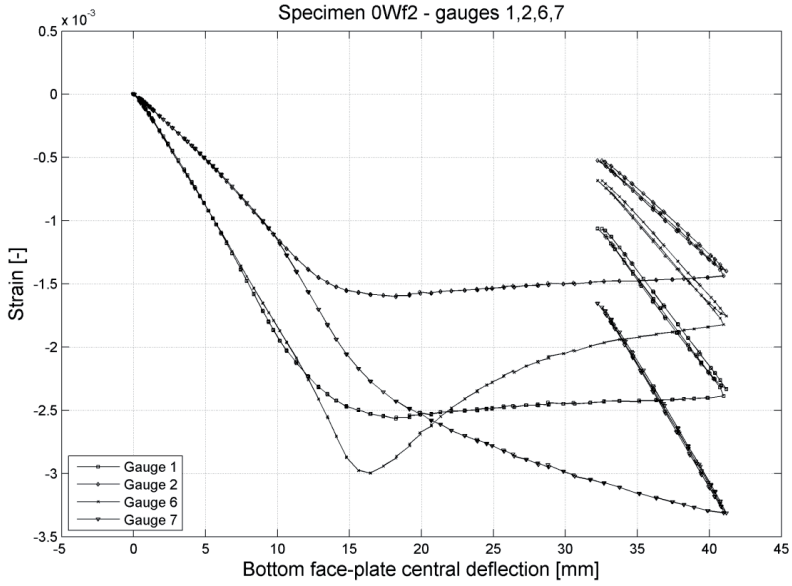

Figure 8-10. Strain measurements

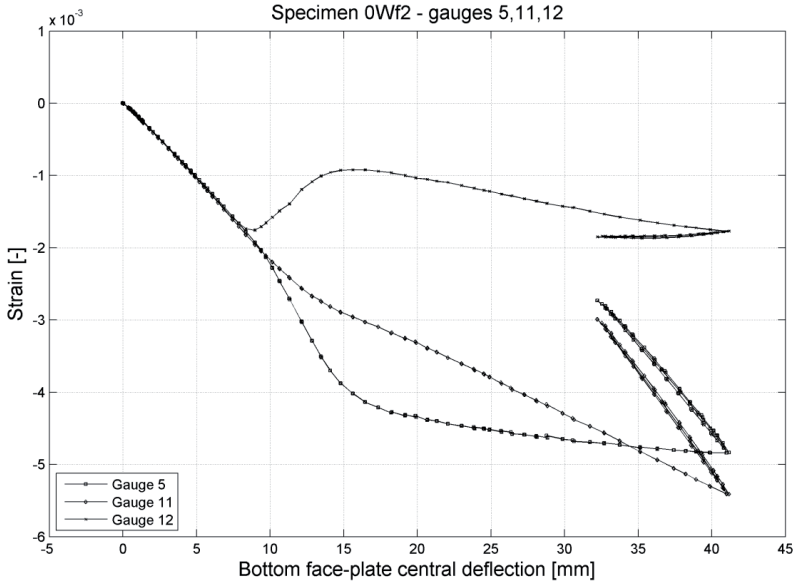

Figure 8-11. Strain measurements

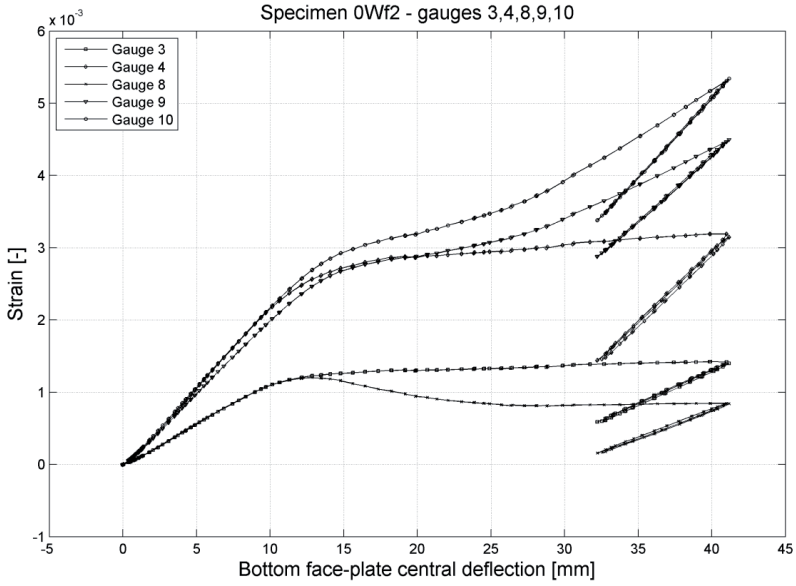

Figure 8-12. Strain measurements

9 Appendix C-W1 – Strain measurements from one-year corroded web-core sandwich beams

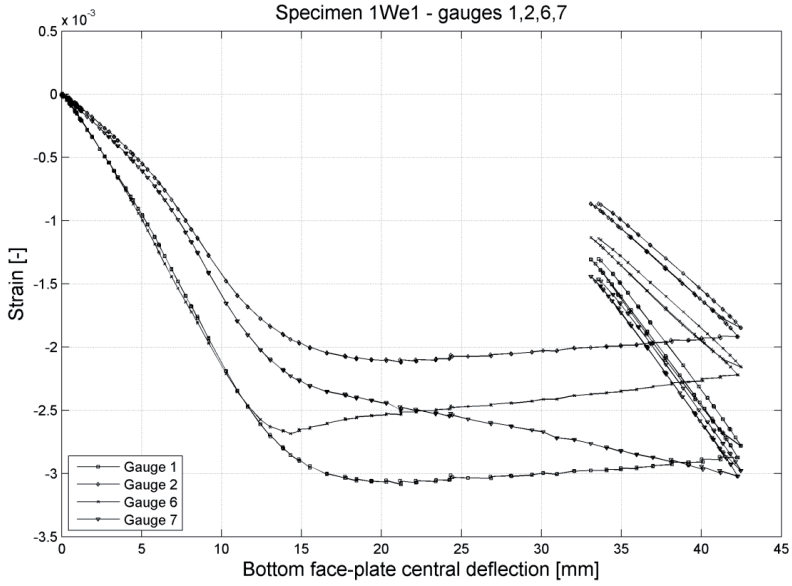

Figure 9-1. Strain measurements

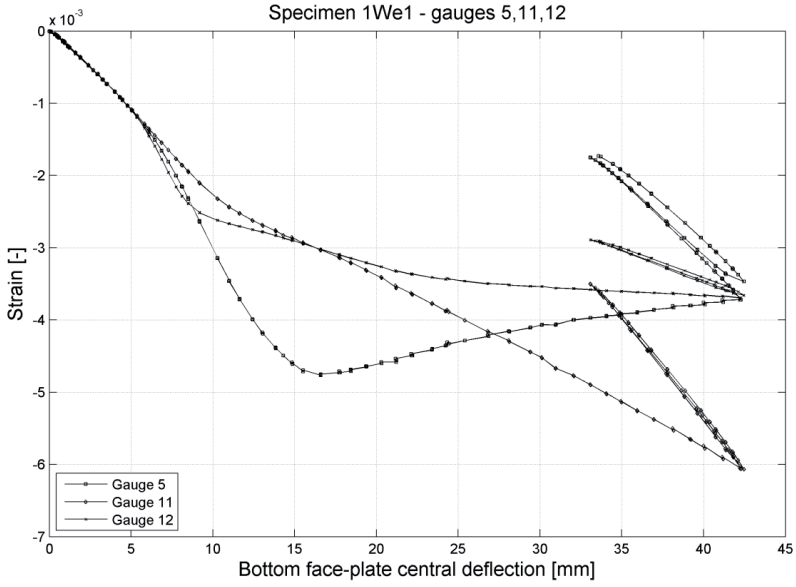

Figure 9-2. Strain measurements

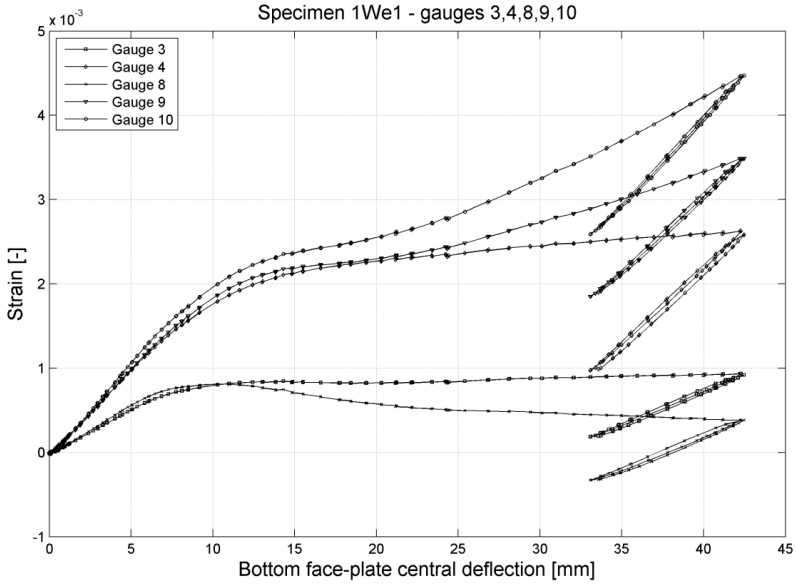

Figure 9-3. Strain measurements

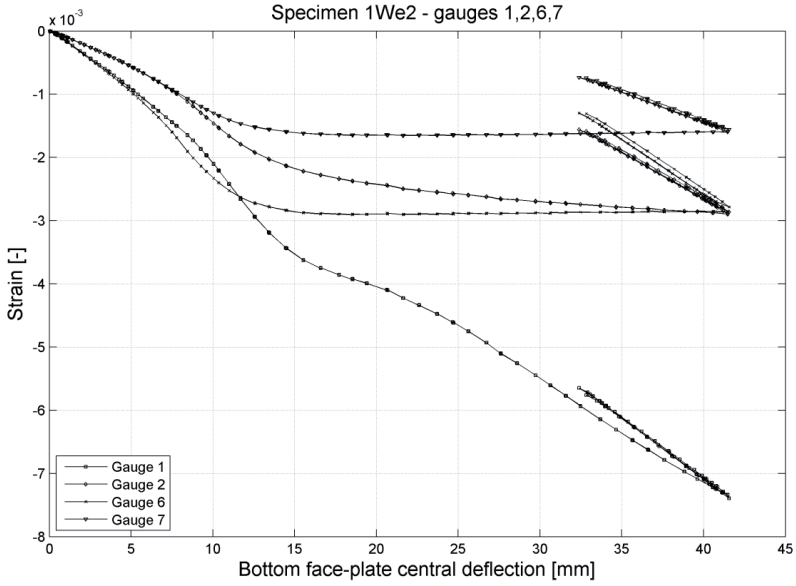

Figure 9-4. Strain measurements

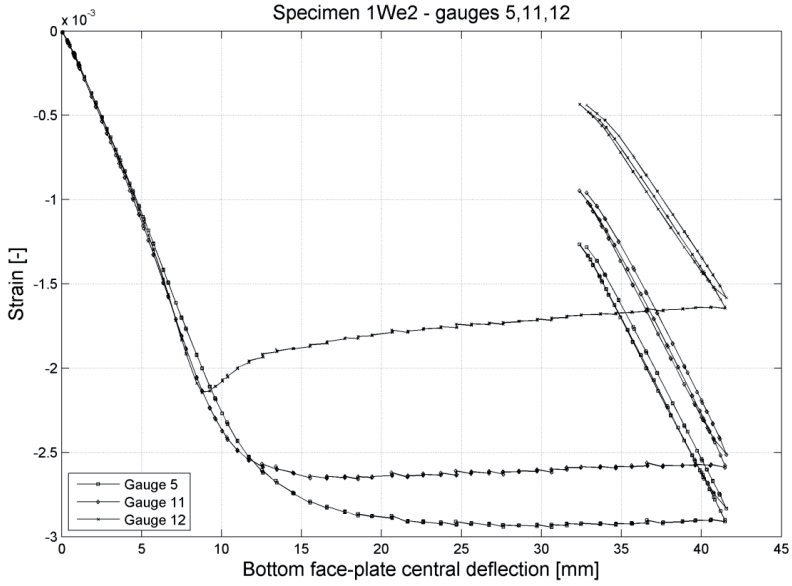

Figure 9-5. Strain measurements

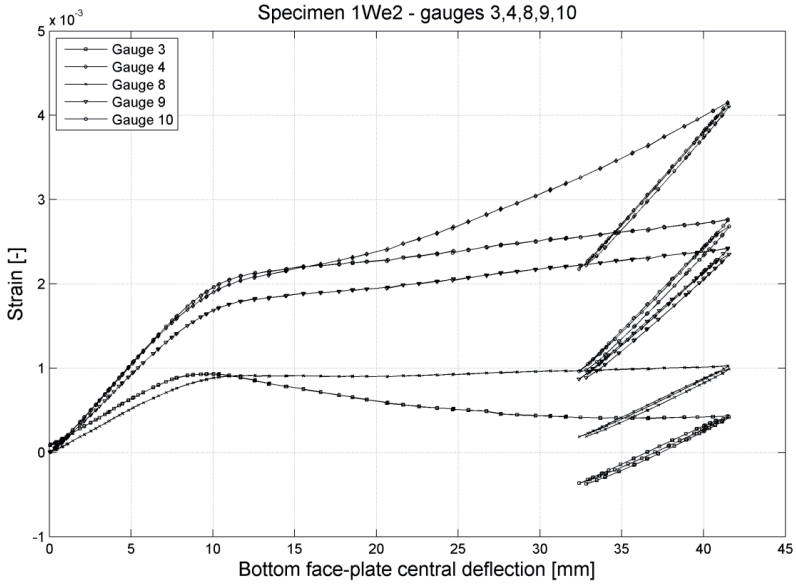

Figure 9-6. Strain measurements

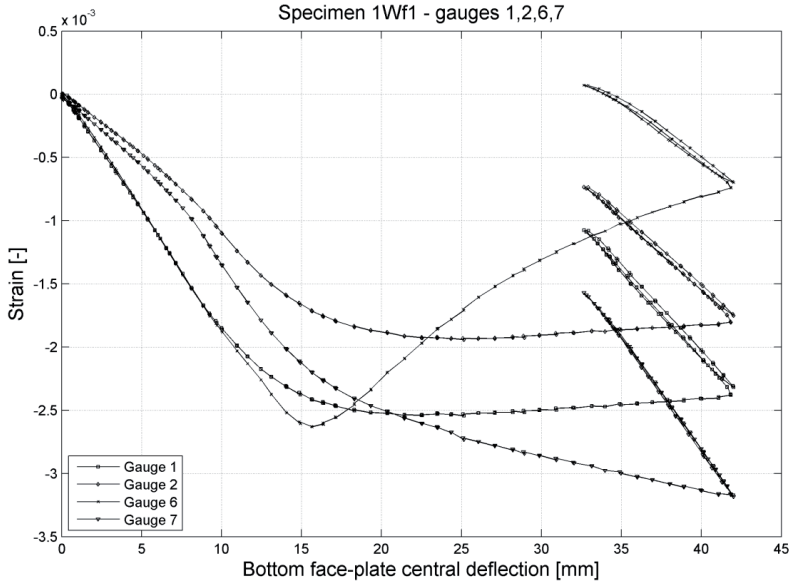

Figure 9-7. Strain measurements

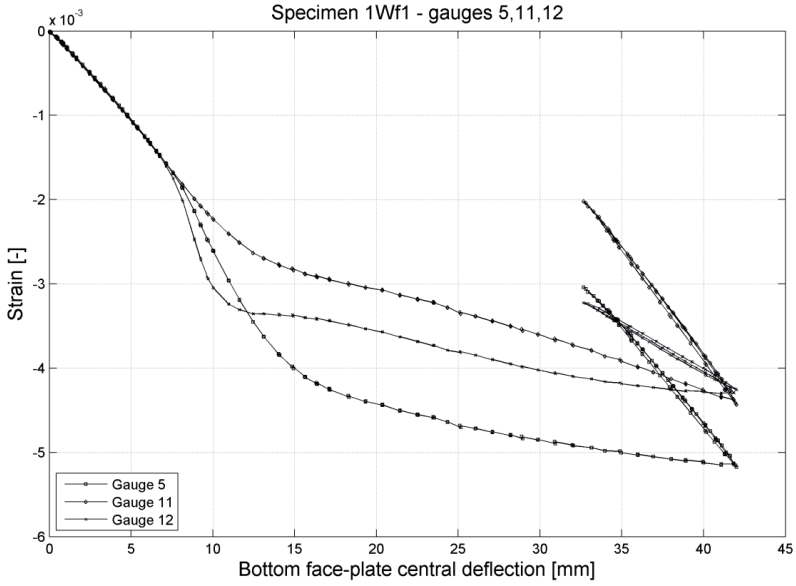

Figure 9-8. Strain measurements

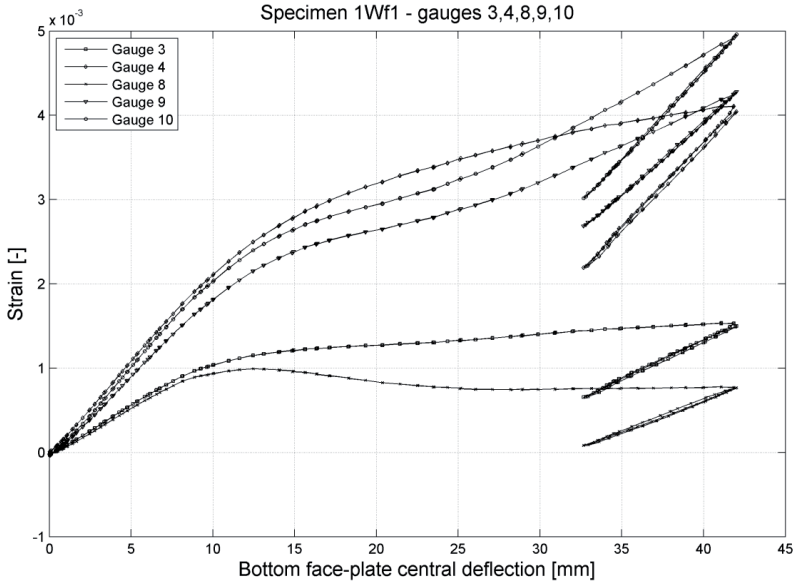

Figure 9-9. Strain measurements

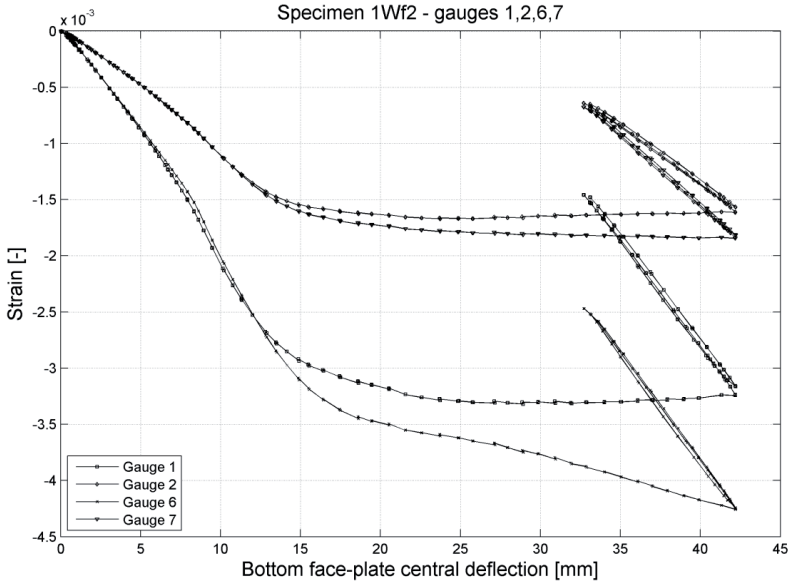

Figure 9-10. Strain measurements

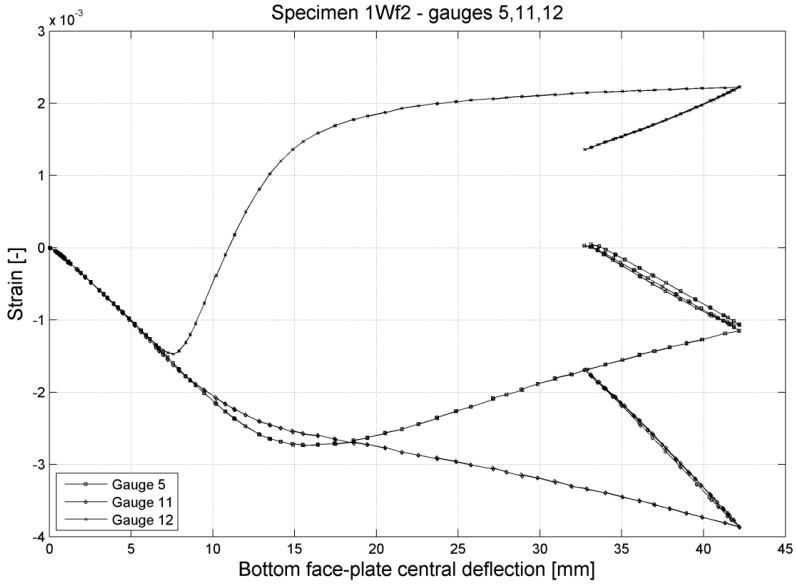

Figure 9-11. Strain measurements

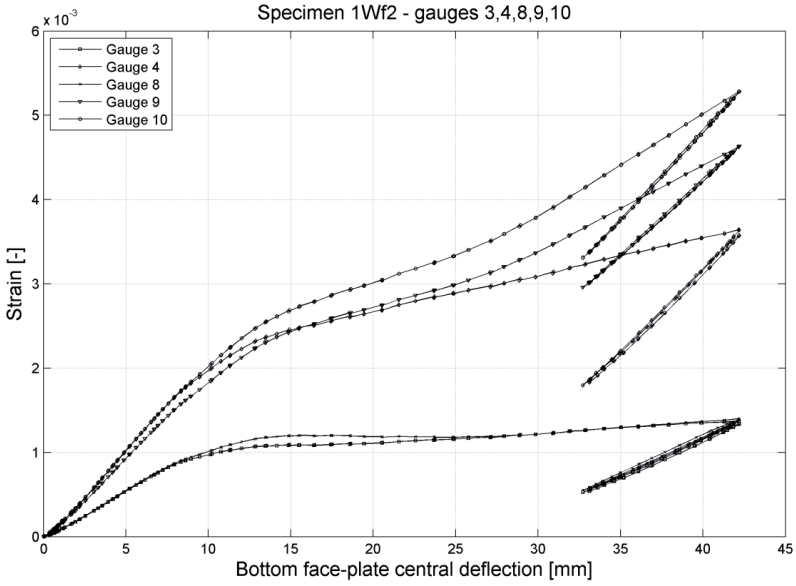

Figure 9-12. Strain measurements

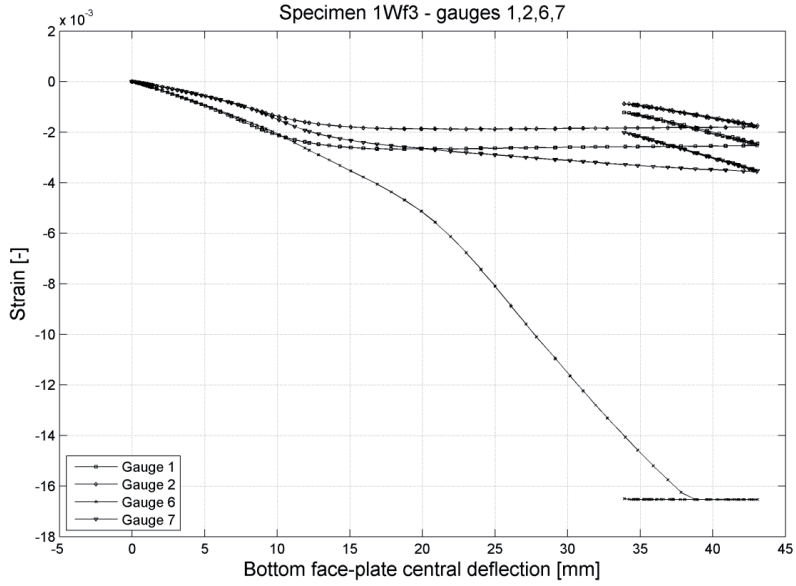

Figure 9-13. Strain measurements

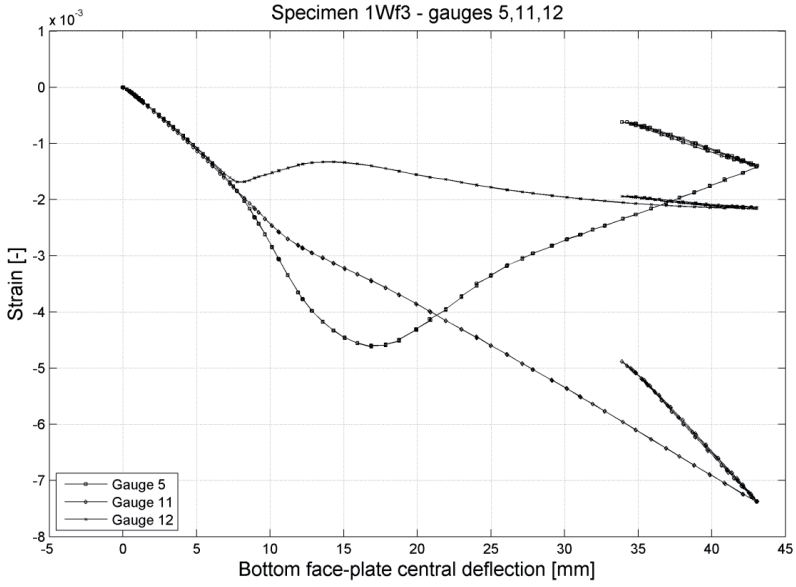

Figure 9-14. Strain measurements

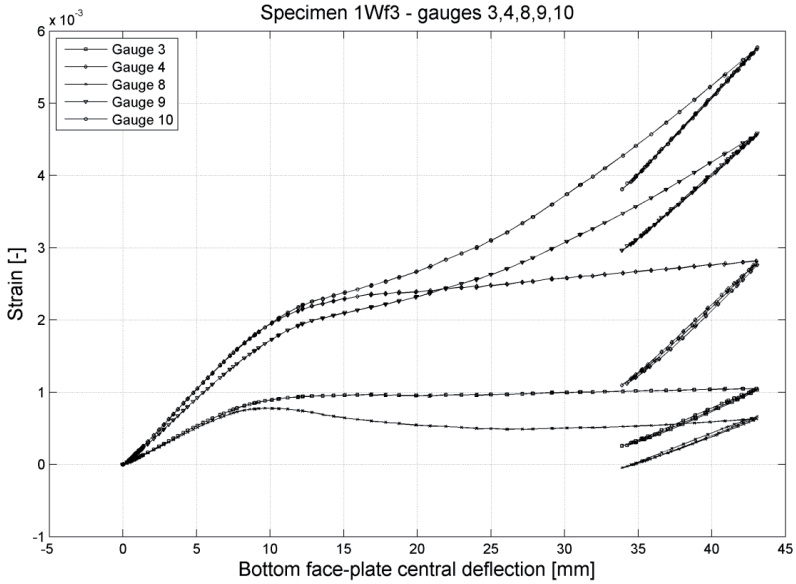

Figure 9-15. Strain measurements

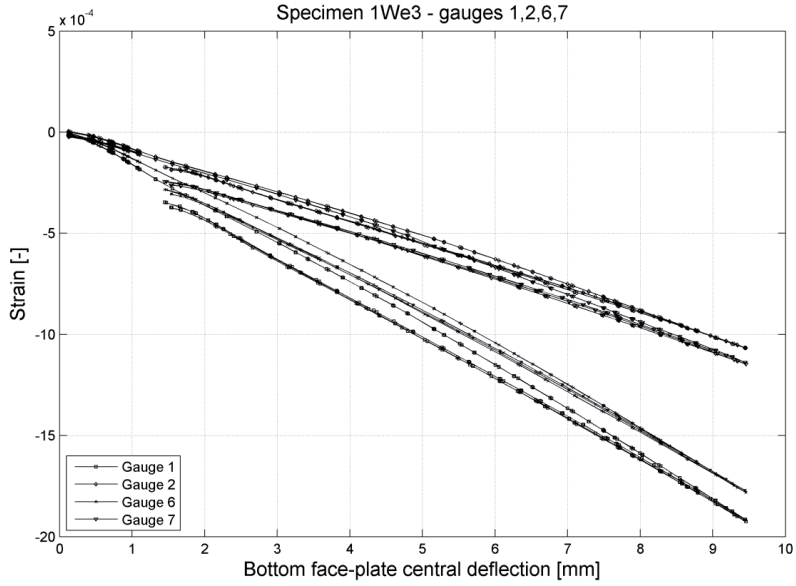

Figure 9-16. Strain measurements

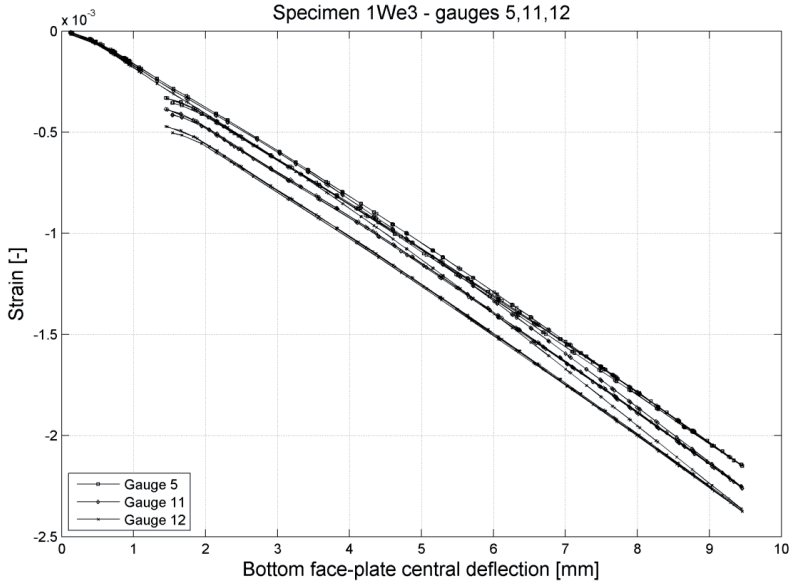

Figure 9-17. Strain measurements

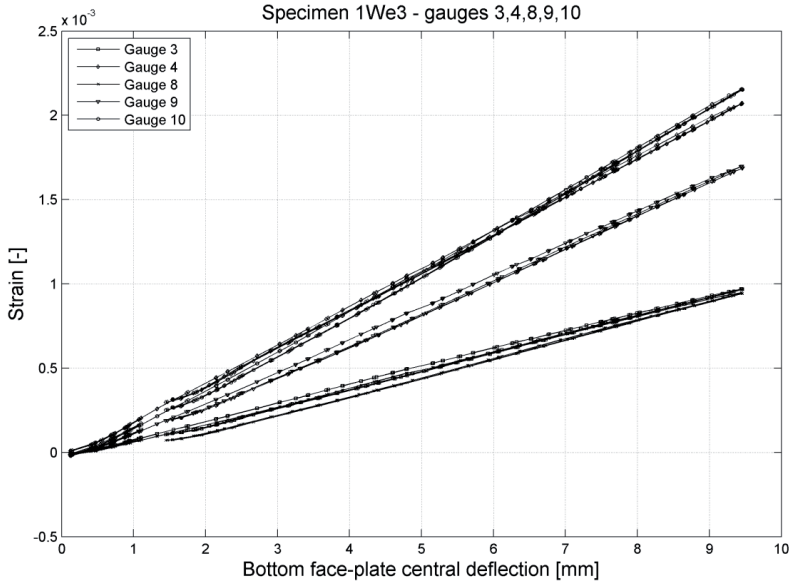

Figure 9-18. Strain measurements

10 Appendix C-W2 – Strain measurements from two-year corroded web-core sandwich beams

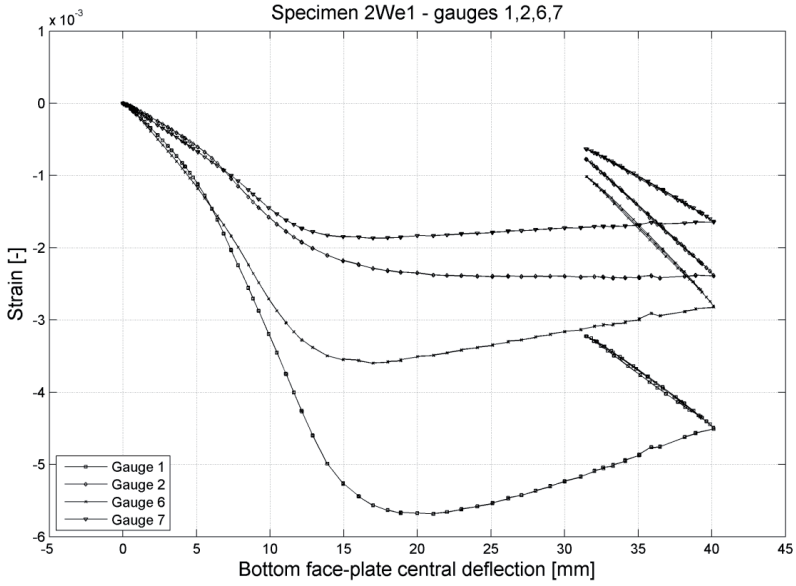

Figure 10-1. Strain measurements

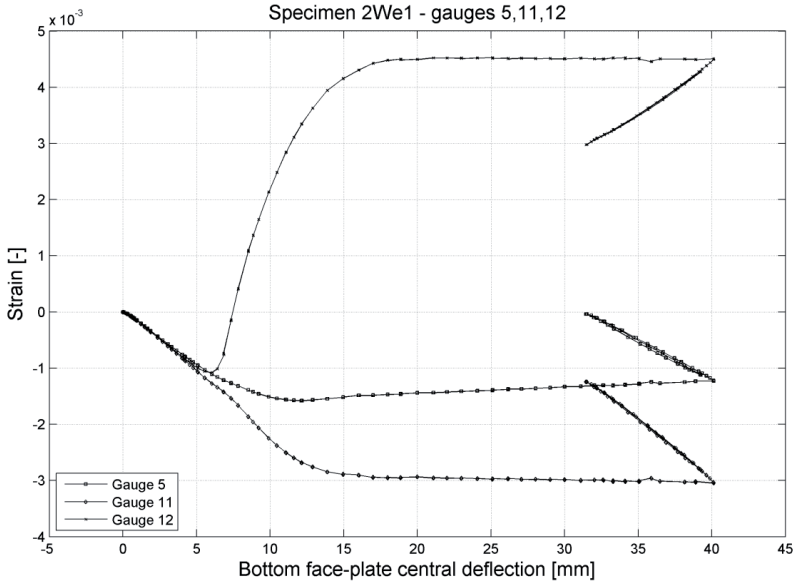

Figure 10-2. Strain measurements

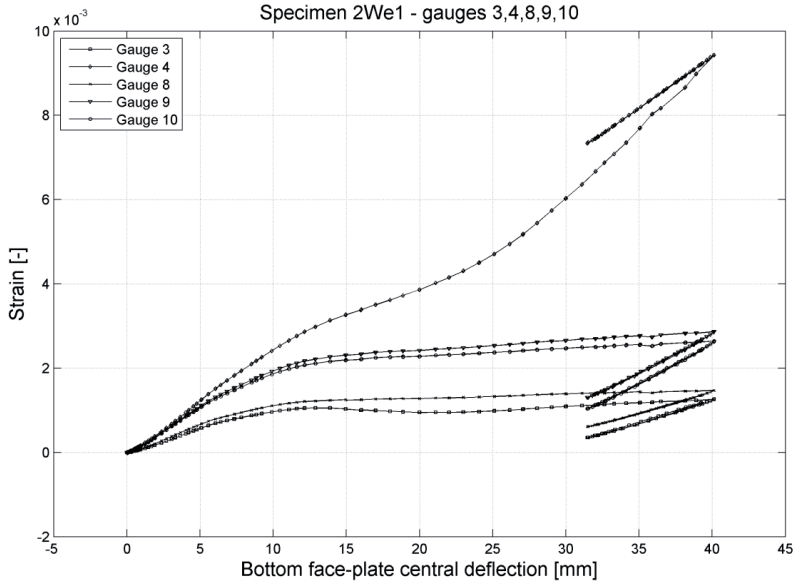

Figure 10-3. Strain measurements

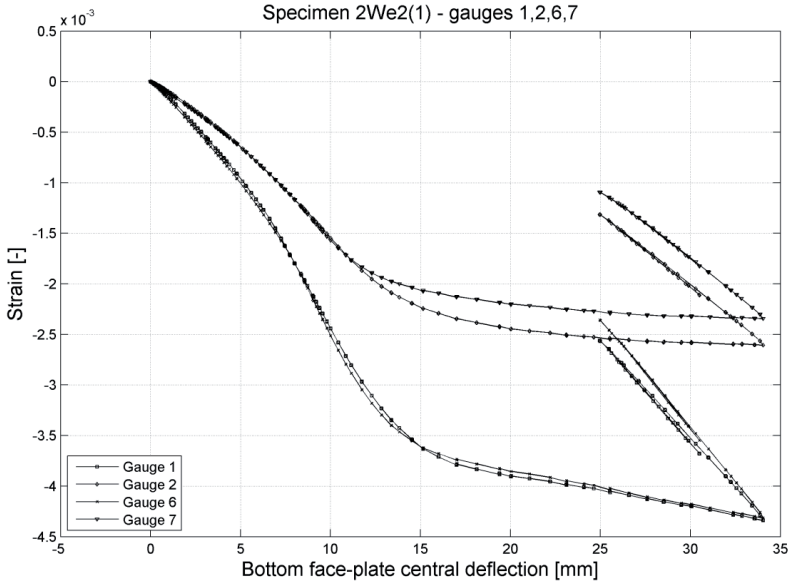

Figure 10-4. Strain measurements

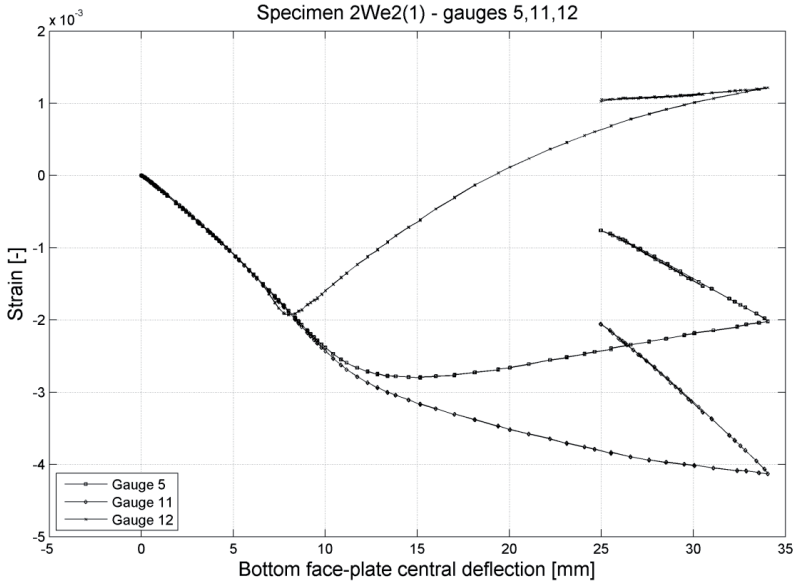

Figure 10-5. Strain measurements

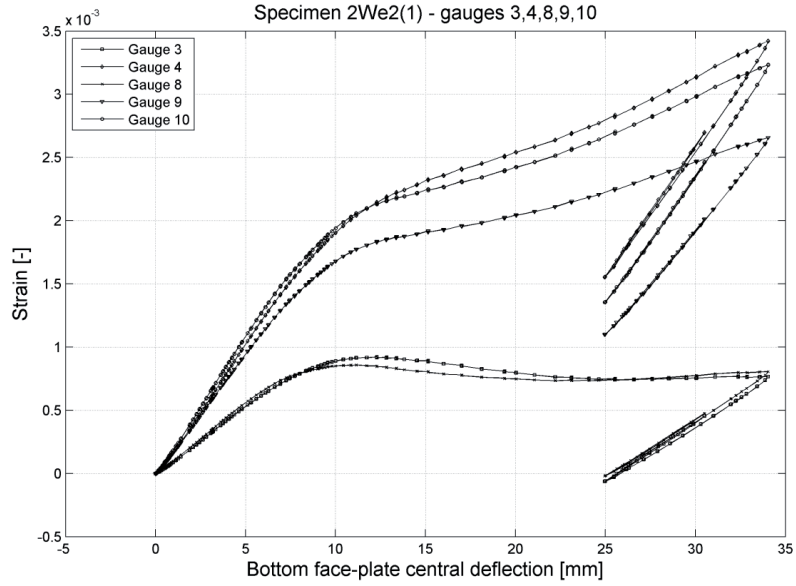

Figure 10-6. Strain measurements

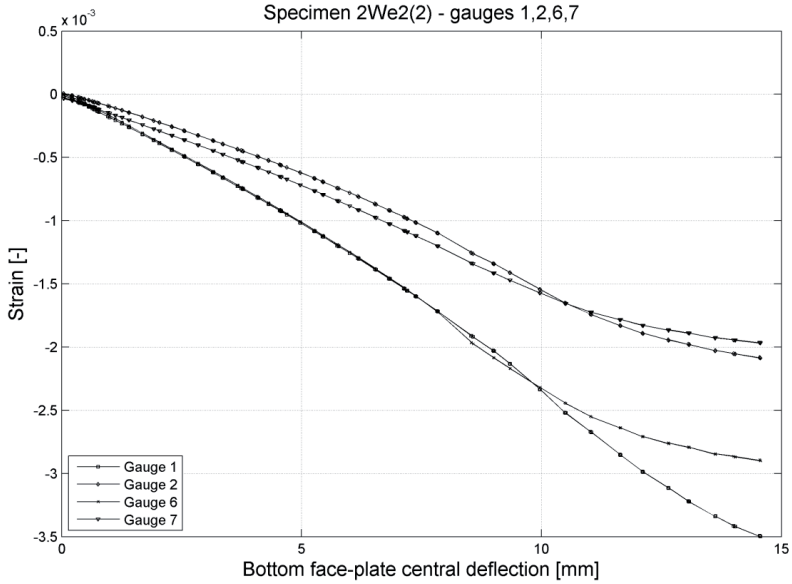

Figure 10-7. Strain measurements

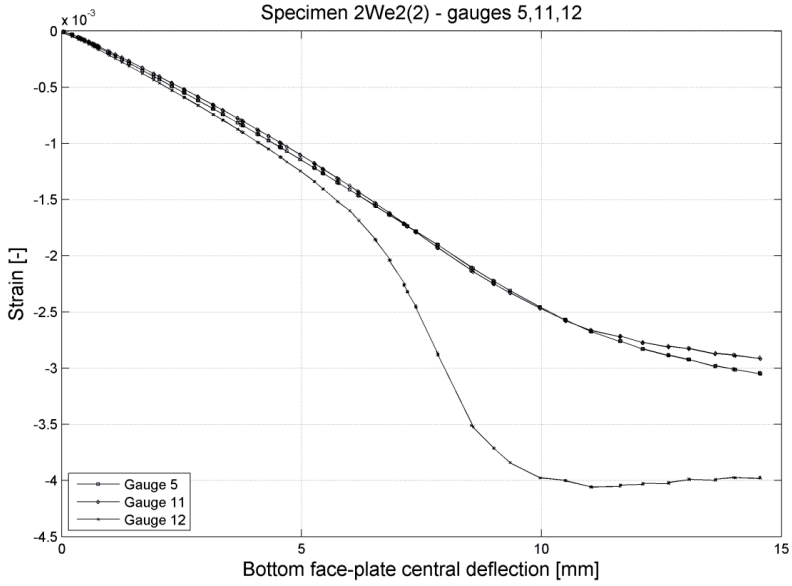

Figure 10-8. Strain measurements

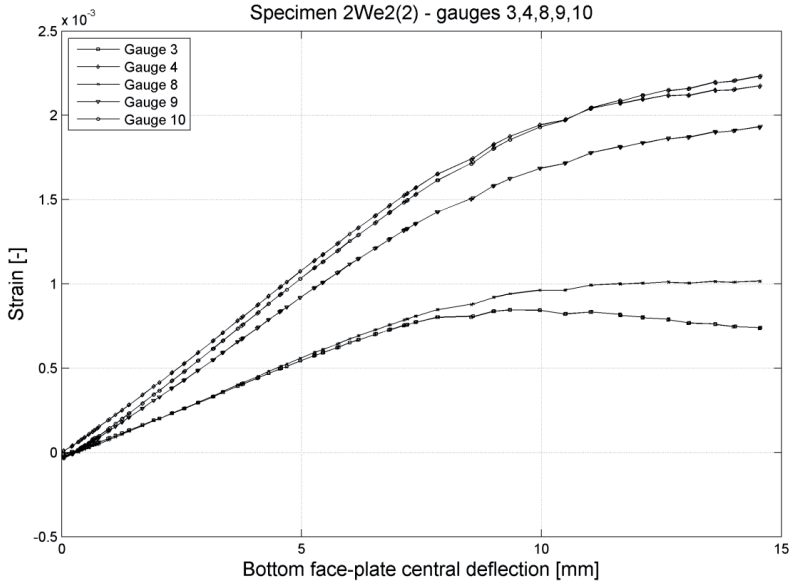

Figure 10-9. Strain measurements

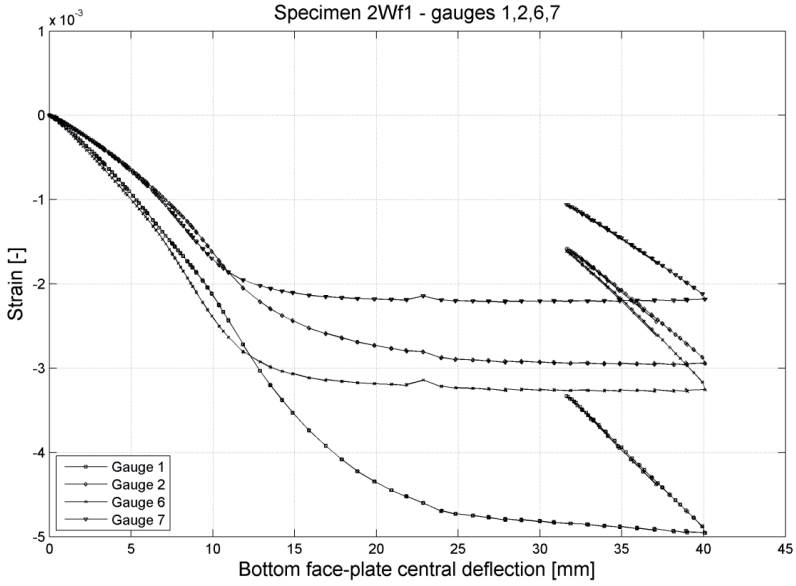

Figure 10-10. Strain measurements

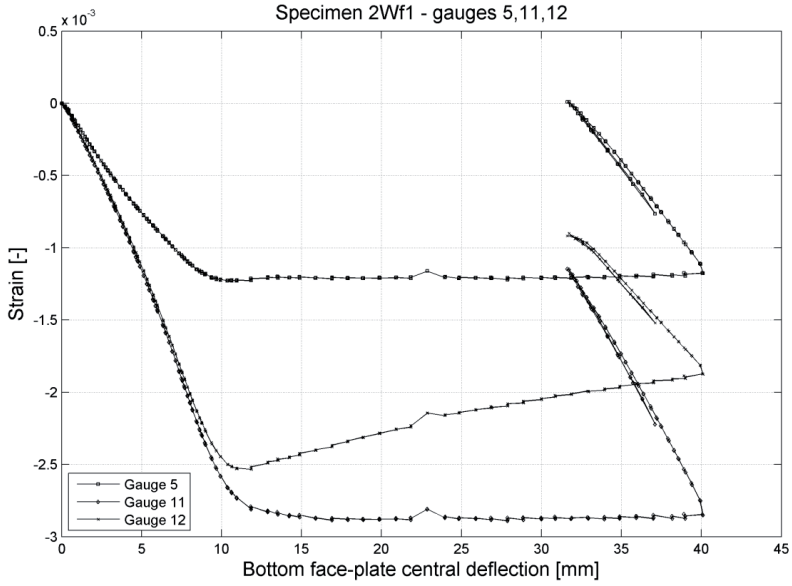

Figure 10-11. Strain measurements

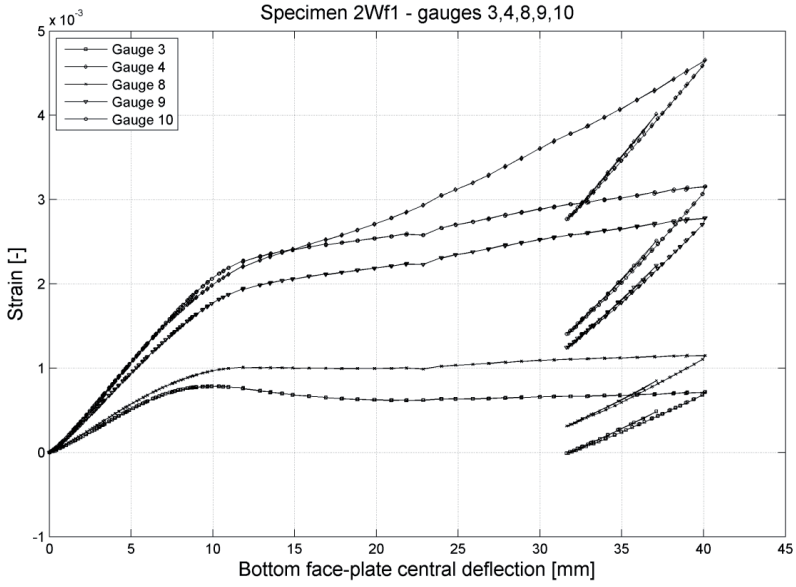

Figure 10-12. Strain measurements

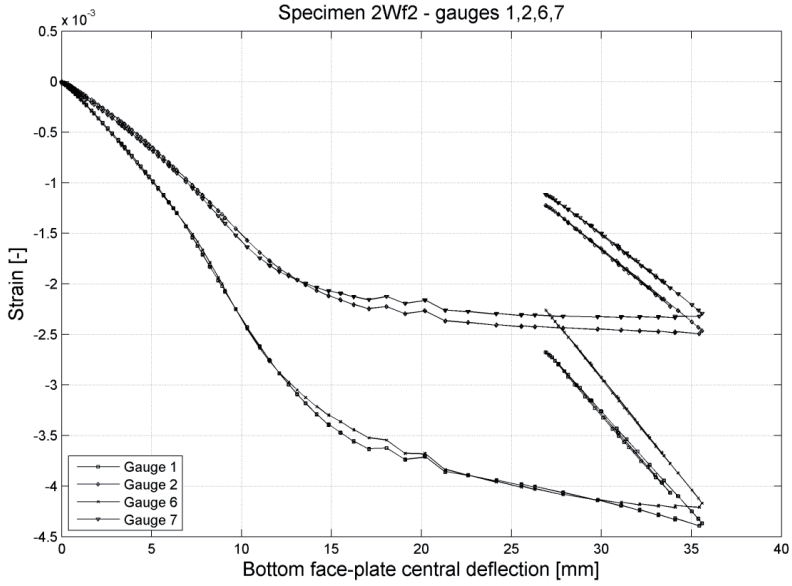

Figure 10-13. Strain measurements

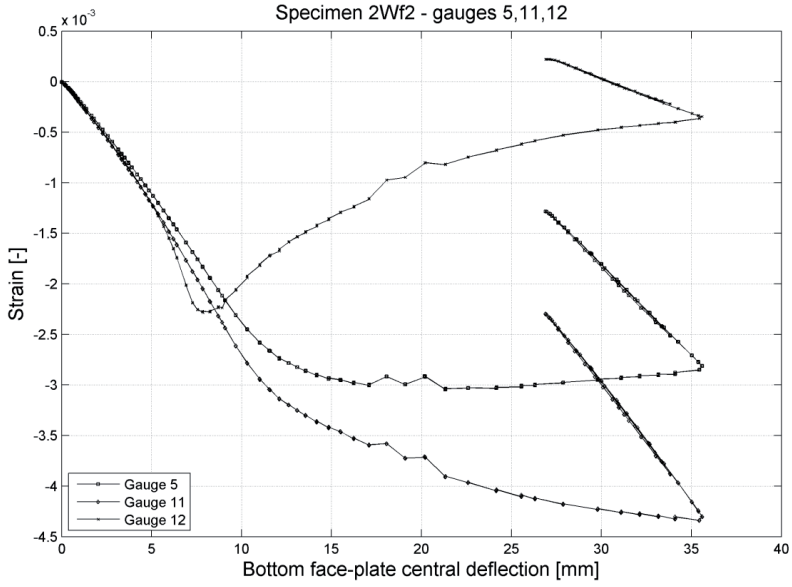

Figure 10-14. Strain measurements

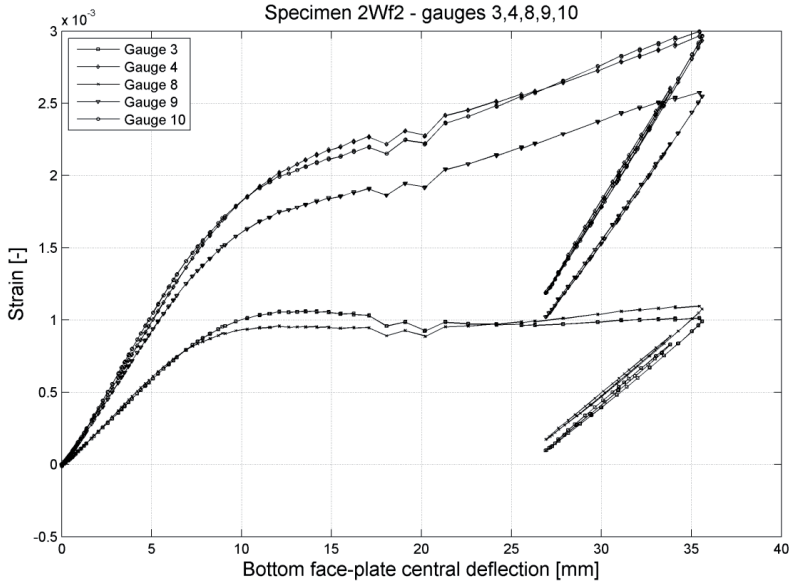

Figure 10-15. Strain measurements

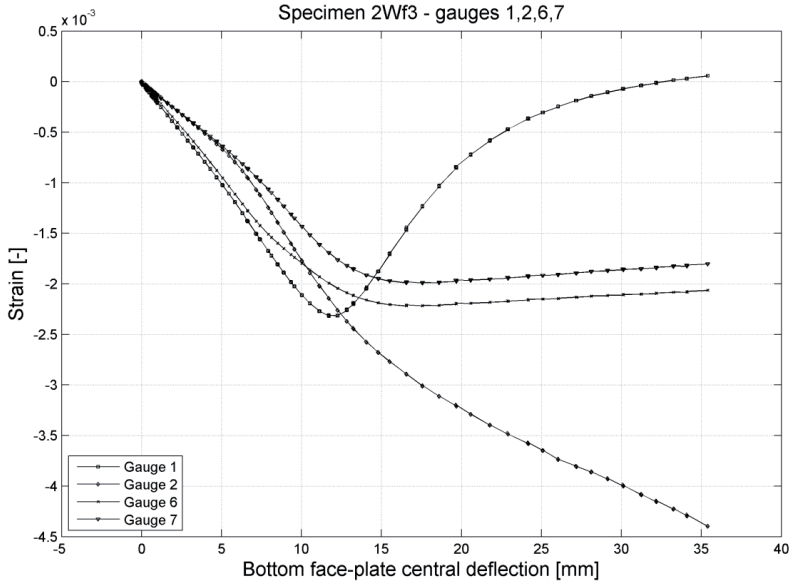

Figure 10-16. Strain measurements

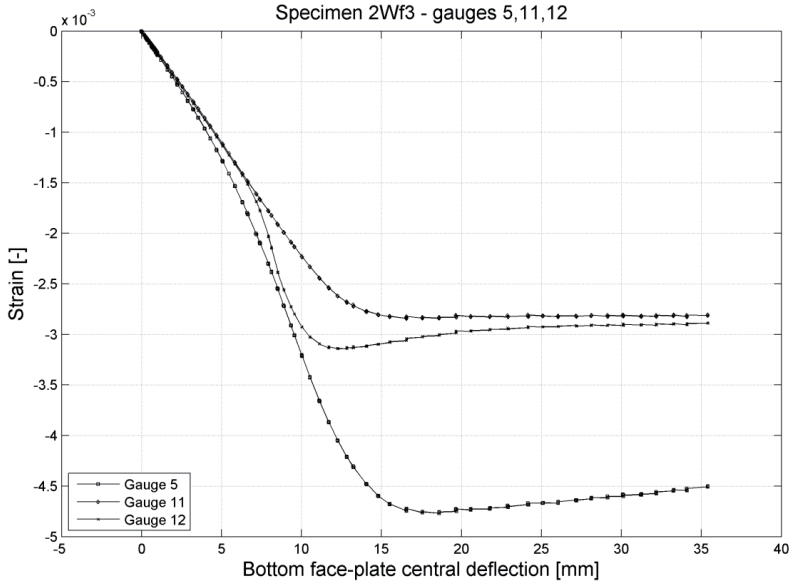

Figure 10-17. Strain measurements

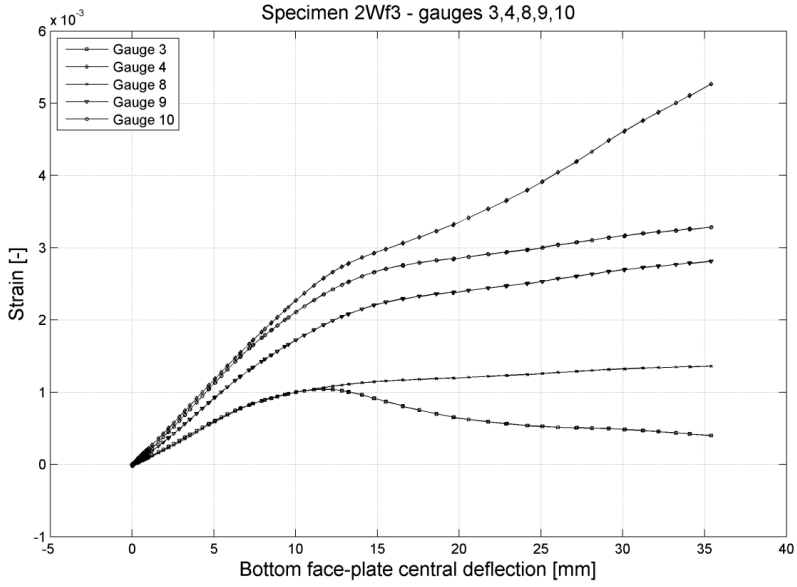

Figure 10-18. Strain measurements

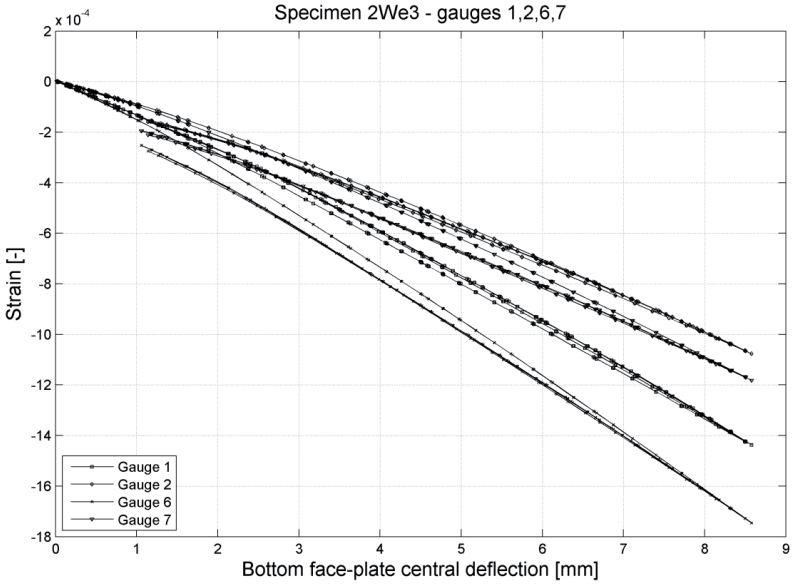

Figure 10-19. Strain measurements

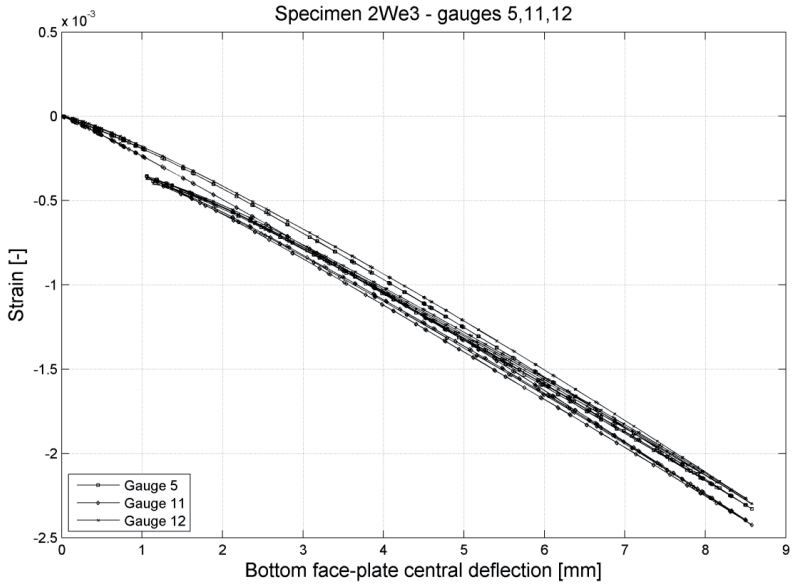

Figure 10-20. Strain measurements

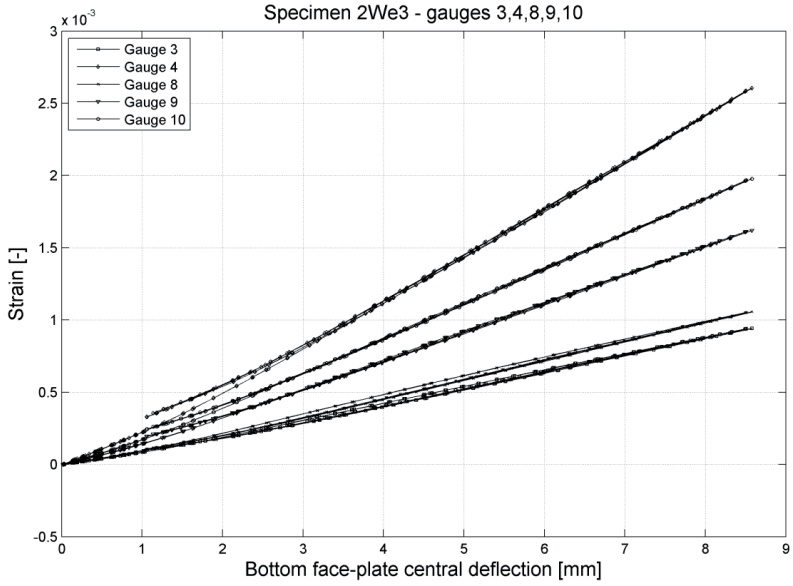

Figure 10-21. Strain measurements

11 Appendix C-C0 – Strain measurements from uncorroded corrugated-core sandwich beams

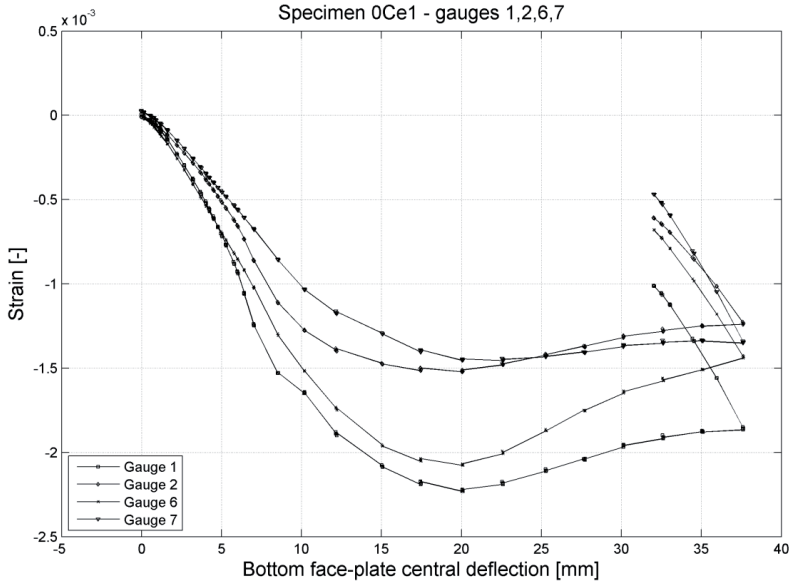

Figure 11-1. Strain measurements

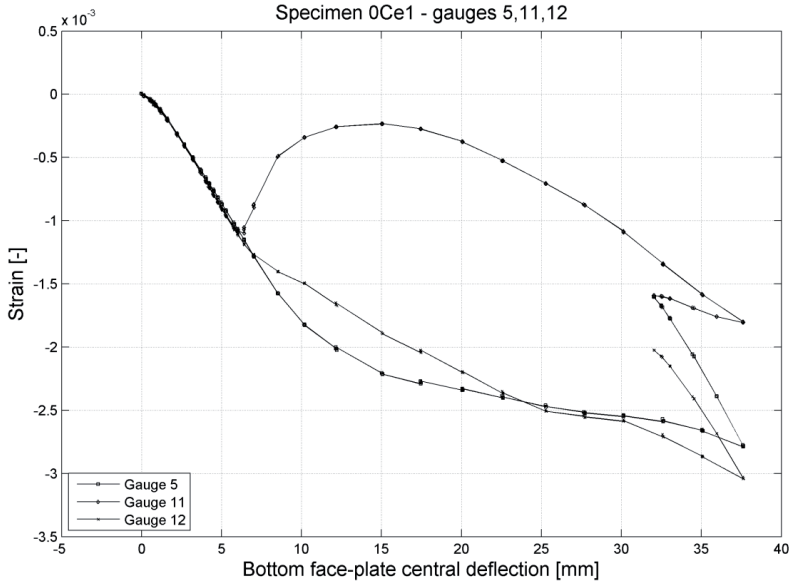

Figure 11-2. Strain measurements

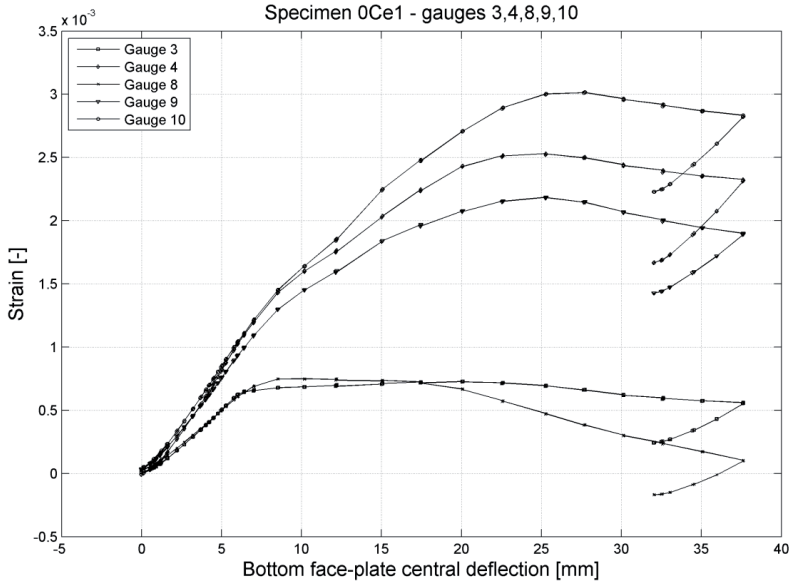

Figure 11-3. Strain measurements

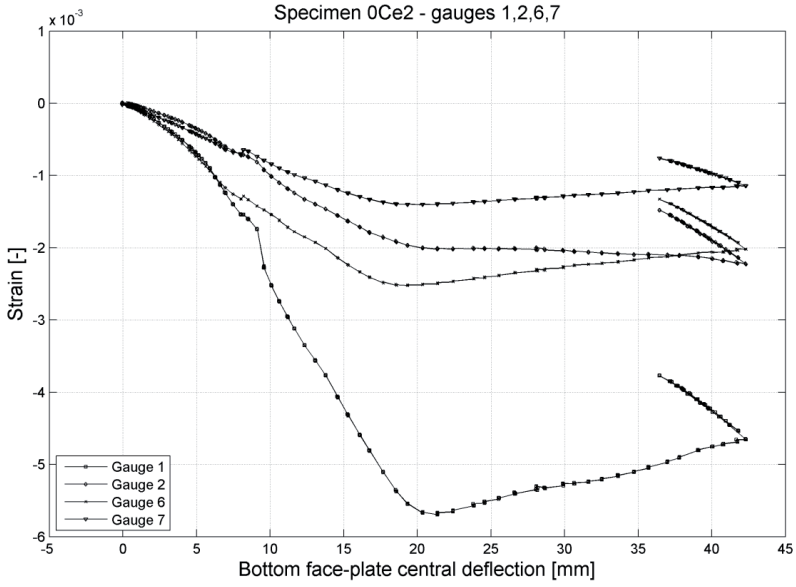

Figure 11-4. Strain measurements

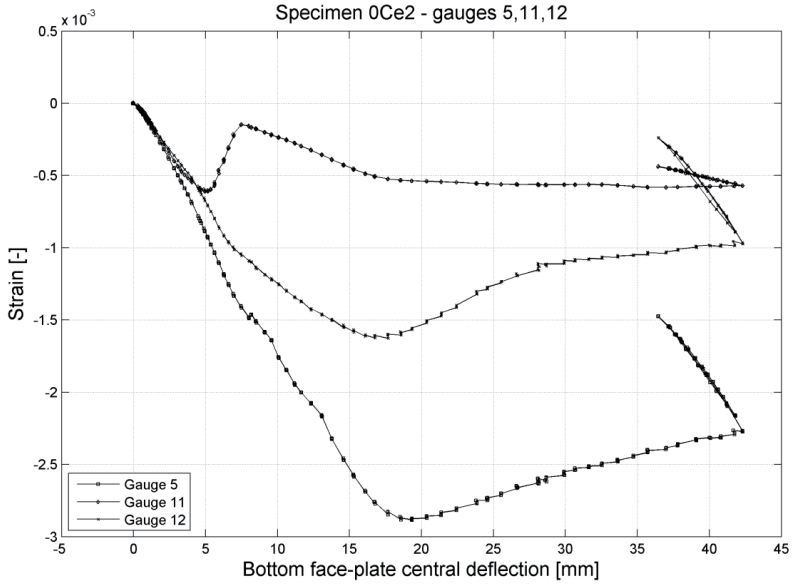

Figure 11-5. Strain measurements

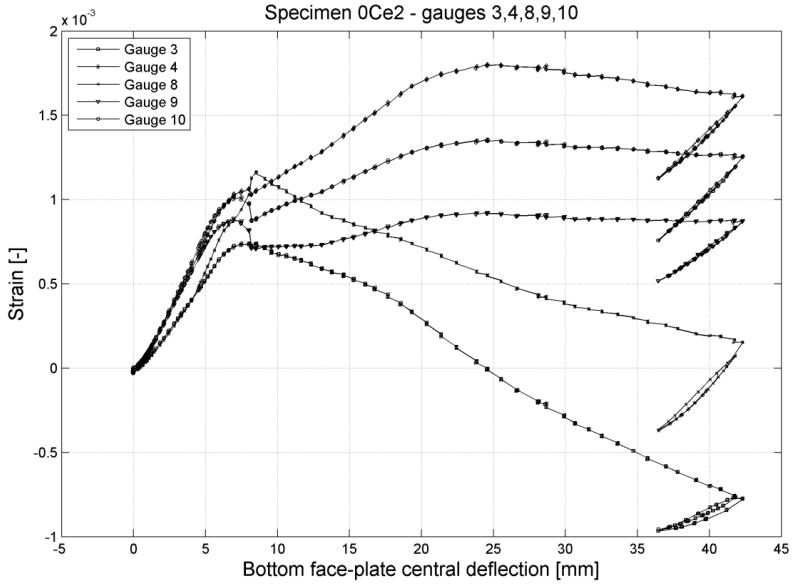

Figure 11-6. Strain measurements

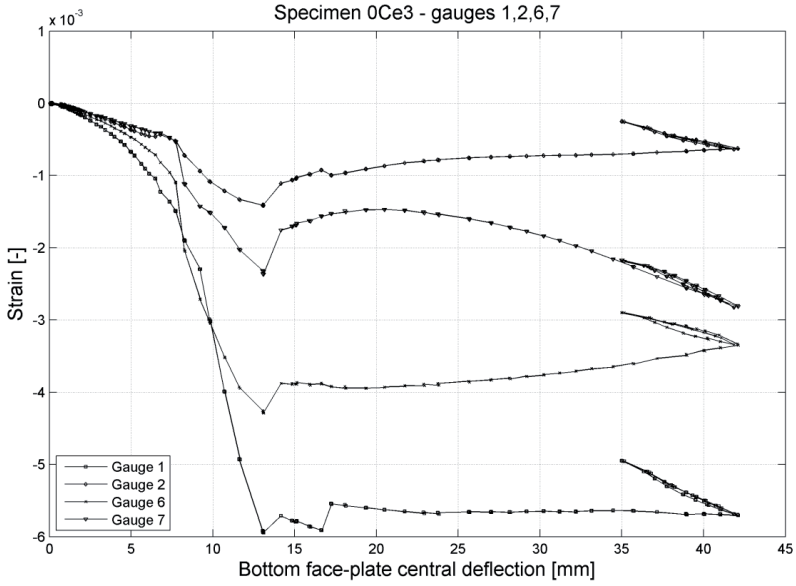

Figure 11-7. Strain measurements

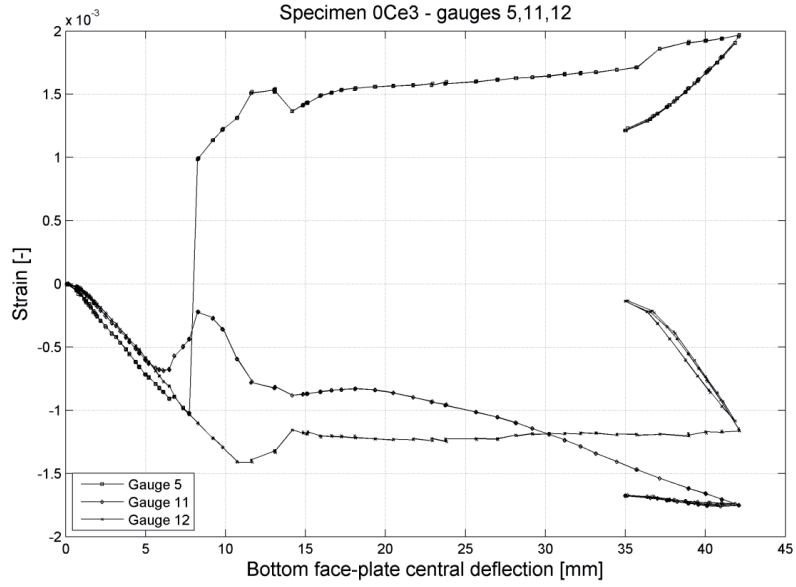

Figure 11-8. Strain measurements

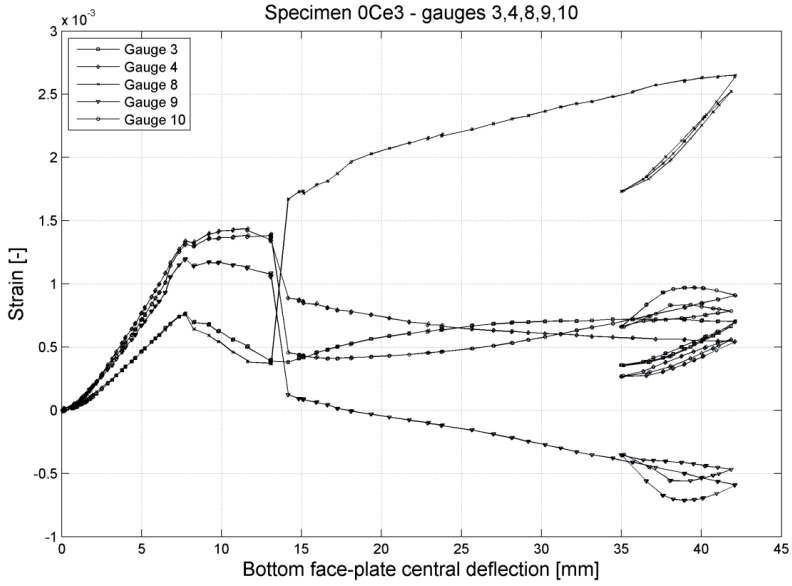

Figure 11-9. Strain measurements

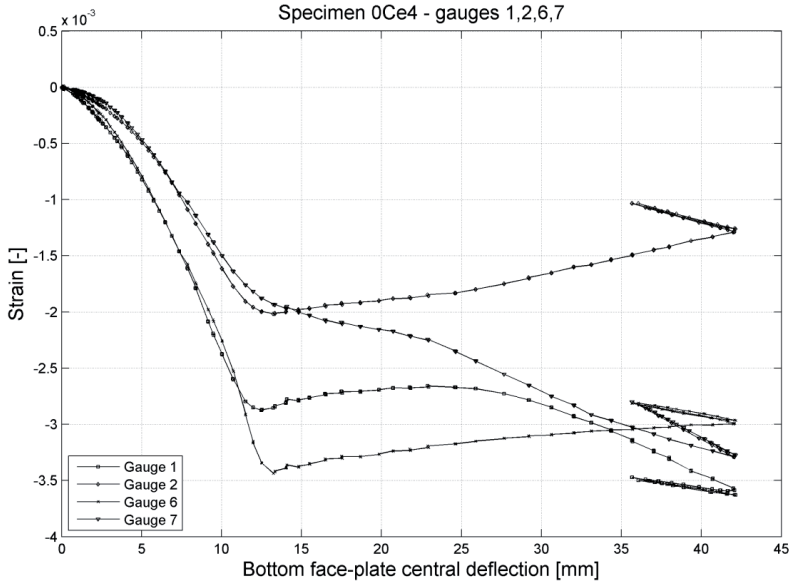

Figure 11-10. Strain measurements

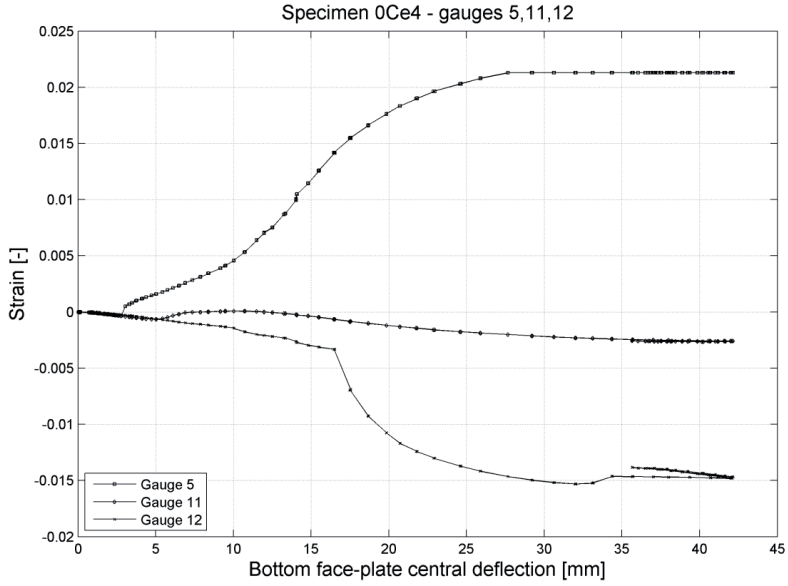

Figure 11-11. Strain measurements

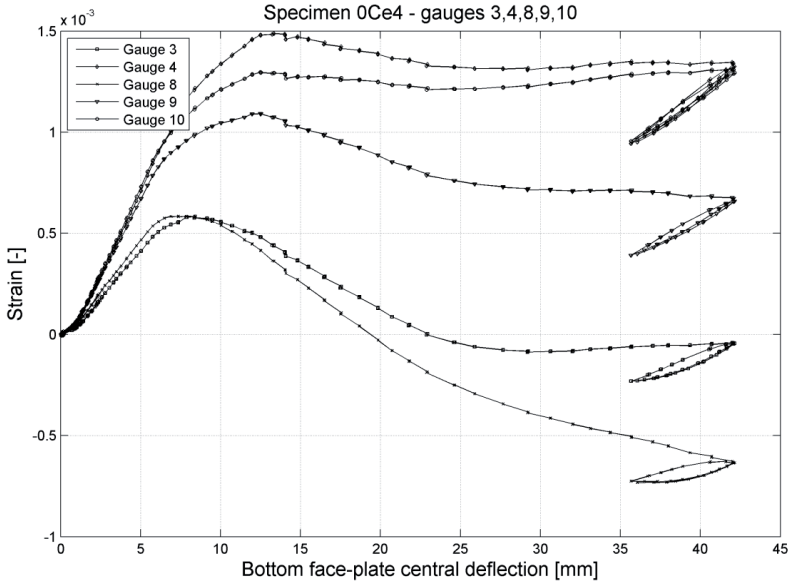

Figure 11-12. Strain measurements

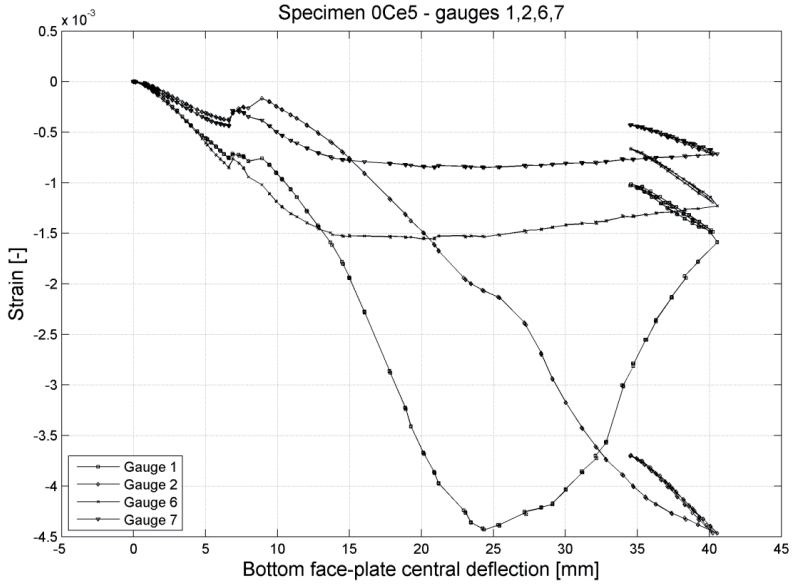

Figure 11-13. Strain measurements

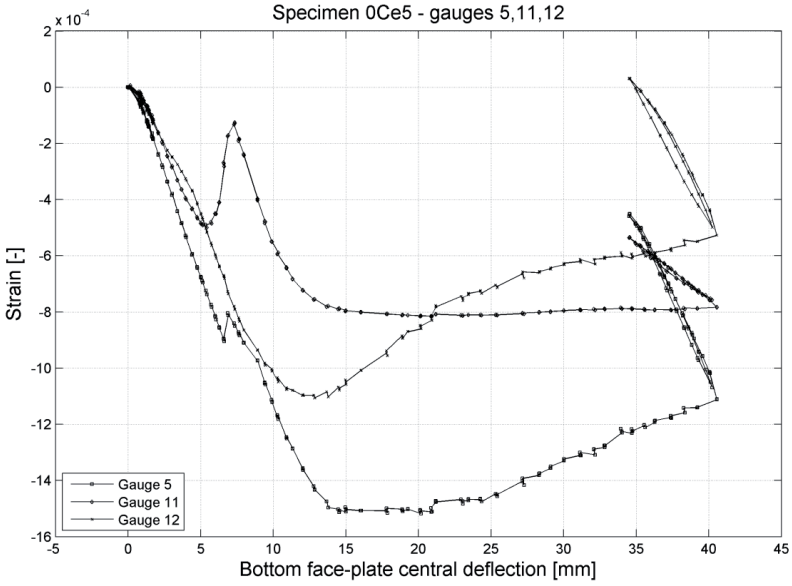

Figure 11-14. Strain measurements

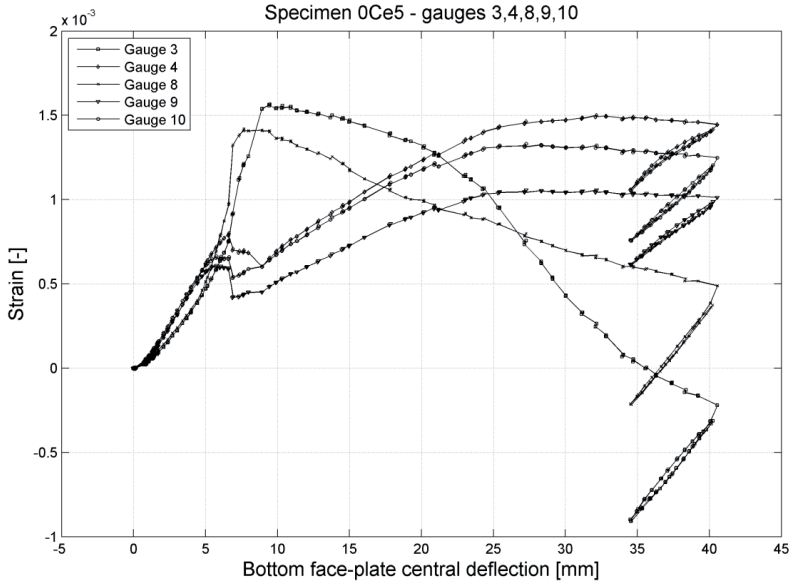

Figure 11-15. Strain measurements

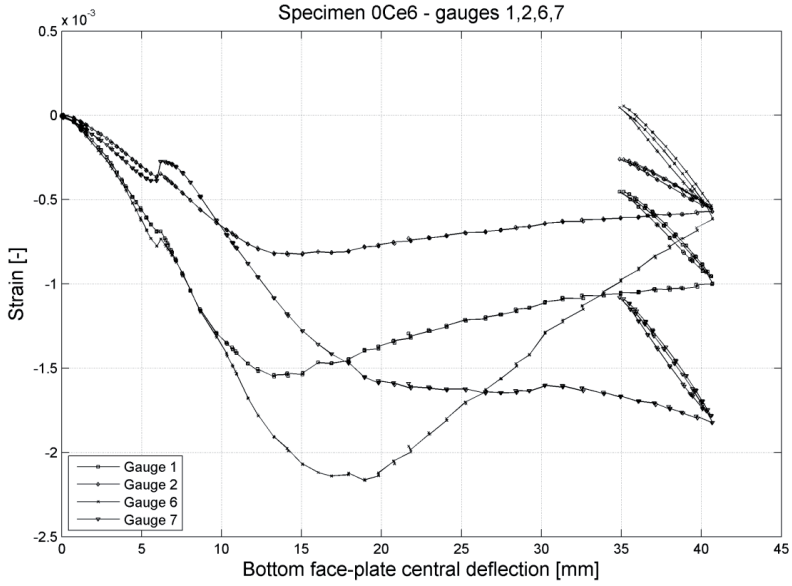

Figure 11-16. Strain measurements

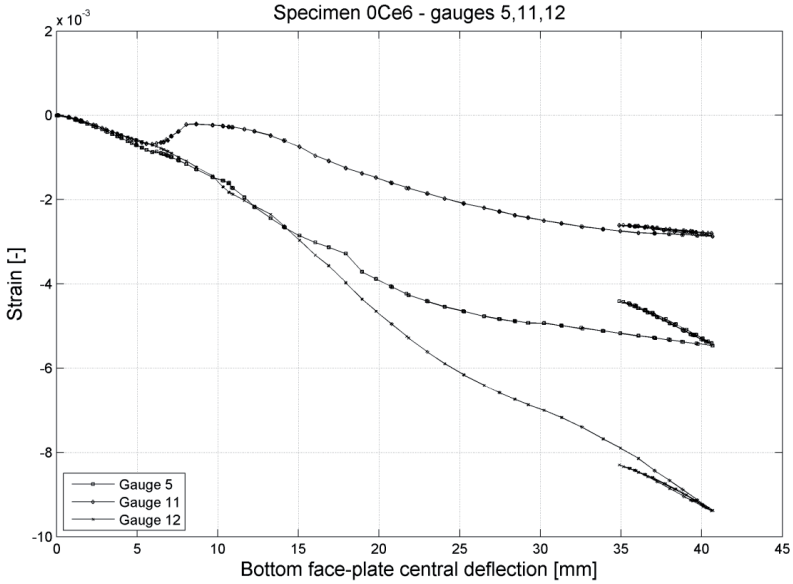

Figure 11-17. Strain measurements

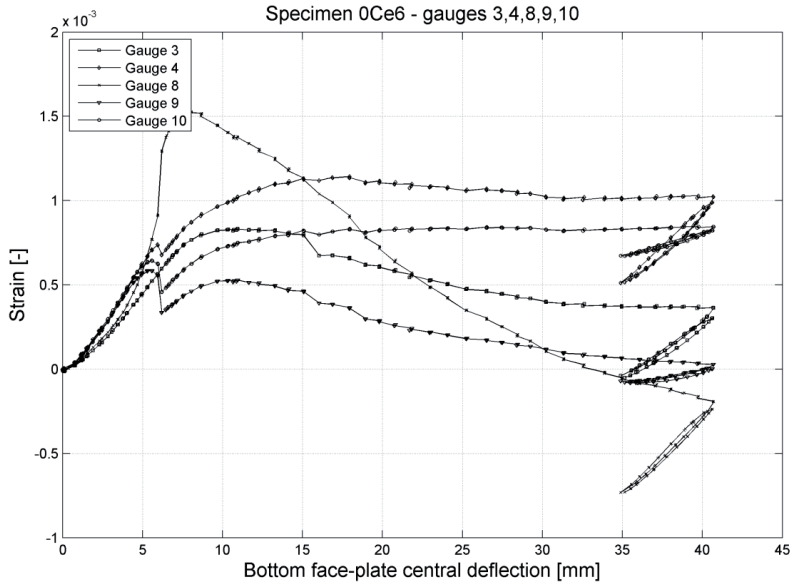

Figure 11-18. Strain measurements

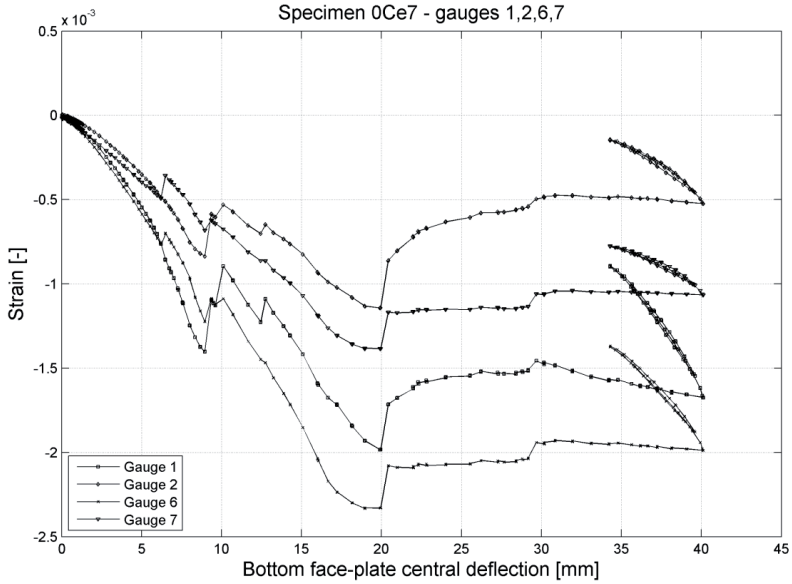

Figure 11-19. Strain measurements

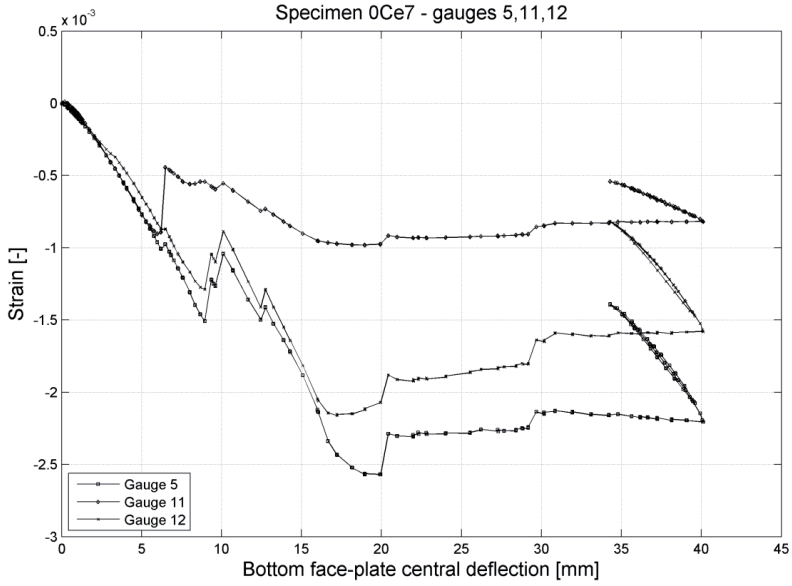

Figure 11-20. Strain measurements

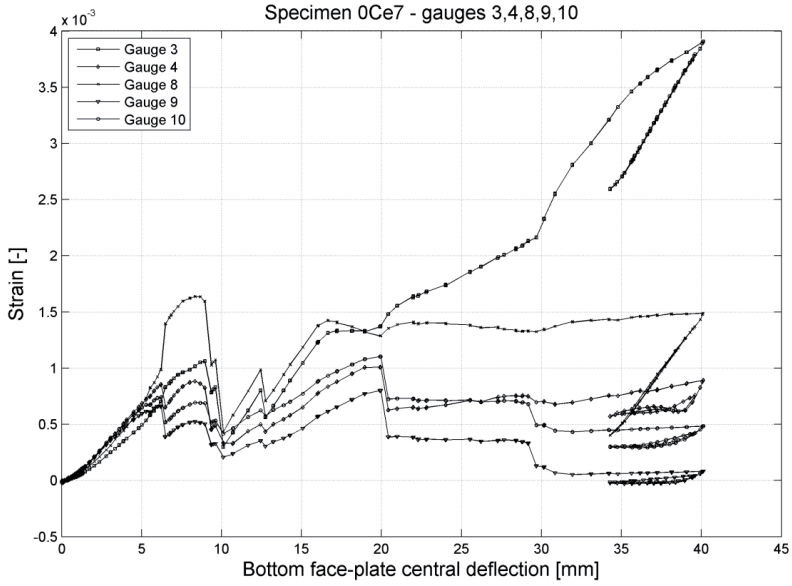

Figure 11-21. Strain measurements

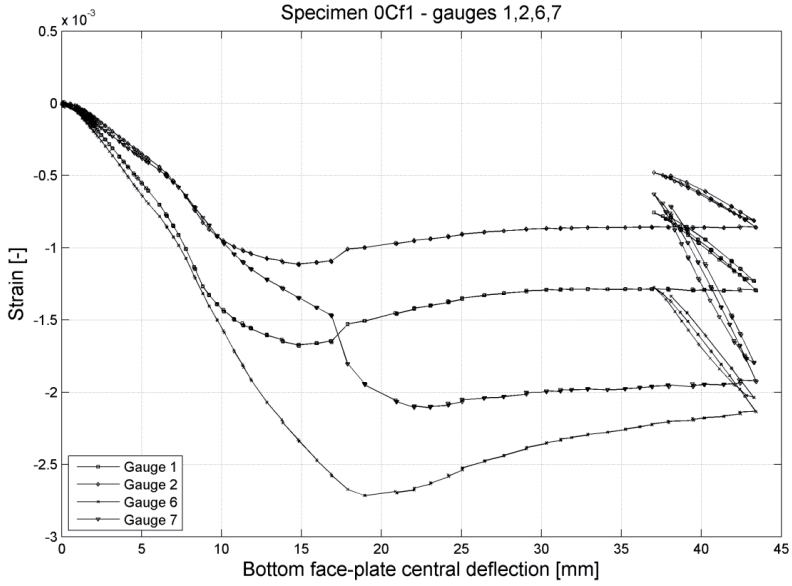

Figure 11-22. Strain measurements

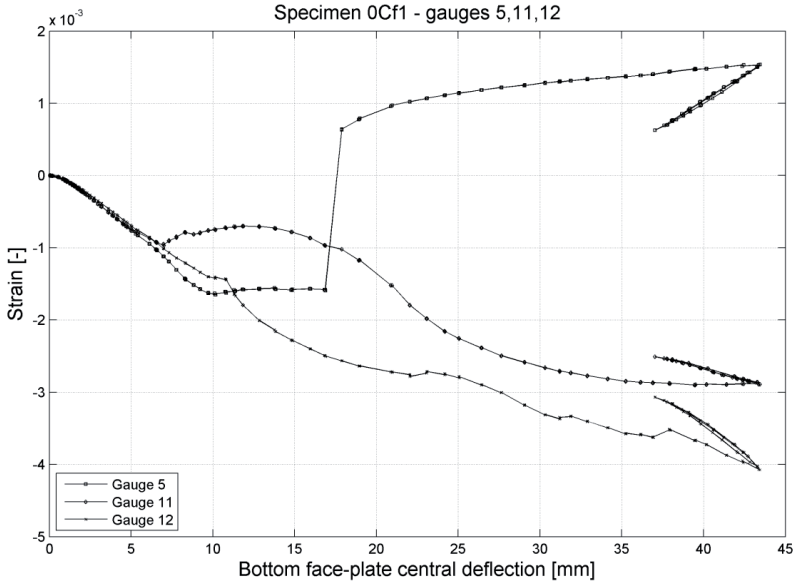

Figure 11-23. Strain measurements

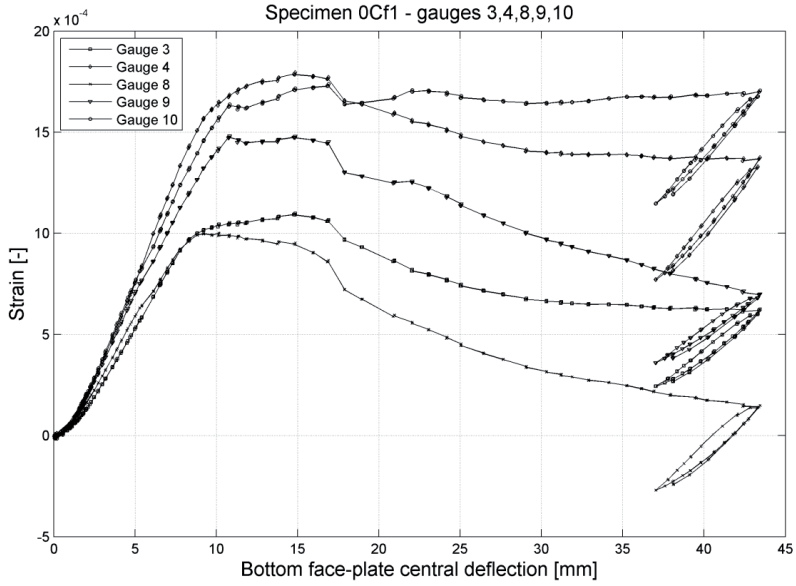

Figure 11-24. Strain measurements

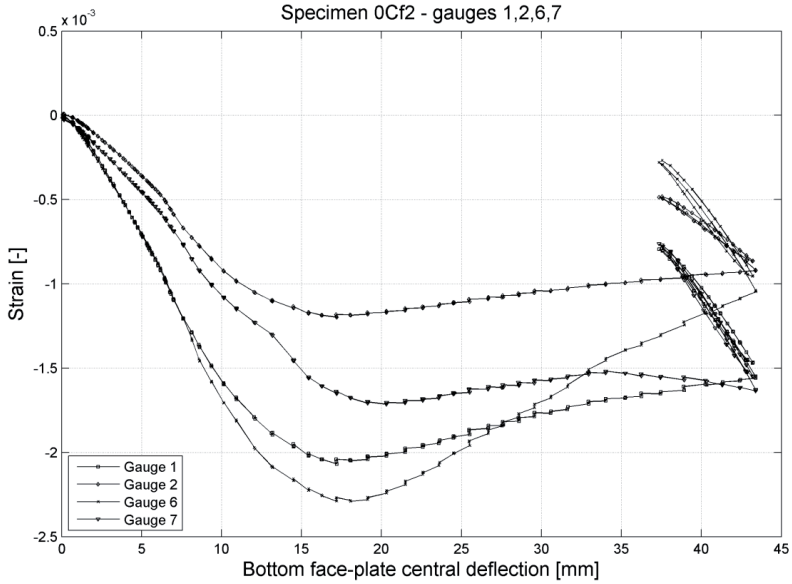

Figure 11-25. Strain measurements

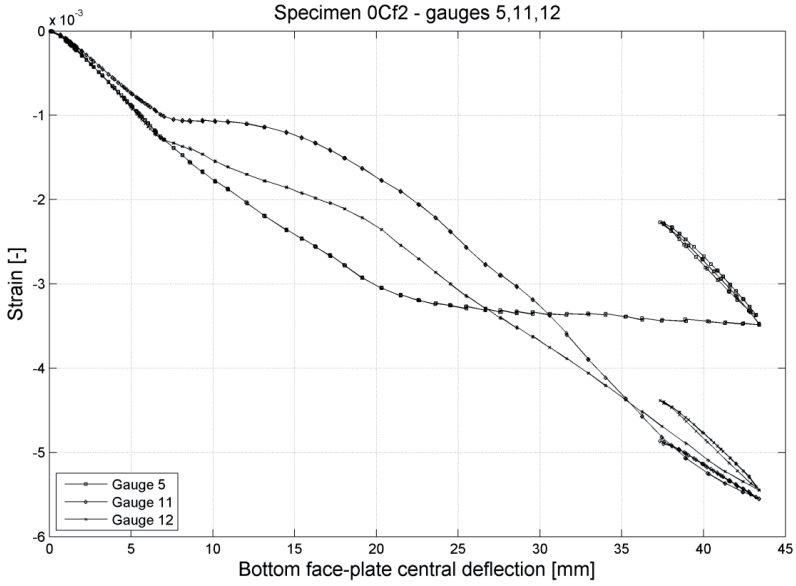

Figure 11-26. Strain measurements

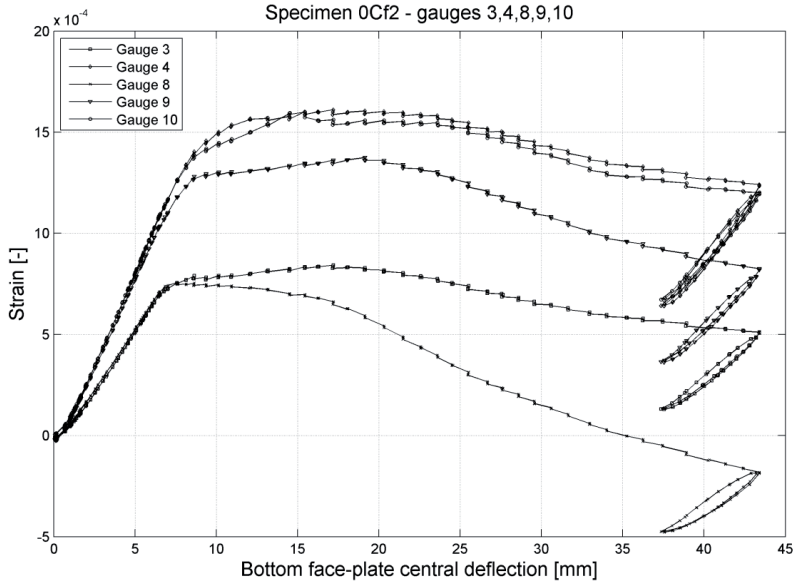

Figure 11-27. Strain measurements

12 Appendix C-C1 – Strain measurements from one-year corroded corrugated-core sandwich beams

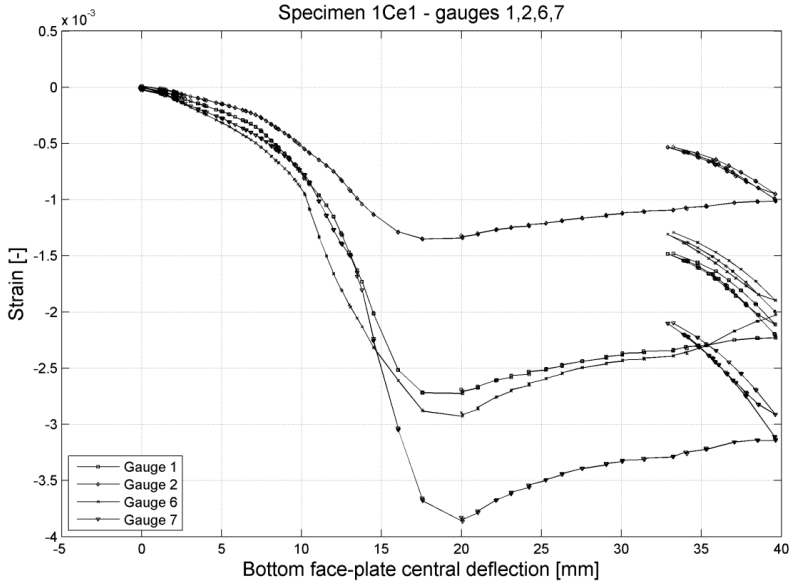

Figure 12-1. Strain measurements

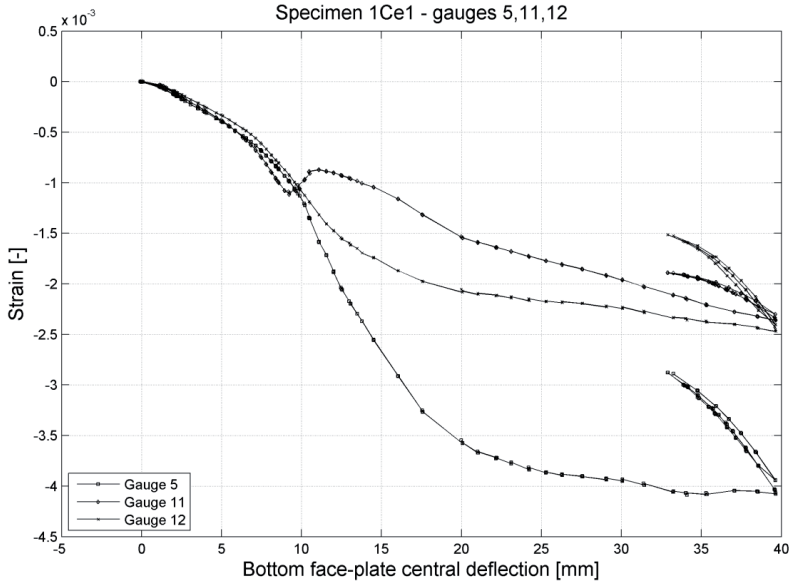

Figure 12-2. Strain measurements

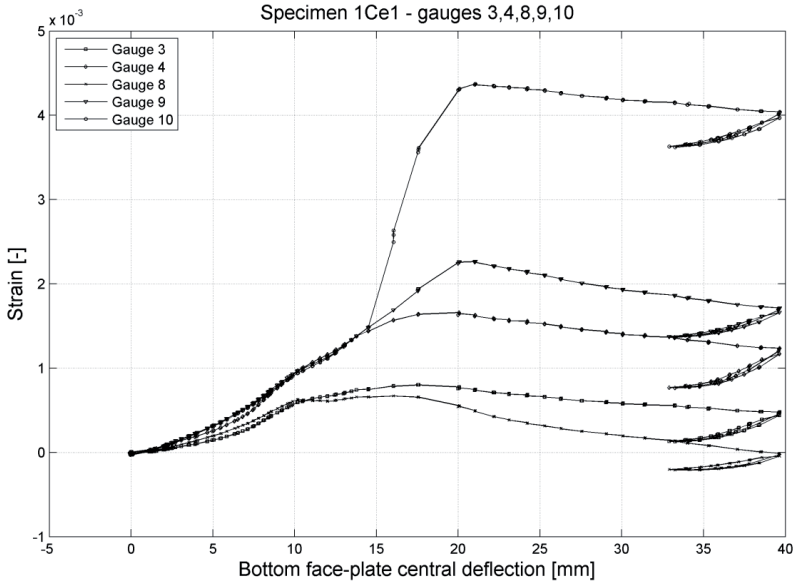

Figure 12-3. Strain measurements

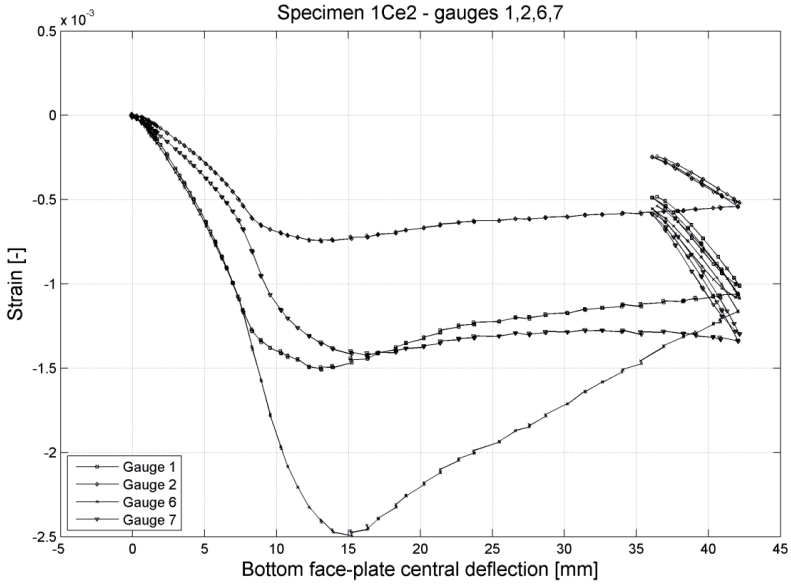

Figure 12-4. Strain measurements

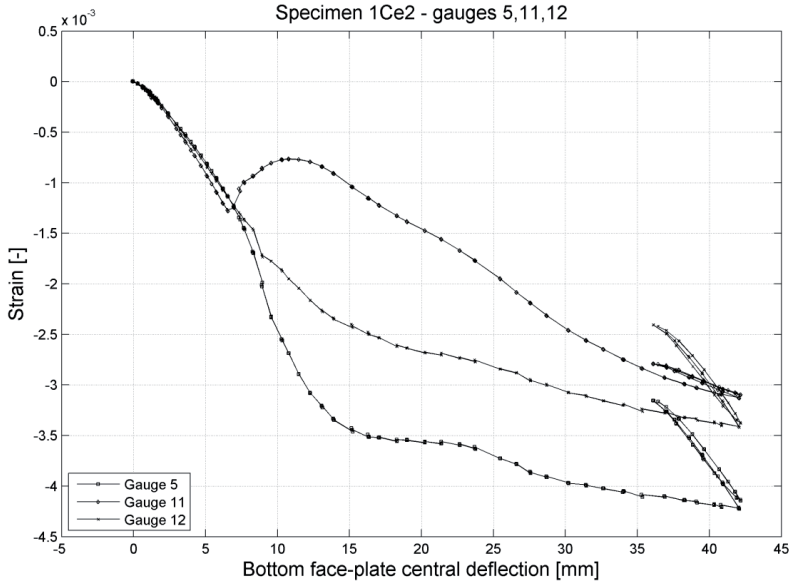

Figure 12-5. Strain measurements

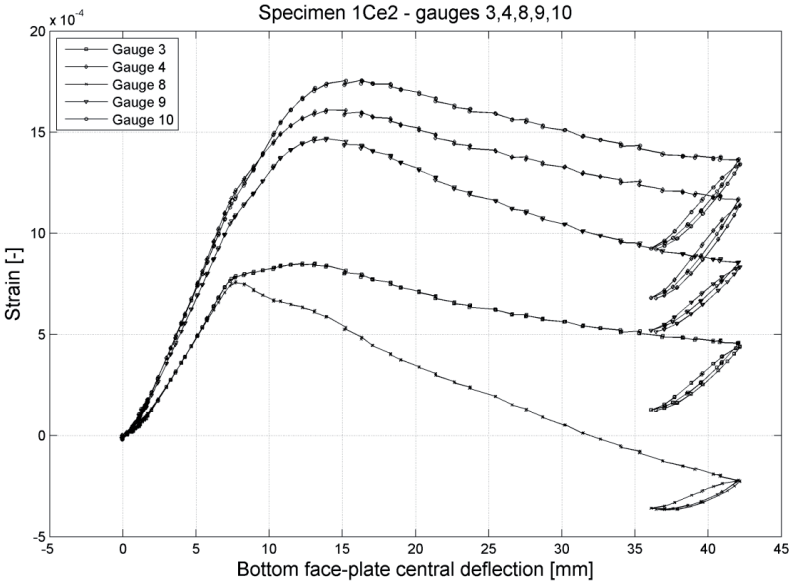

Figure 12-6. Strain measurements

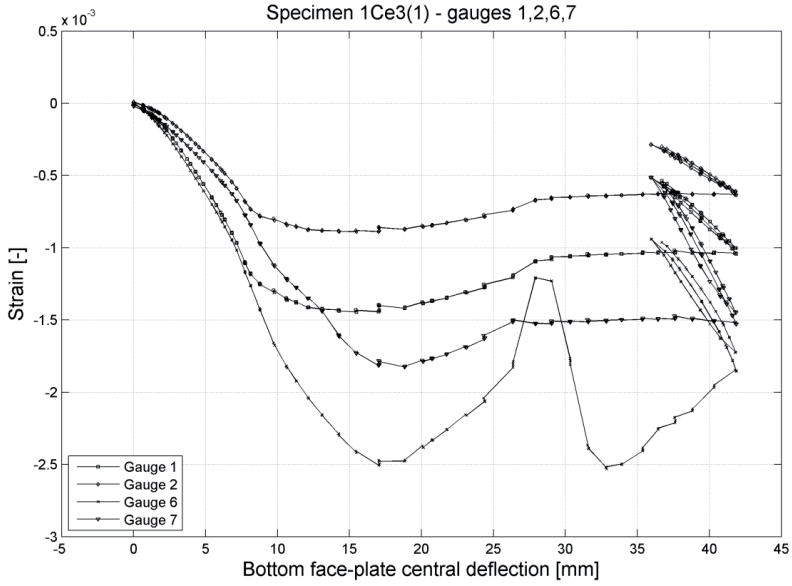

Figure 12-7. Strain measurements

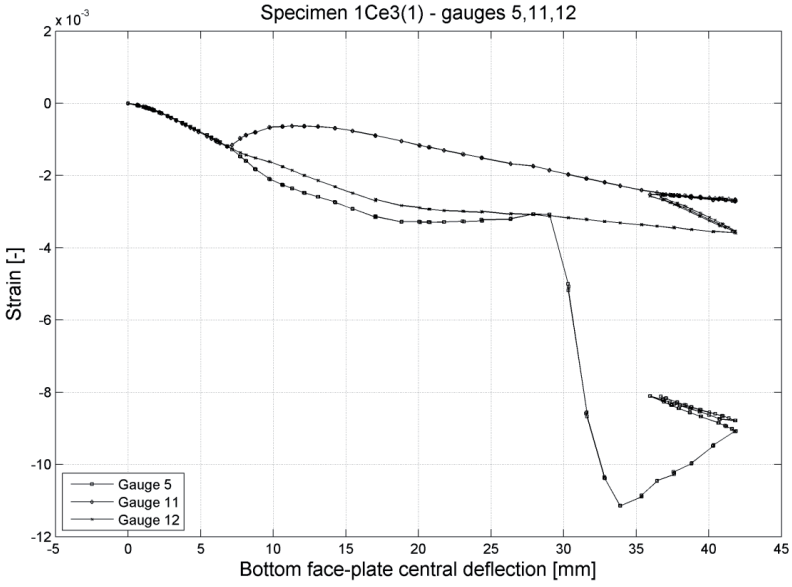

Figure 12-8. Strain measurements

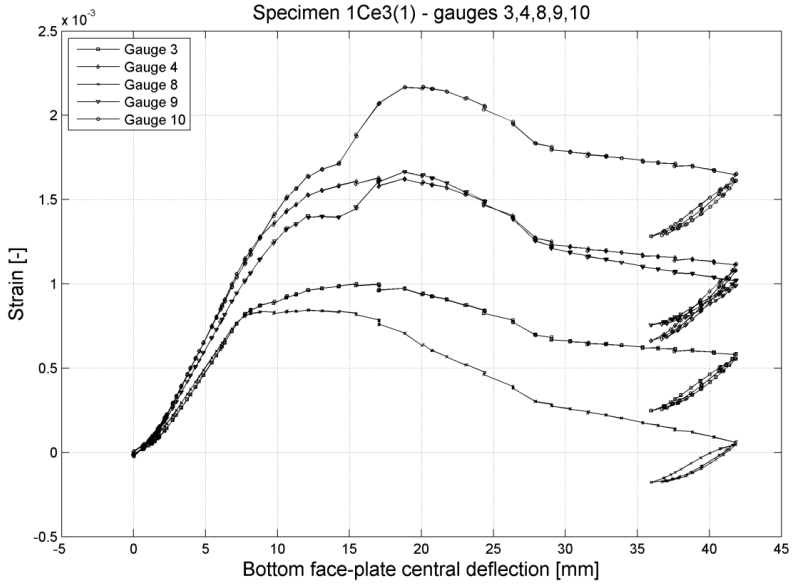

Figure 12-9. Strain measurements

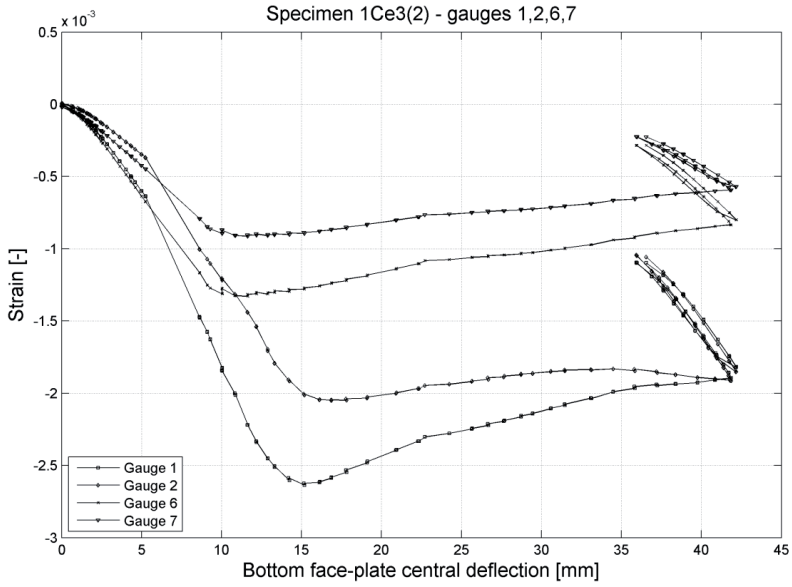

Figure 12-10. Strain measurements

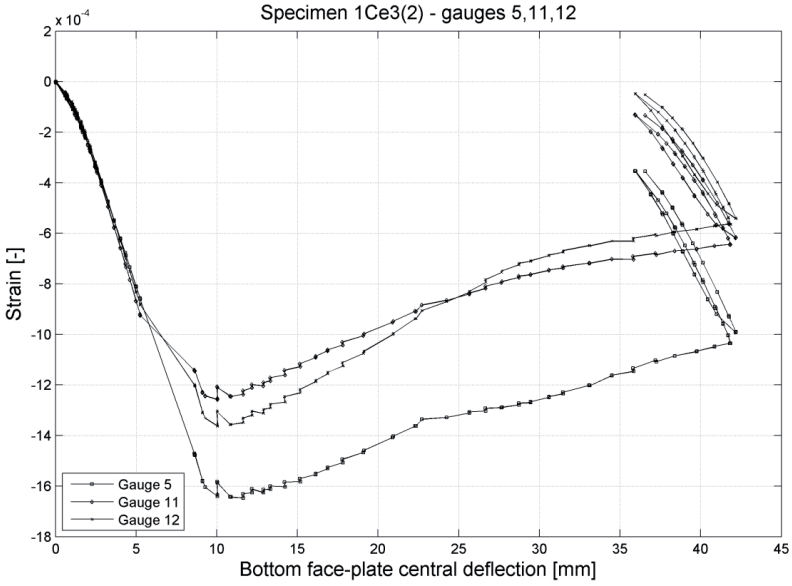

Figure 12-11. Strain measurements

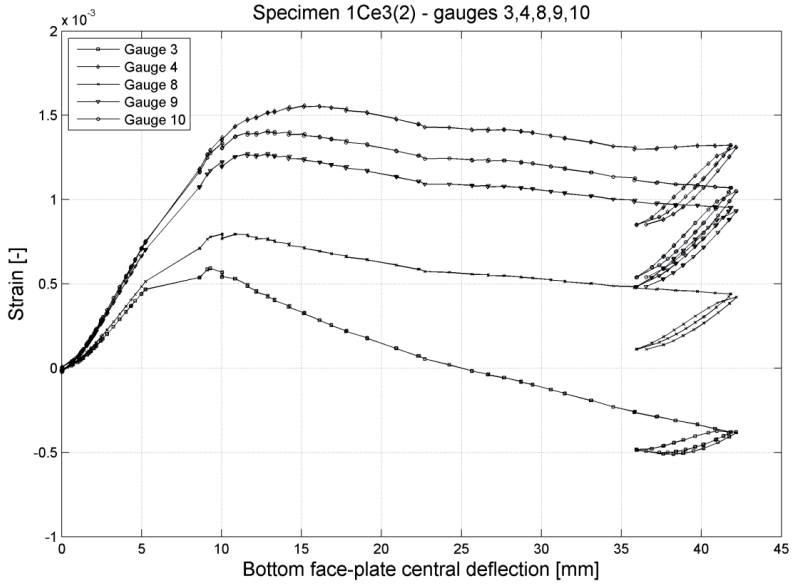

Figure 12-12. Strain measurements

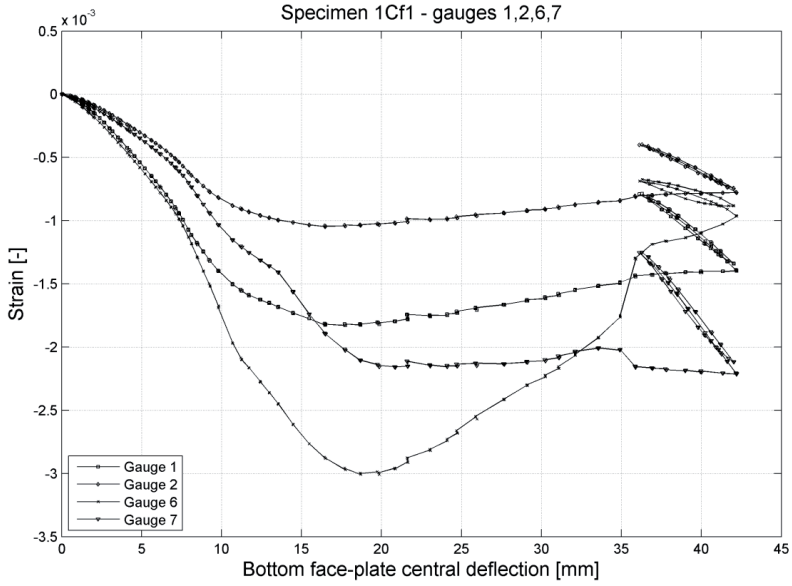

Figure 12-13. Strain measurements

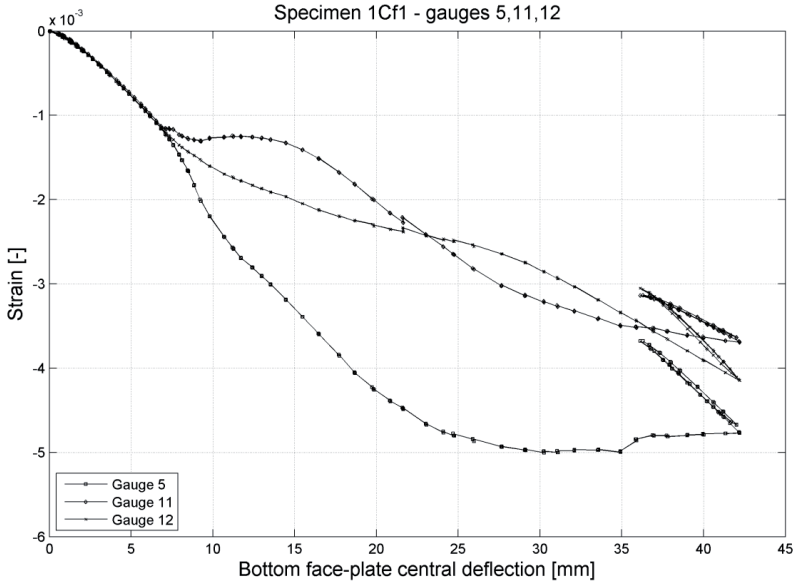

Figure 12-14. Strain measurements

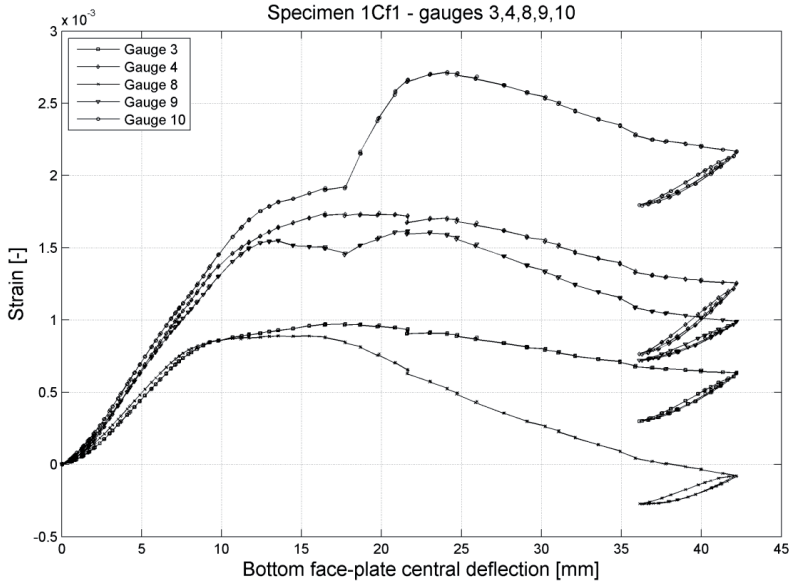

Figure 12-15. Strain measurements

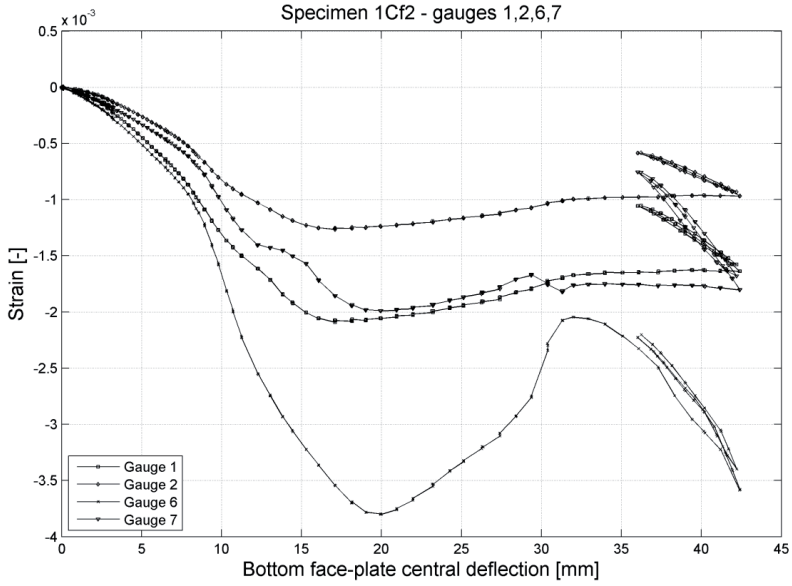

Figure 12-16. Strain measurements

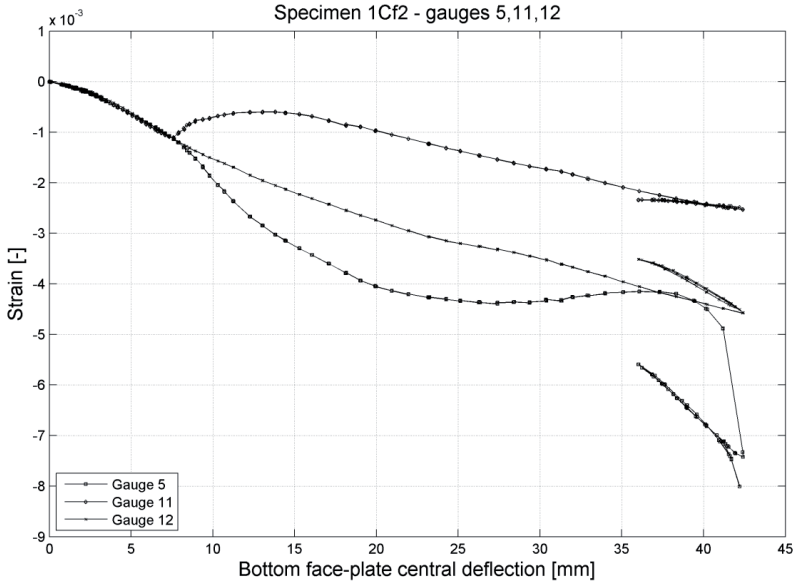

Figure 12-17. Strain measurements

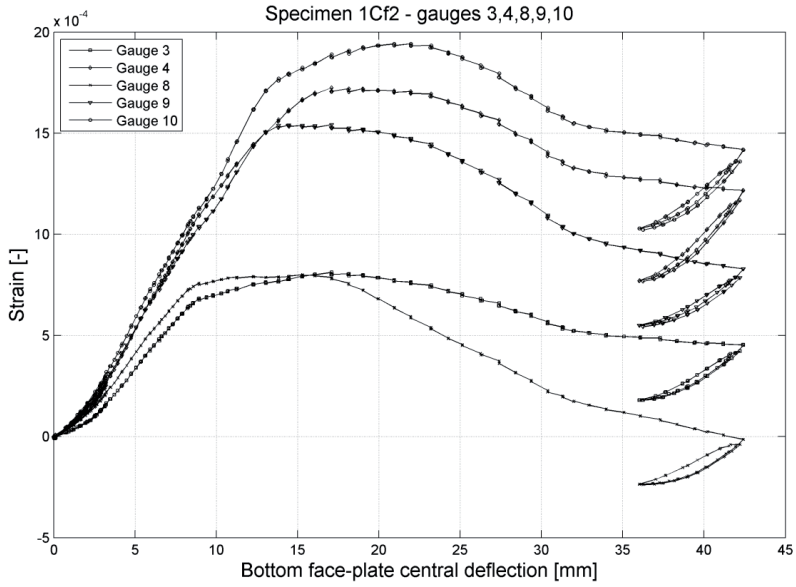

Figure 12-18. Strain measurements

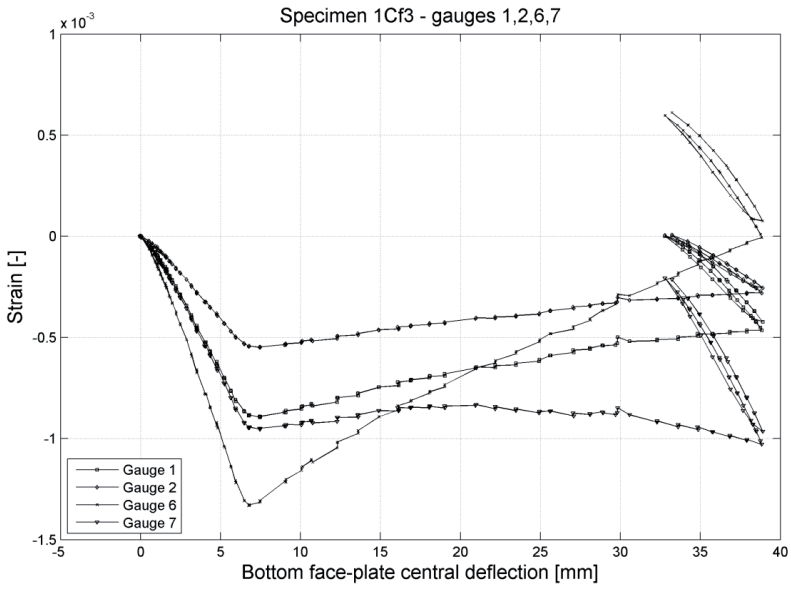

Figure 12-19. Strain measurements

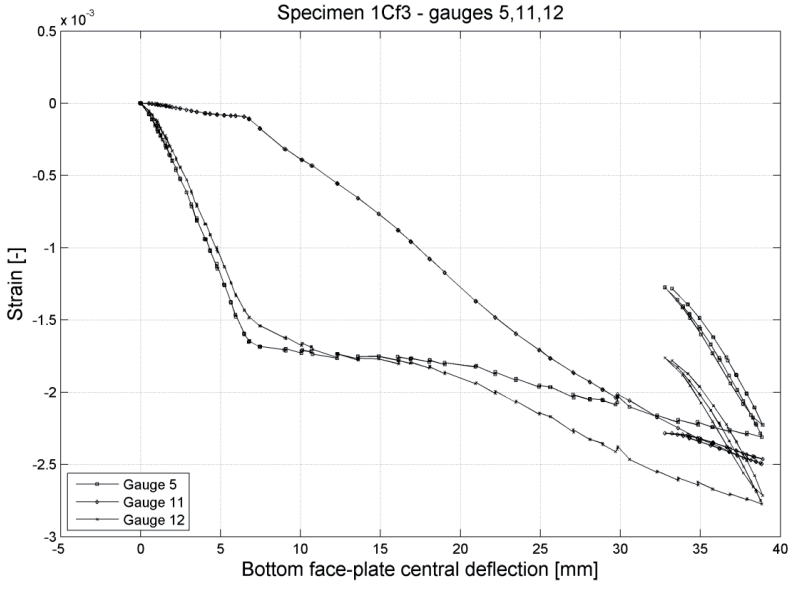

Figure 12-20. Strain measurements

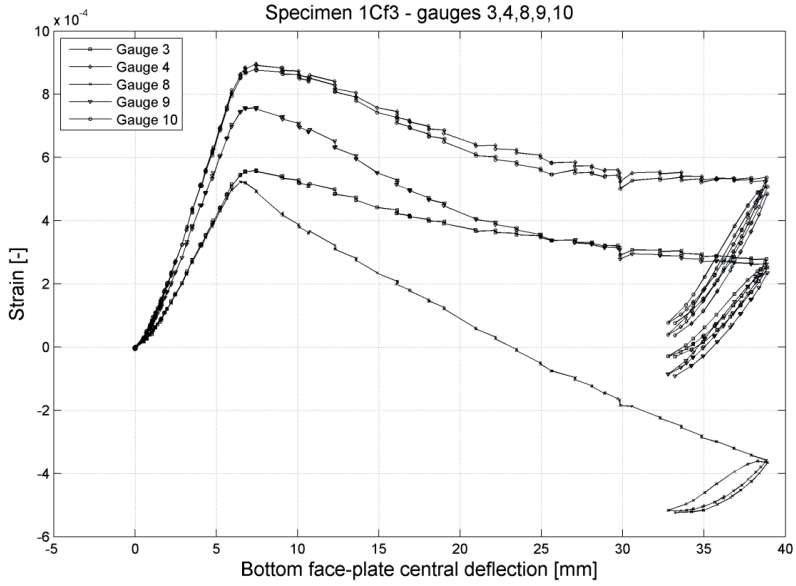

Figure 12-21. Strain measurements

13 Appendix C-C2 – Strain measurements from two-year corroded corrugated-core sandwich beams

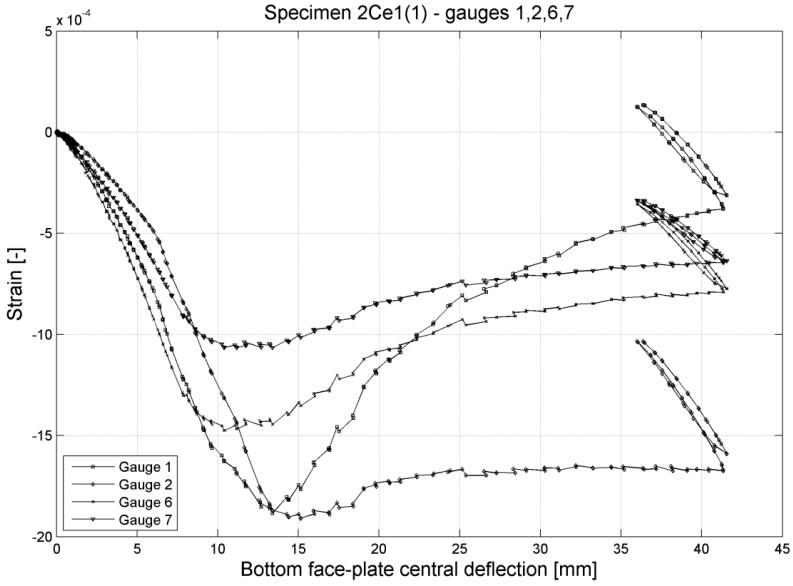

Figure 13-1. Strain measurements

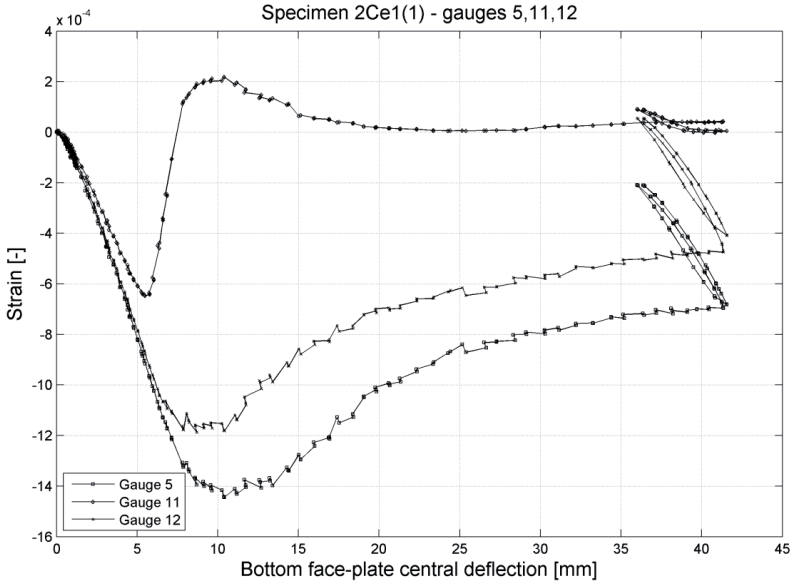

Figure 13-2. Strain measurements

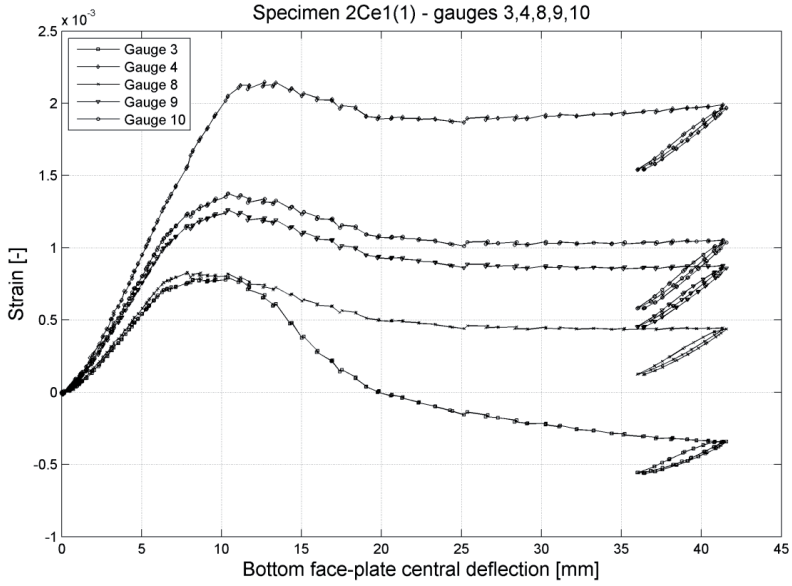

Figure 13-3. Strain measurements

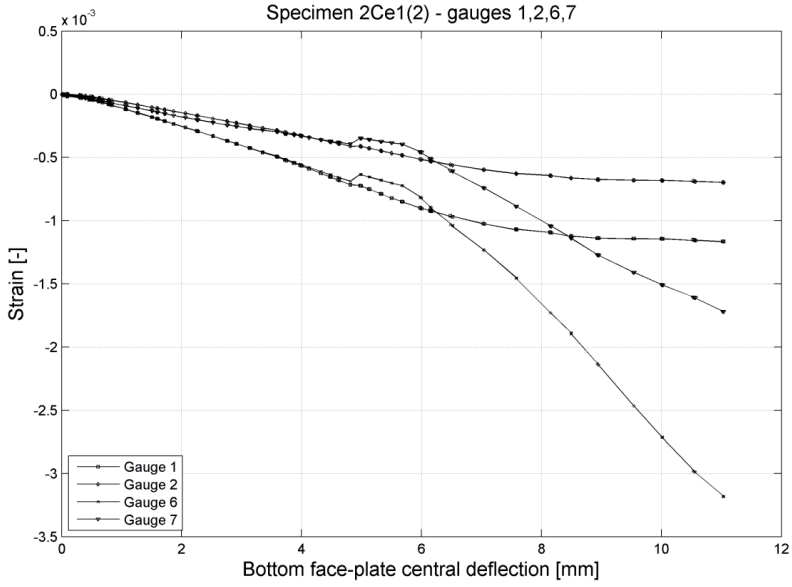

Figure 13-4. Strain measurements

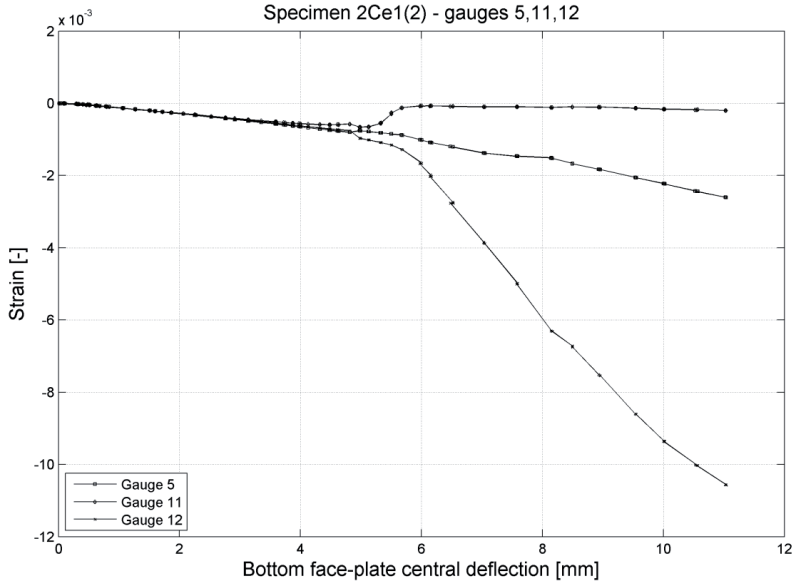

Figure 13-5. Strain measurements

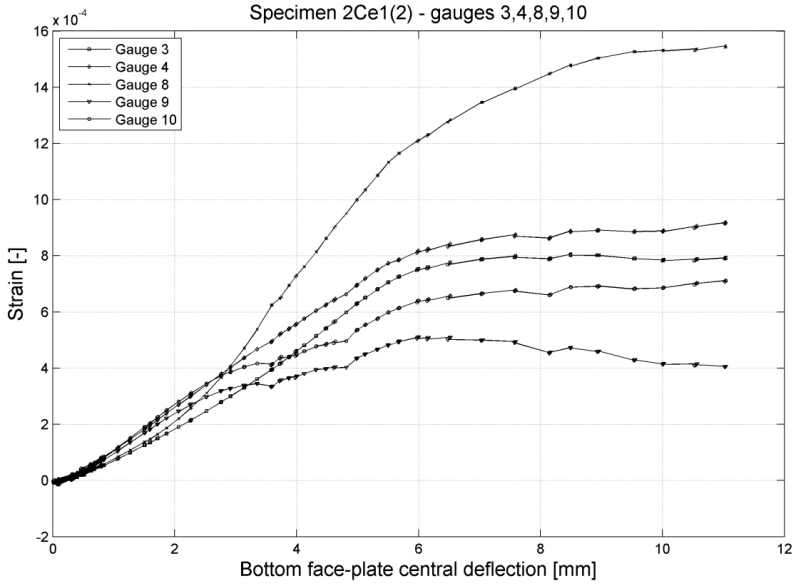

Figure 13-6. Strain measurements

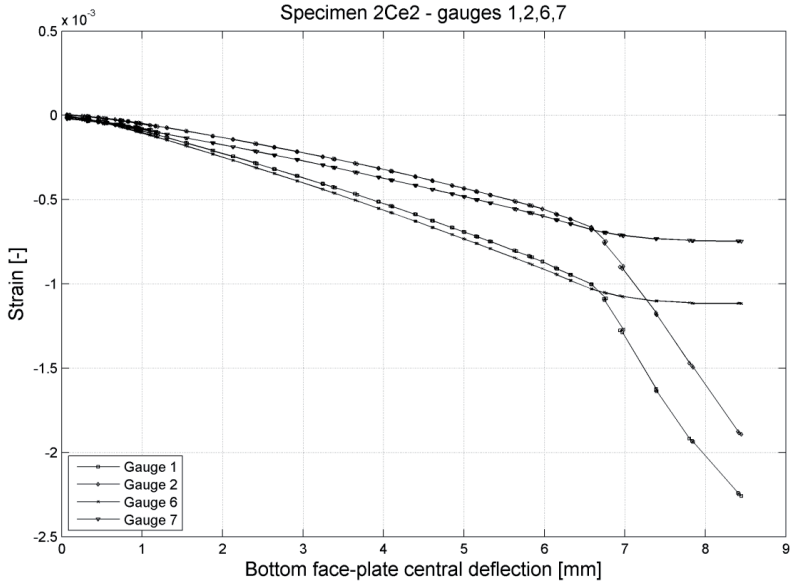

Figure 13-7. Strain measurements

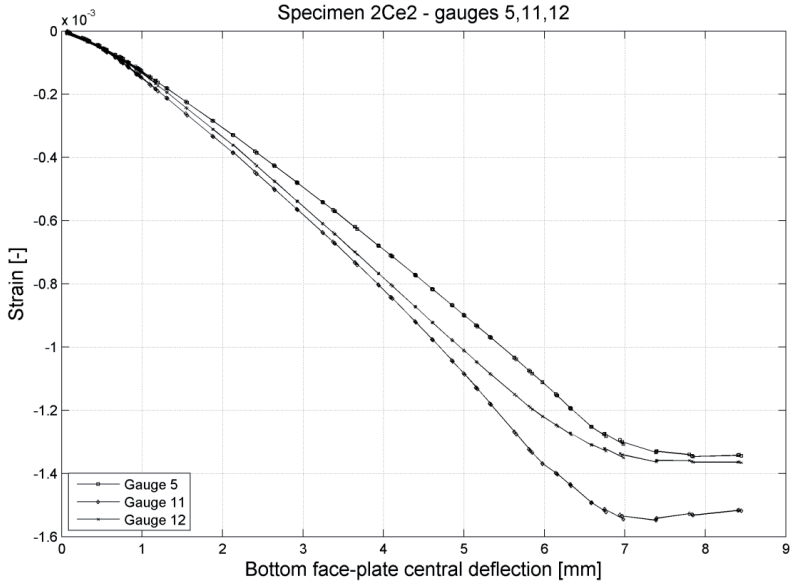

Figure 13-8. Strain measurements

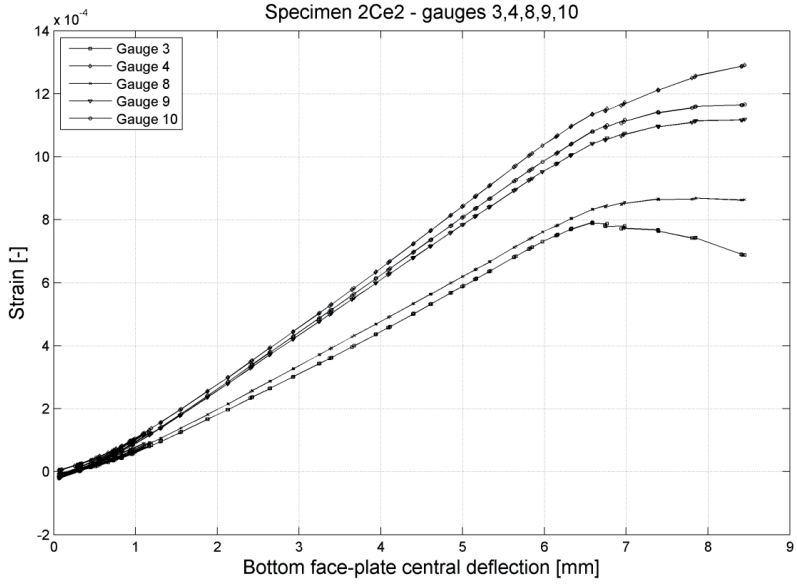

Figure 13-9. Strain measurements

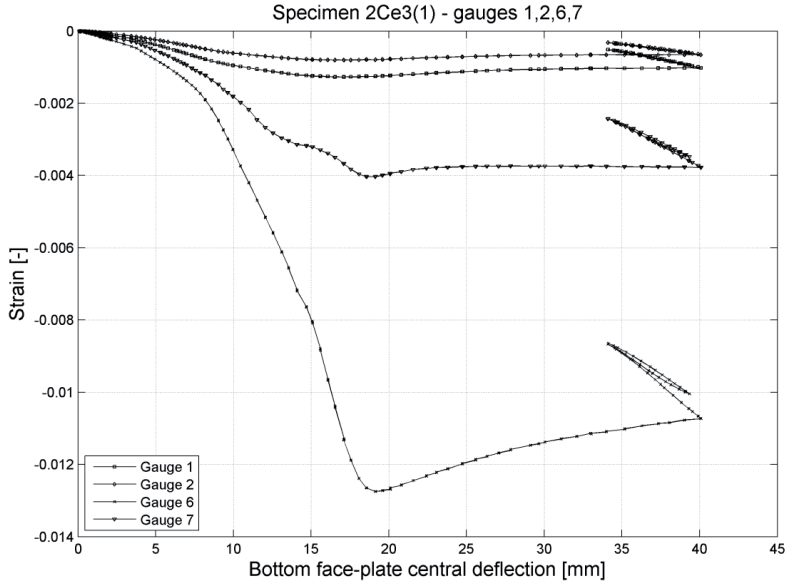

Figure 13-10. Strain measurements

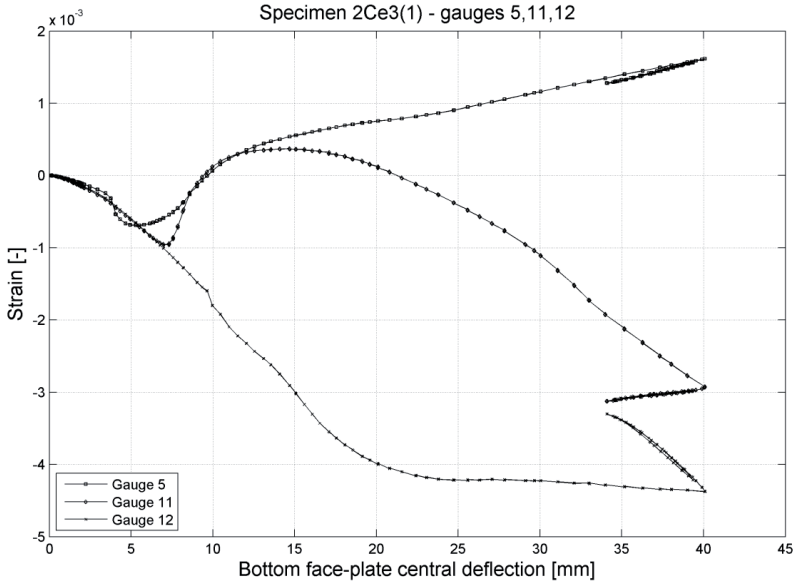

Figure 13-11. Strain measurements

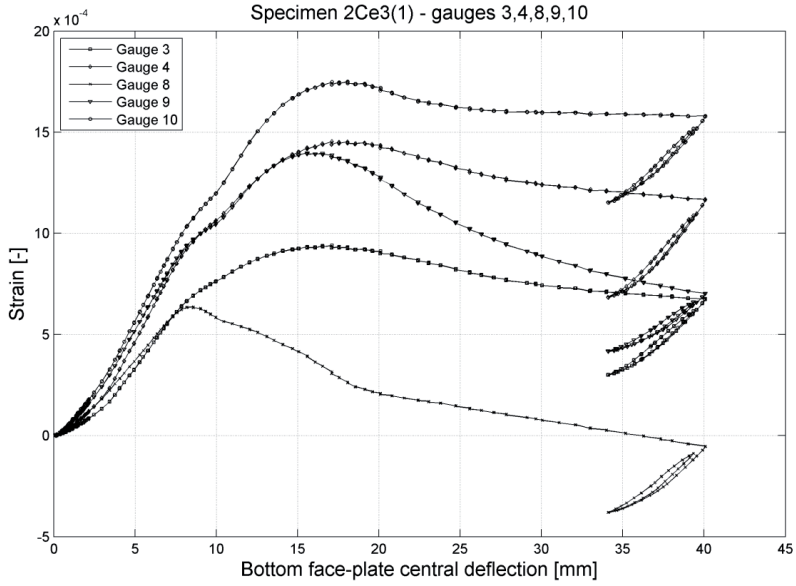

Figure 13-12. Strain measurements

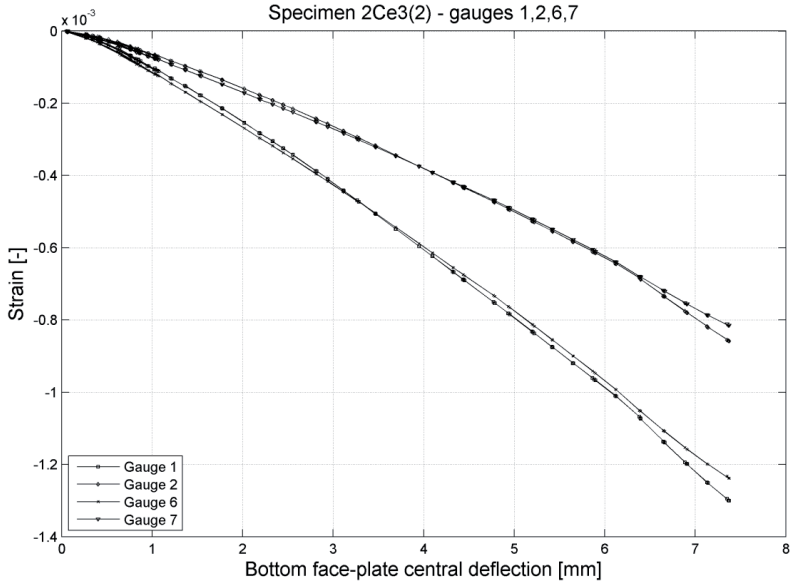

Figure 13-13. Strain measurements

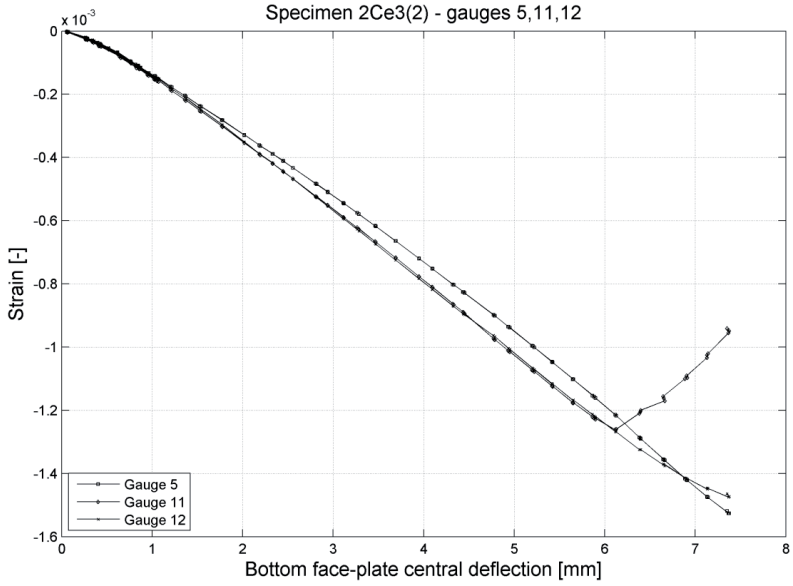

Figure 13-14. Strain measurements

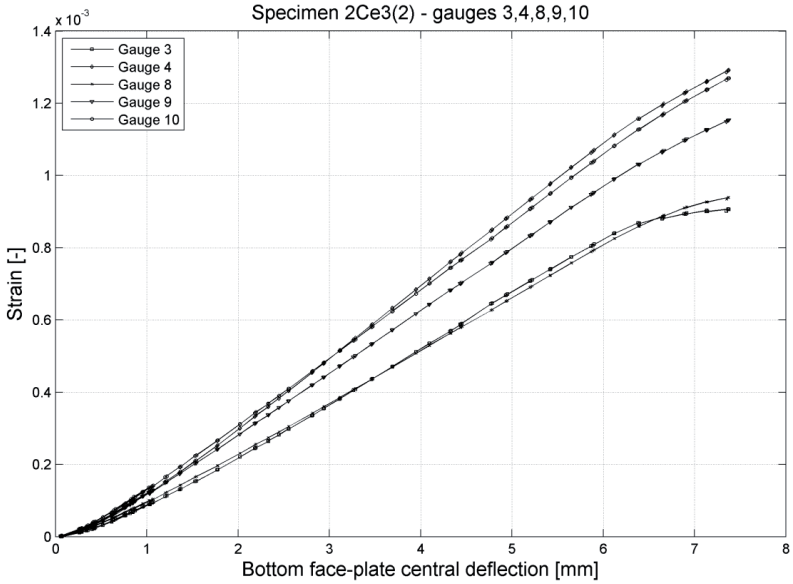

Figure 13-15. Strain measurements

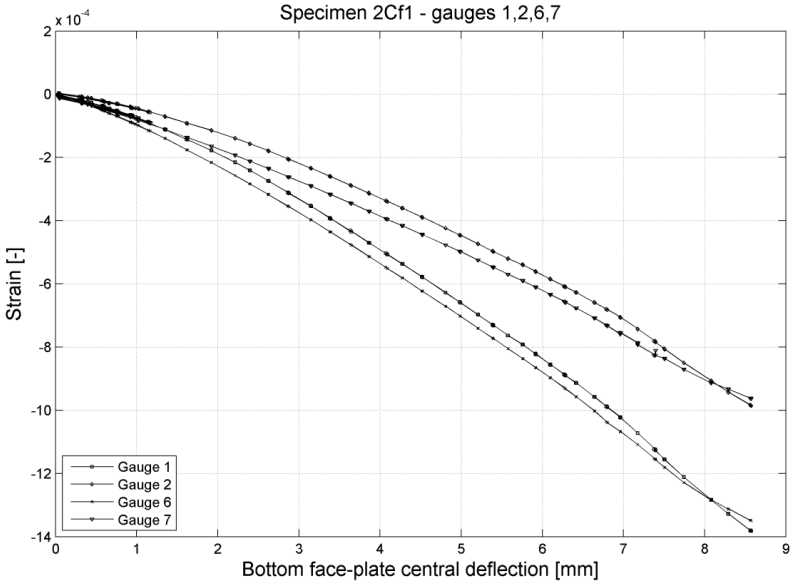

Figure 13-16. Strain measurements

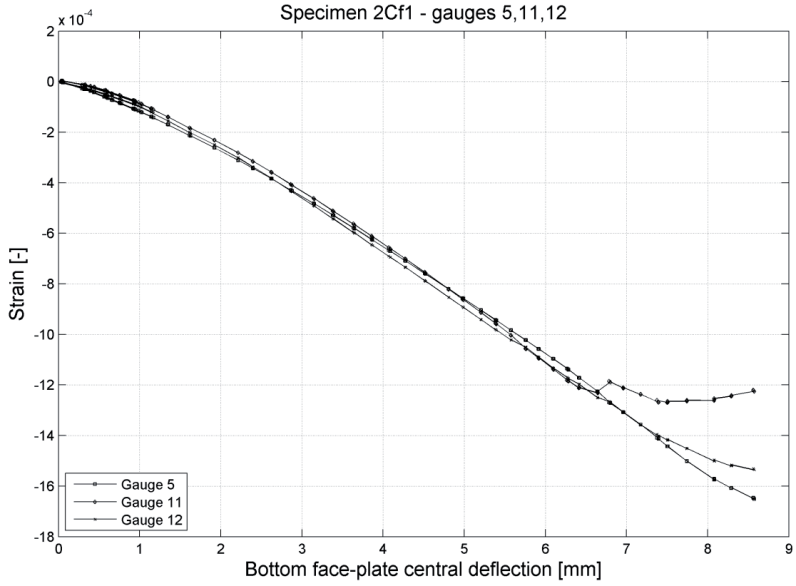

Figure 13-17. Strain measurements

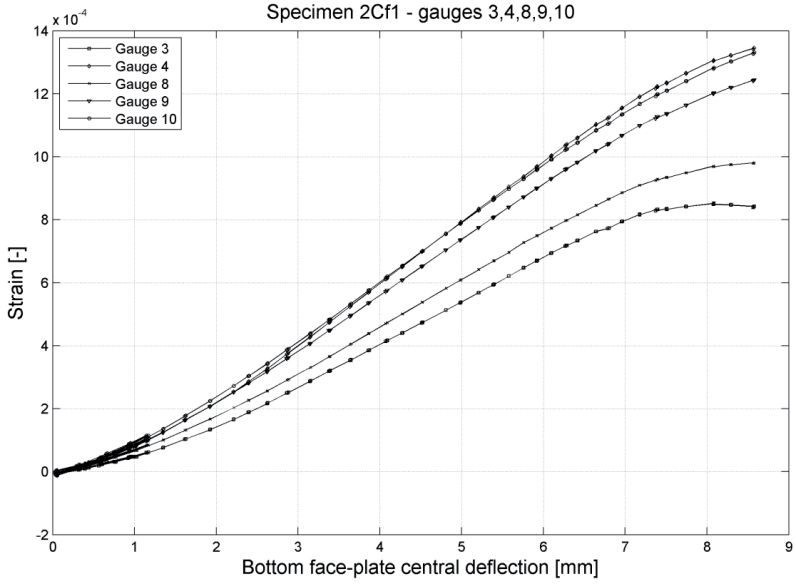

Figure 13-18. Strain measurements

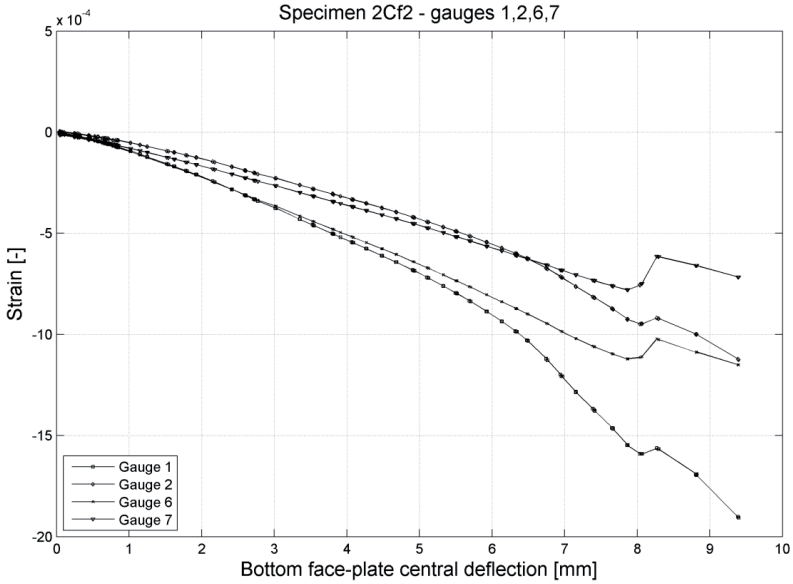

Figure 13-19. Strain measurements

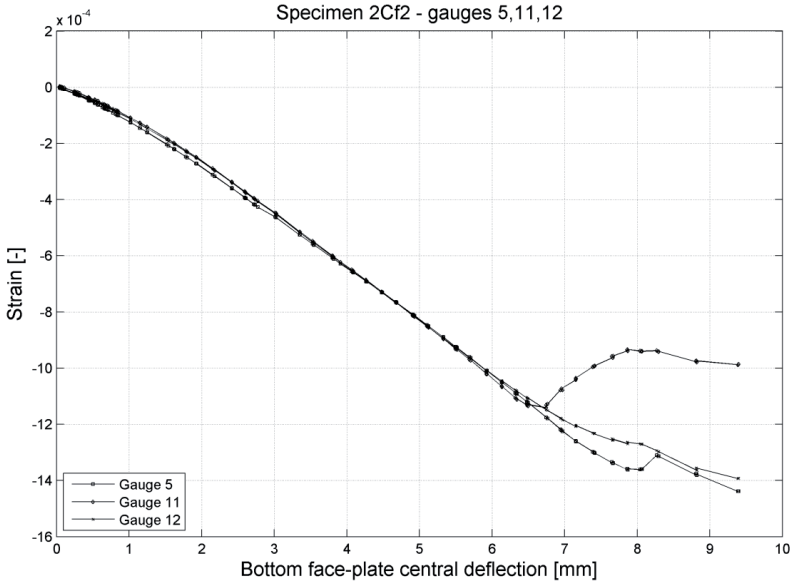

Figure 13-20. Strain measurements

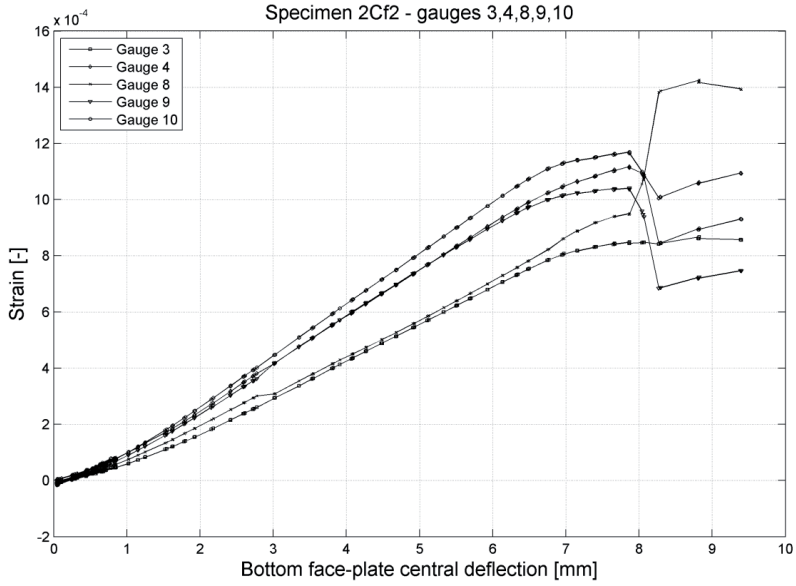

Figure 13-21. Strain measurements

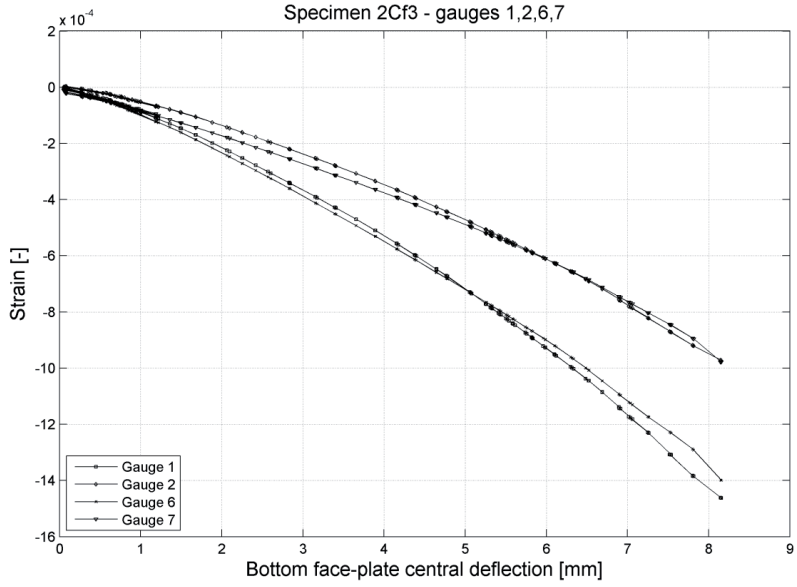

Figure 13-22. Strain measurements

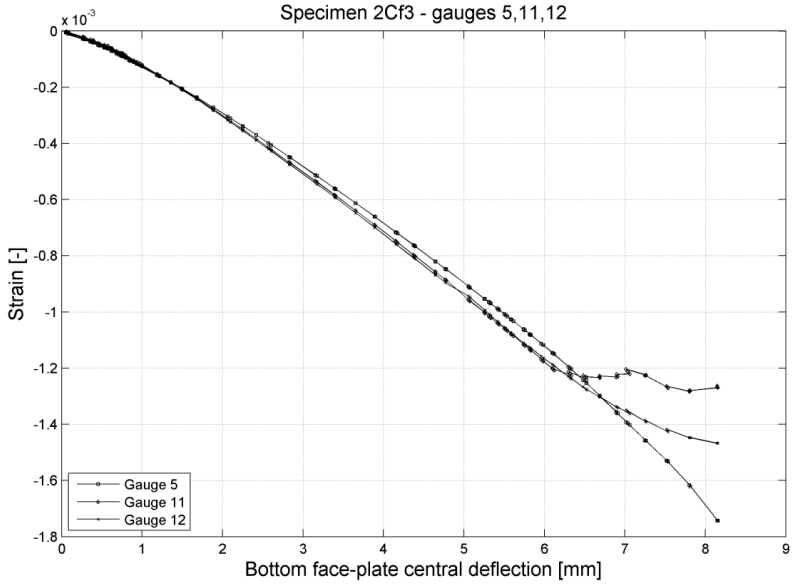

Figure 13-23. Strain measurements

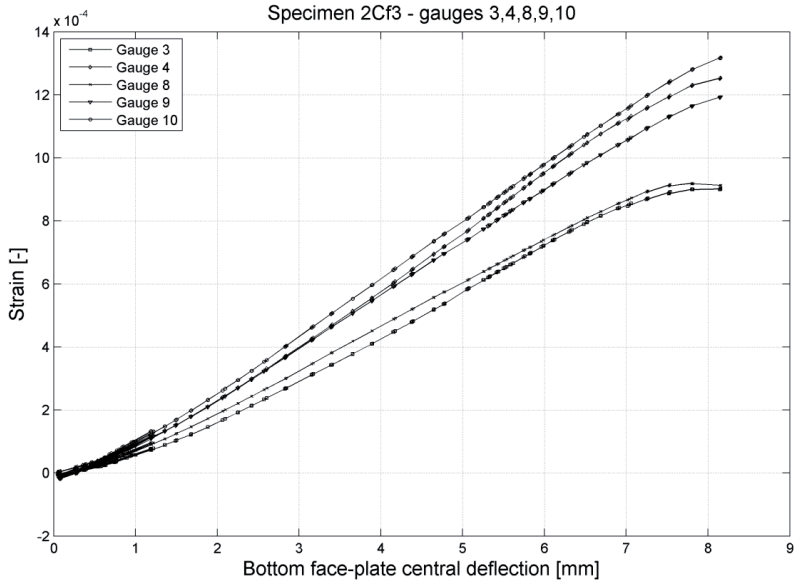

Figure 13-24. Strain measurements

14 Appendix D – Stiffness of the sandwich beams

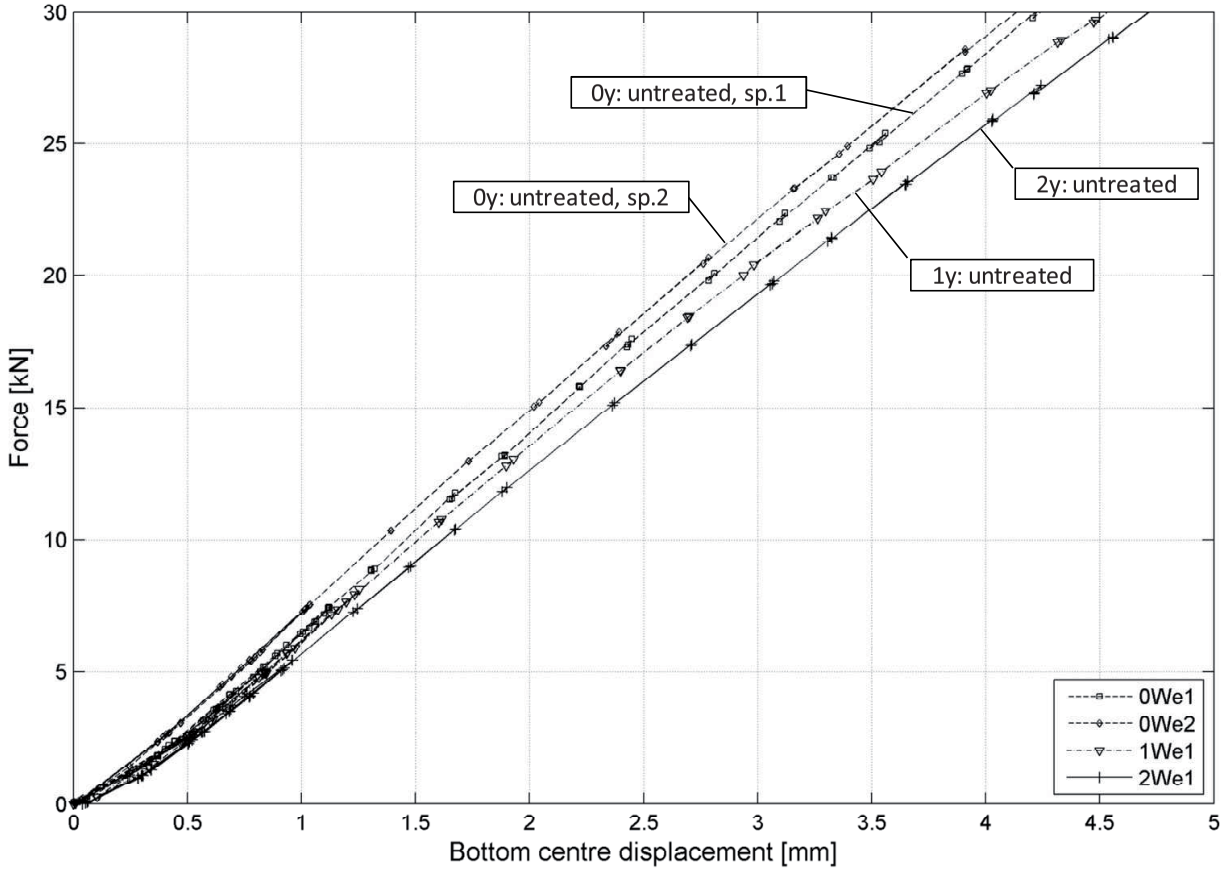

14-1. Stiffness of the web-core beams.

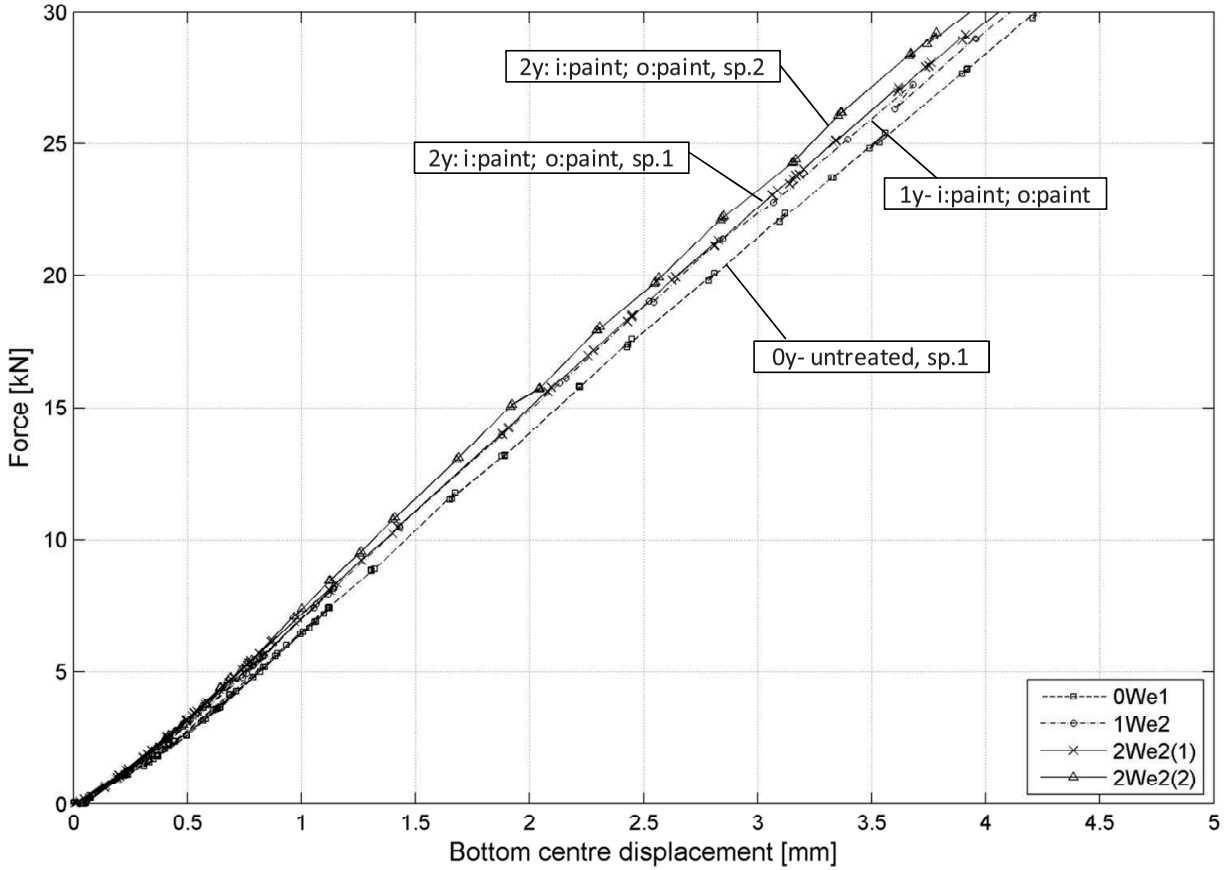

Figure 14-2. Stiffness of the web-core beams.

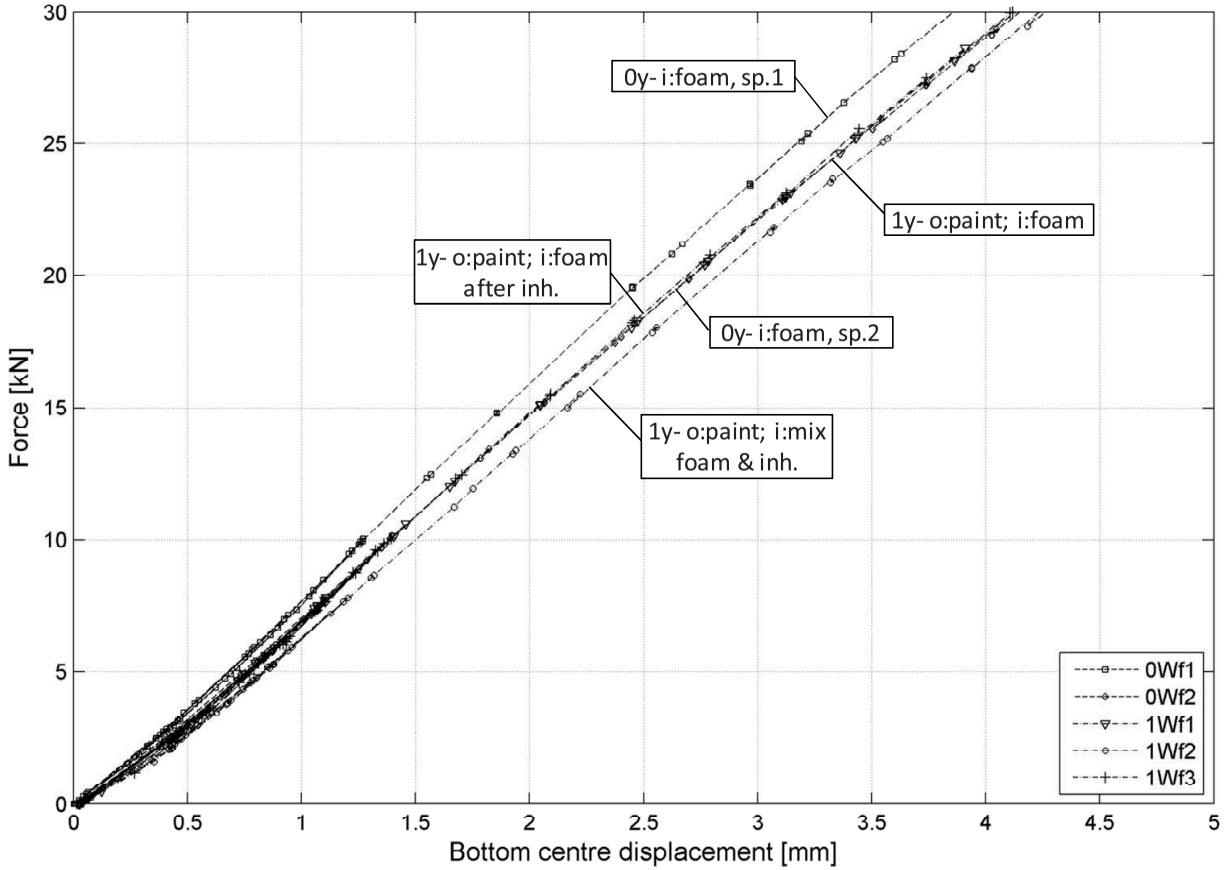

Figure 14-3. Stiffness of the web-core beams.

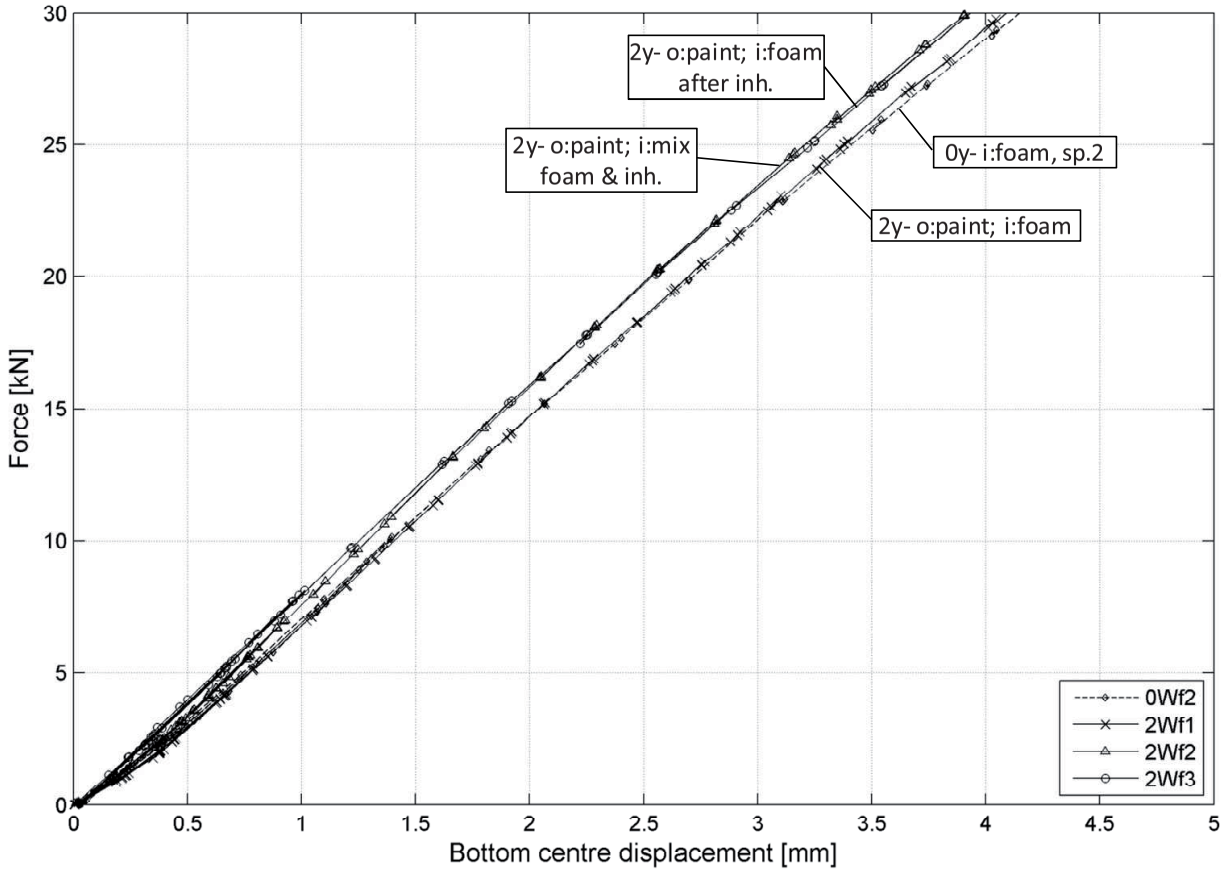

Figure 14-4. Stiffness of the web-core beams.

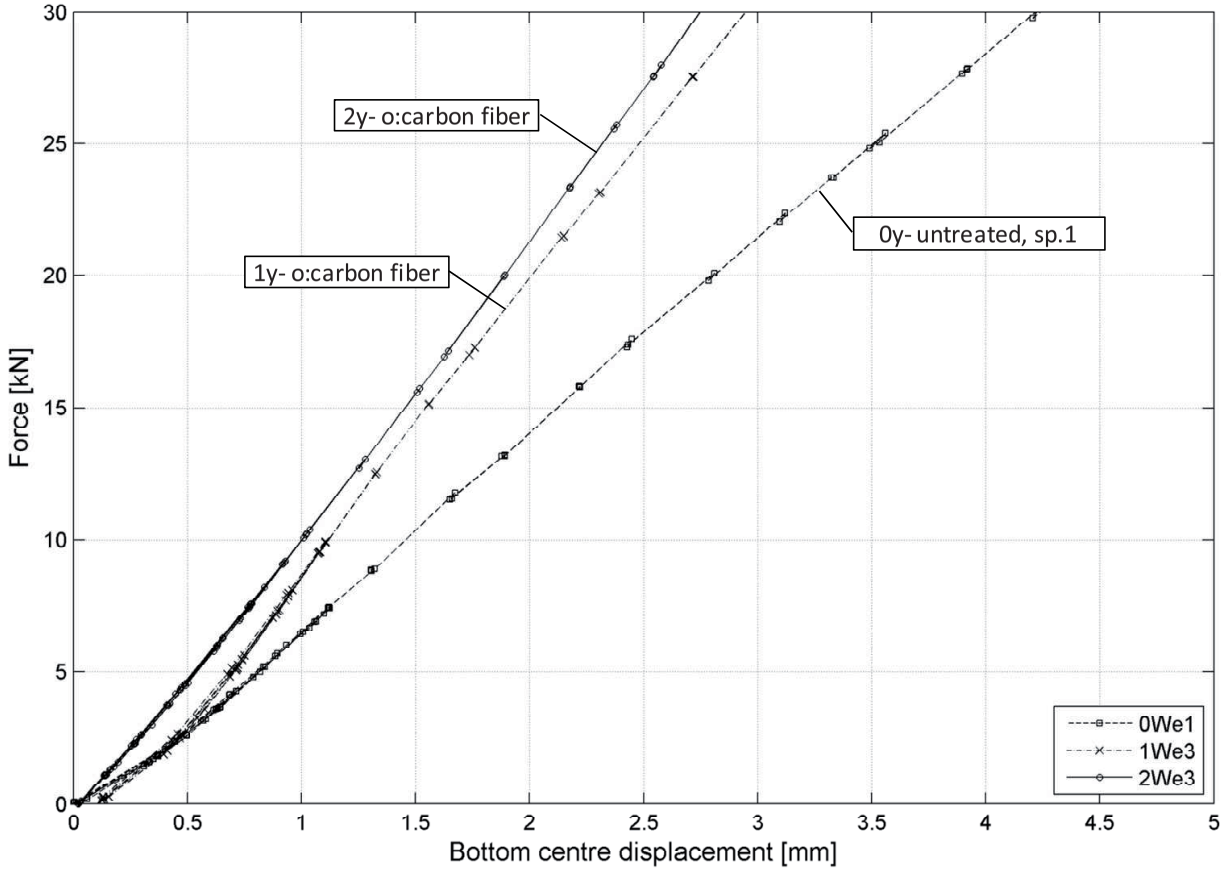

Figure 14-5. Stiffness of the web-core beams.

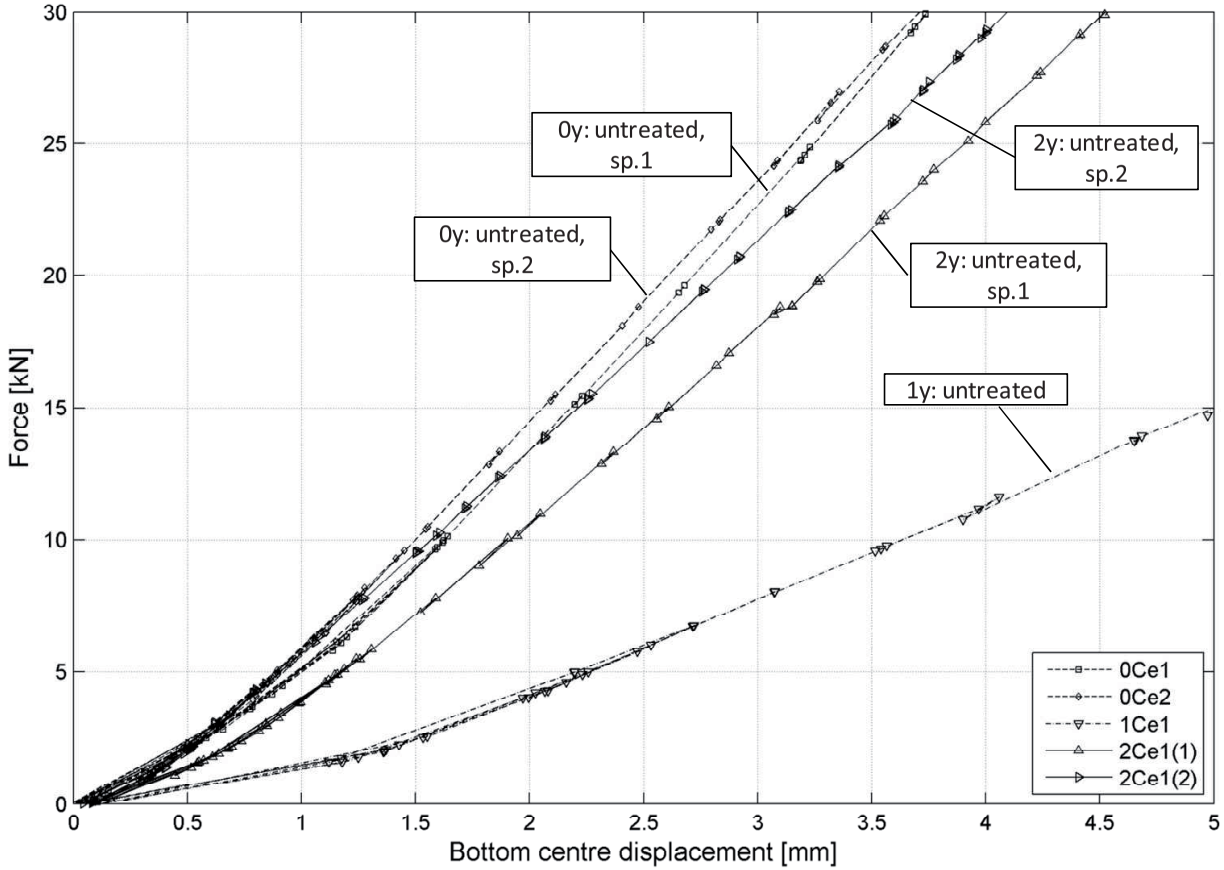

Figure 14-6. Stiffness of the corrugated-core beams.

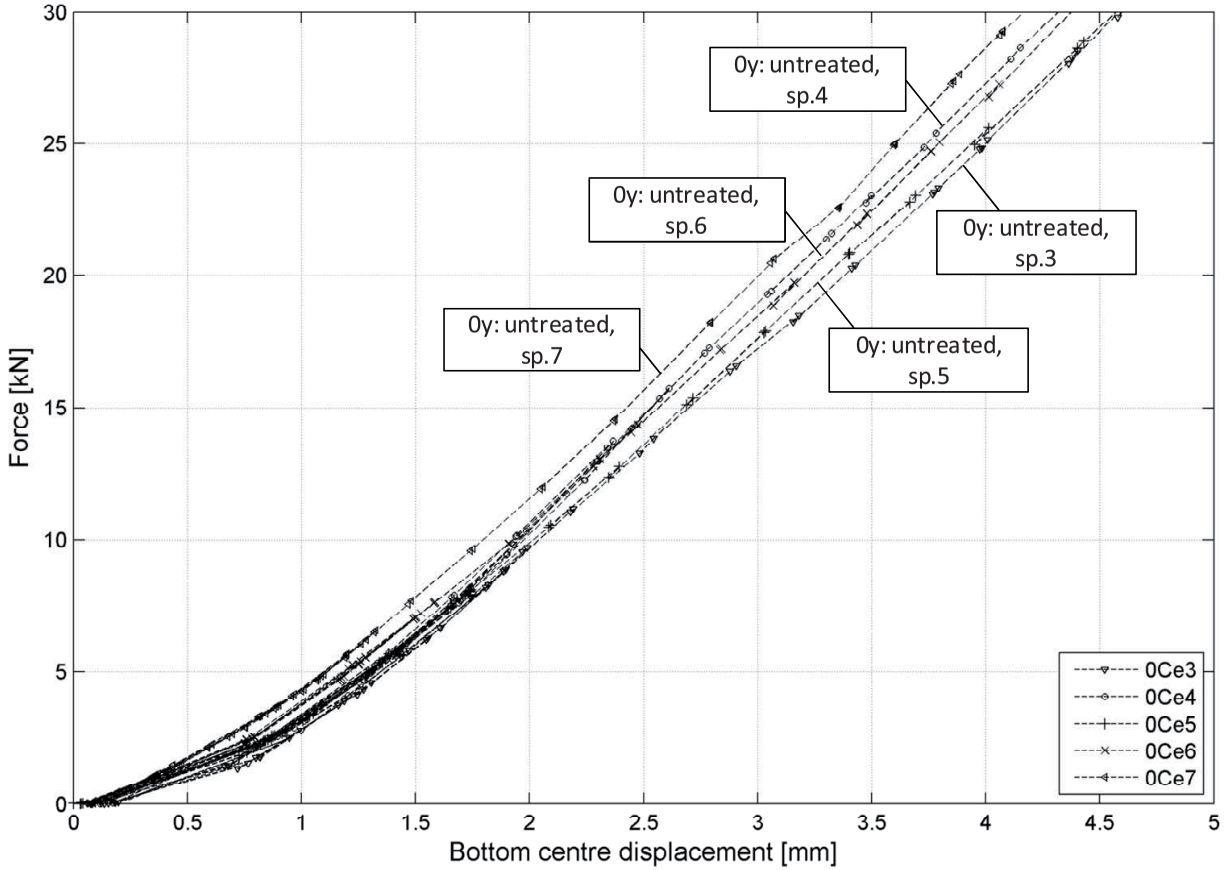

Figure 14-7. Stiffness of the corrugated-core beams.

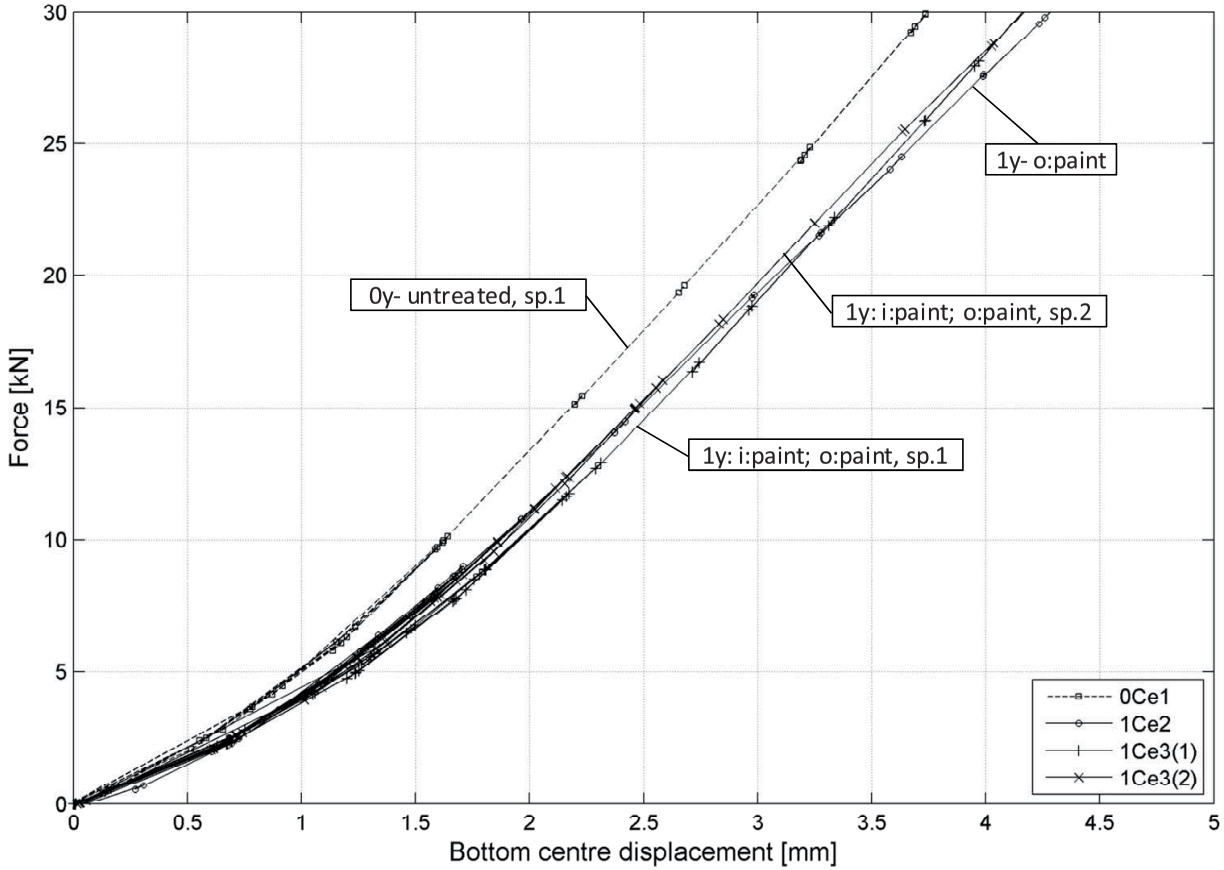

Figure 14-8. Stiffness of the corrugated-core beams.

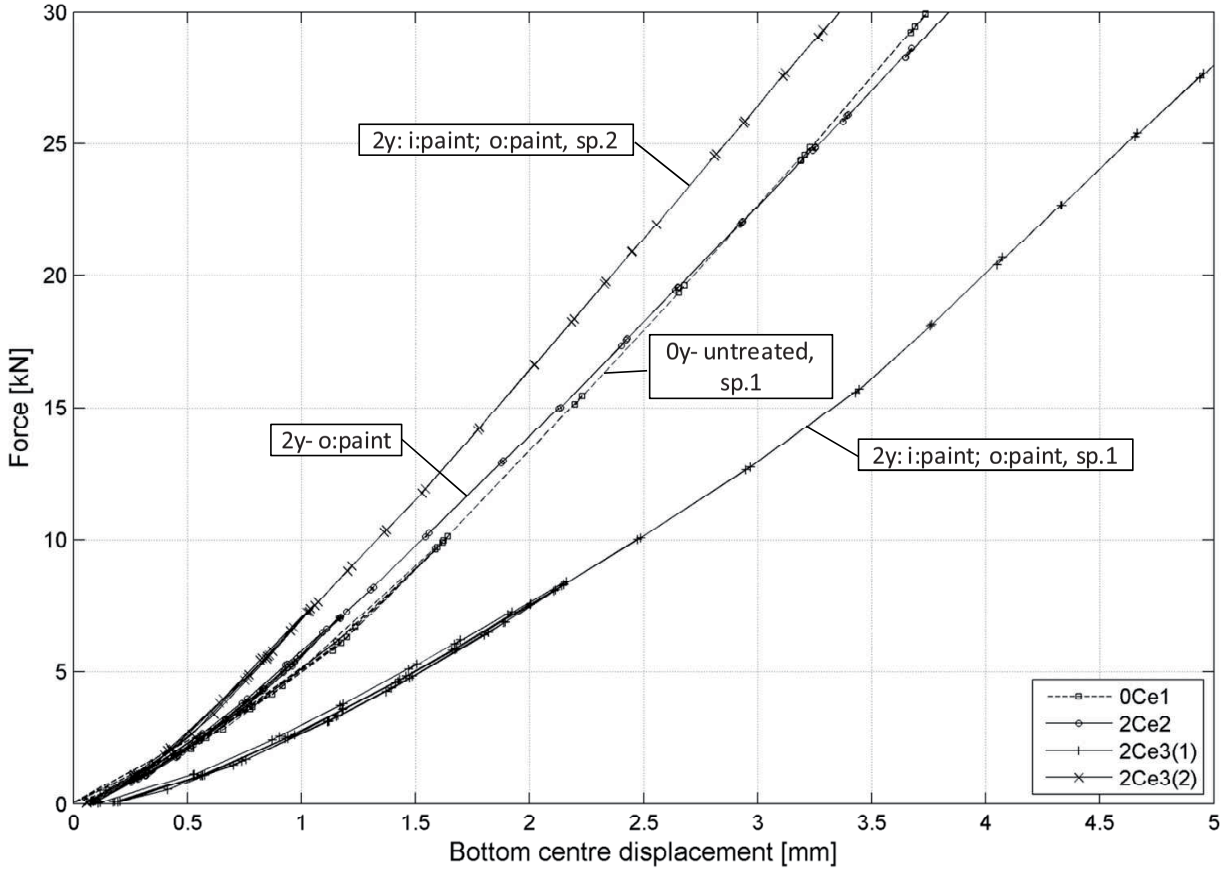

Figure 14-9. Stiffness of the corrugated-core beams.

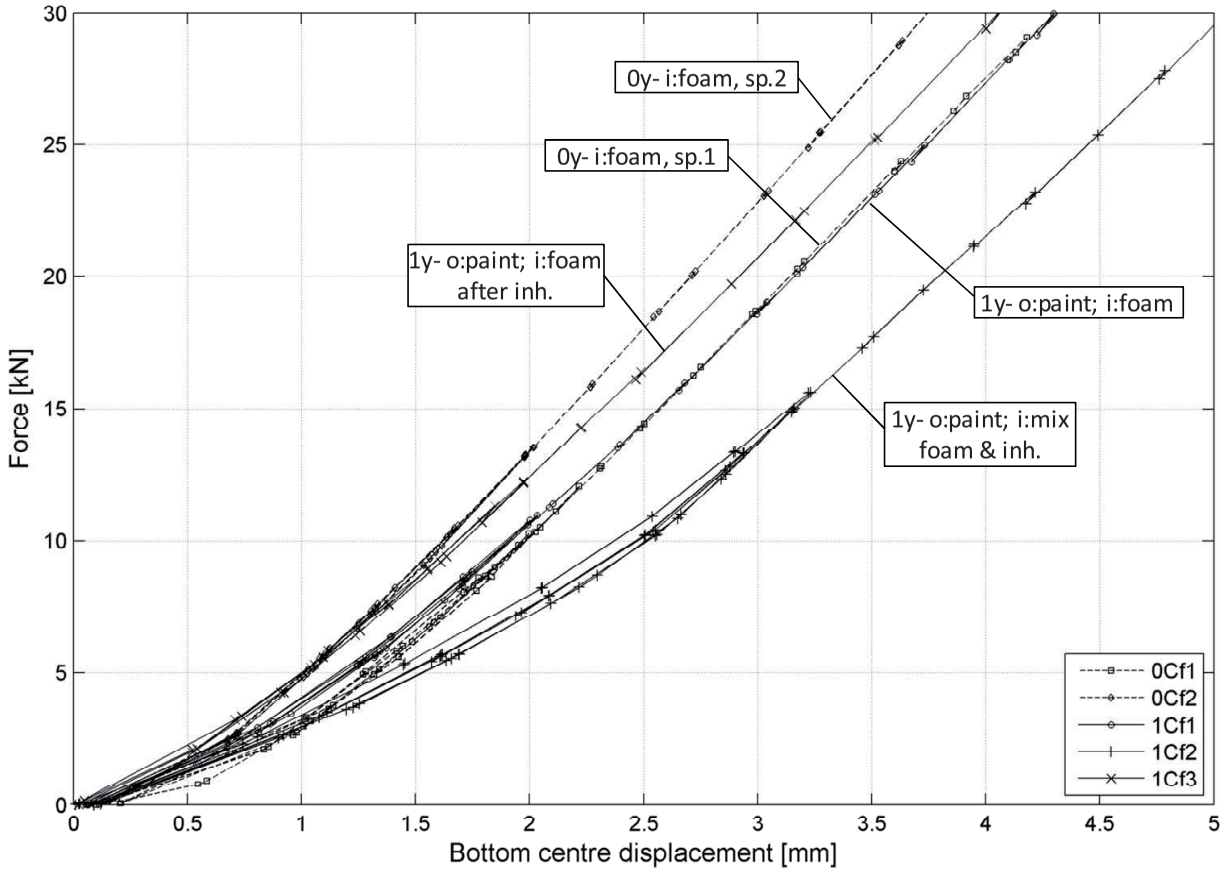

Figure 14-10. Stiffness of the corrugated-core beams.

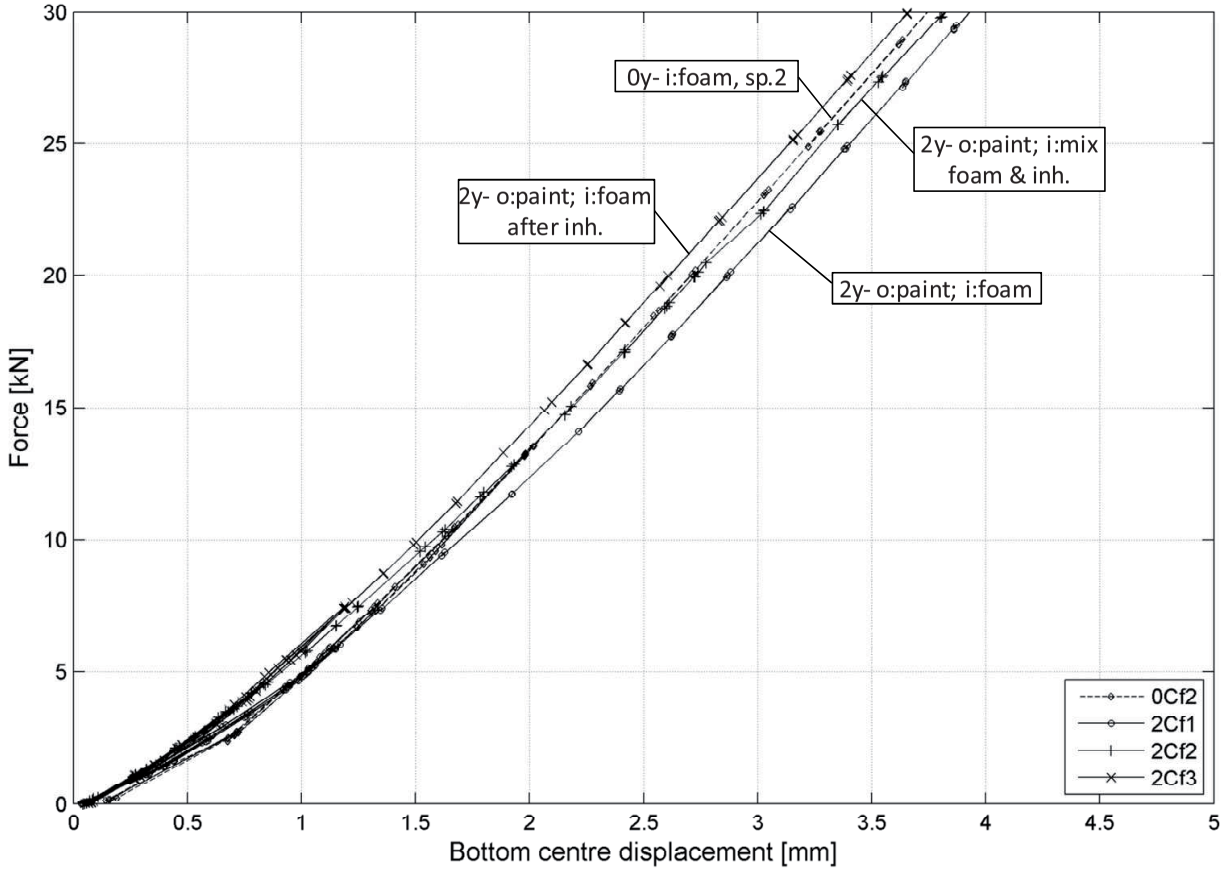

Figure 14-11. Stiffness of the corrugated-core beams.

15 Appendix E – Strength test results

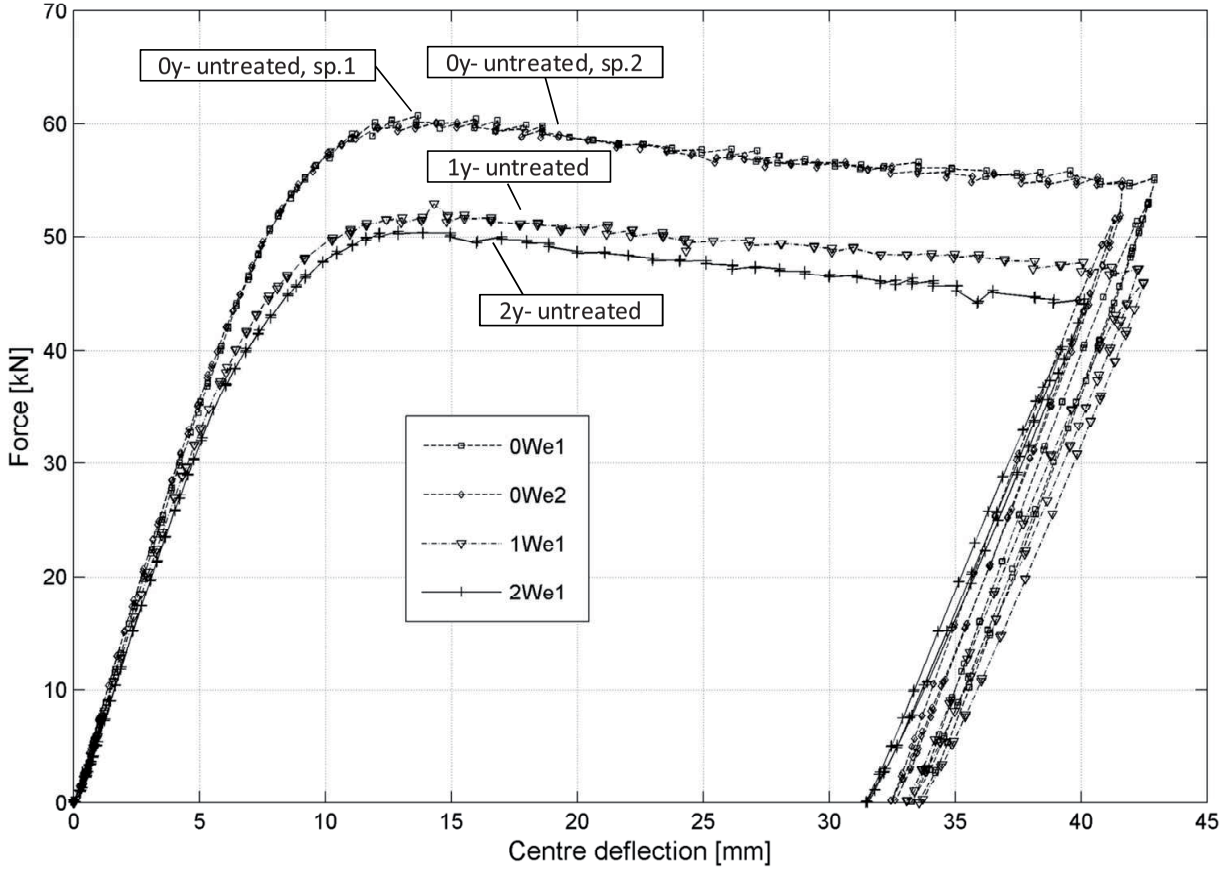

Figure 15-1. Strength results of the web-core beams.

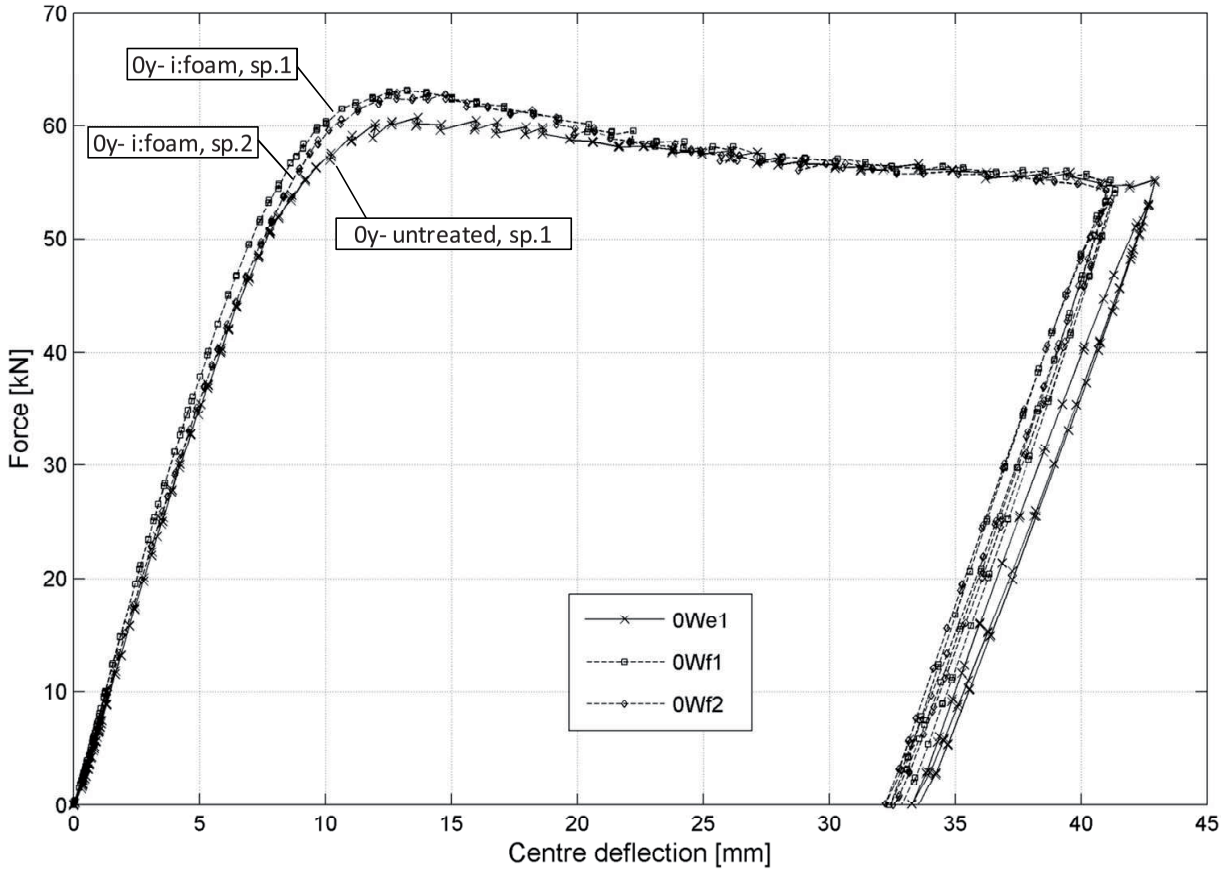

Figure 15-2. Strength results of the web-core beams.

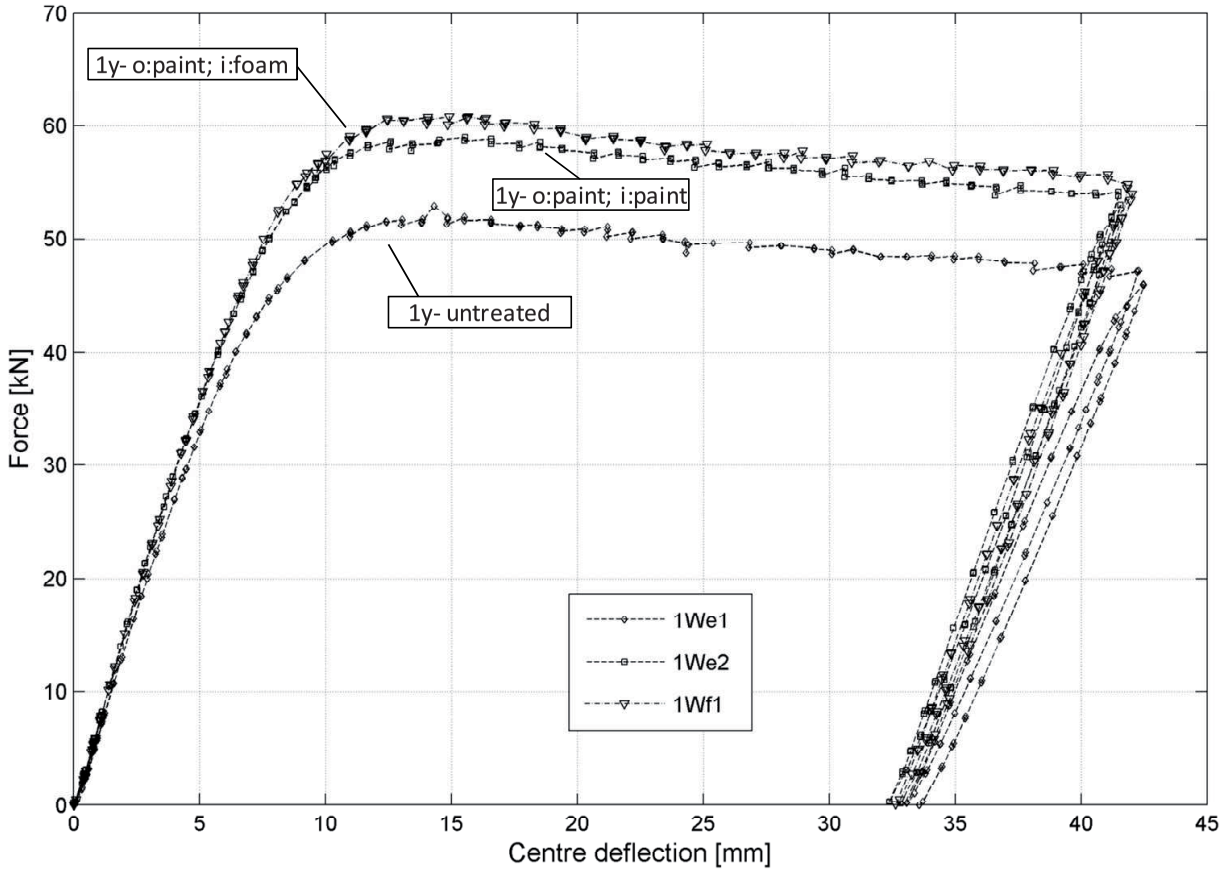

Figure 15-3. Strength results of the web-core beams.

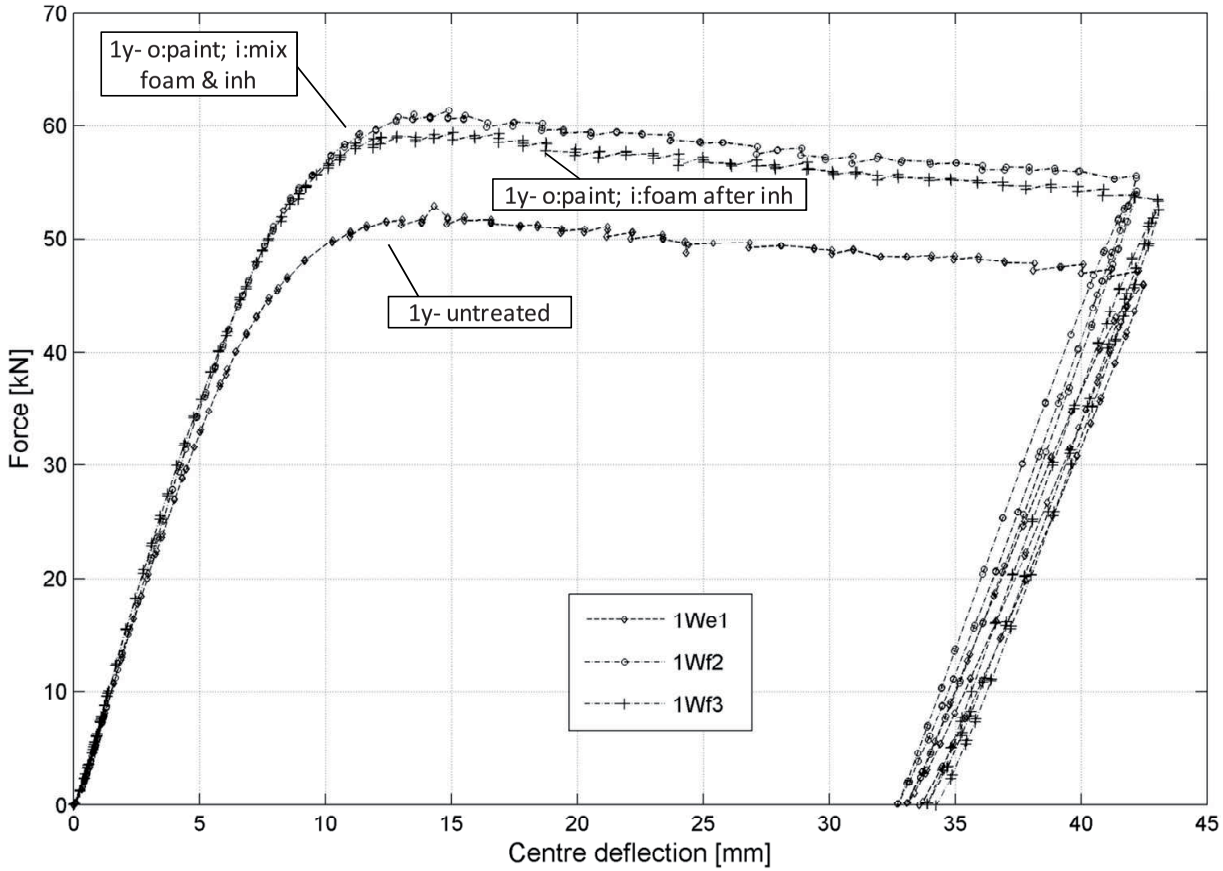

Figure 15-4. Strength results of the web-core beams.

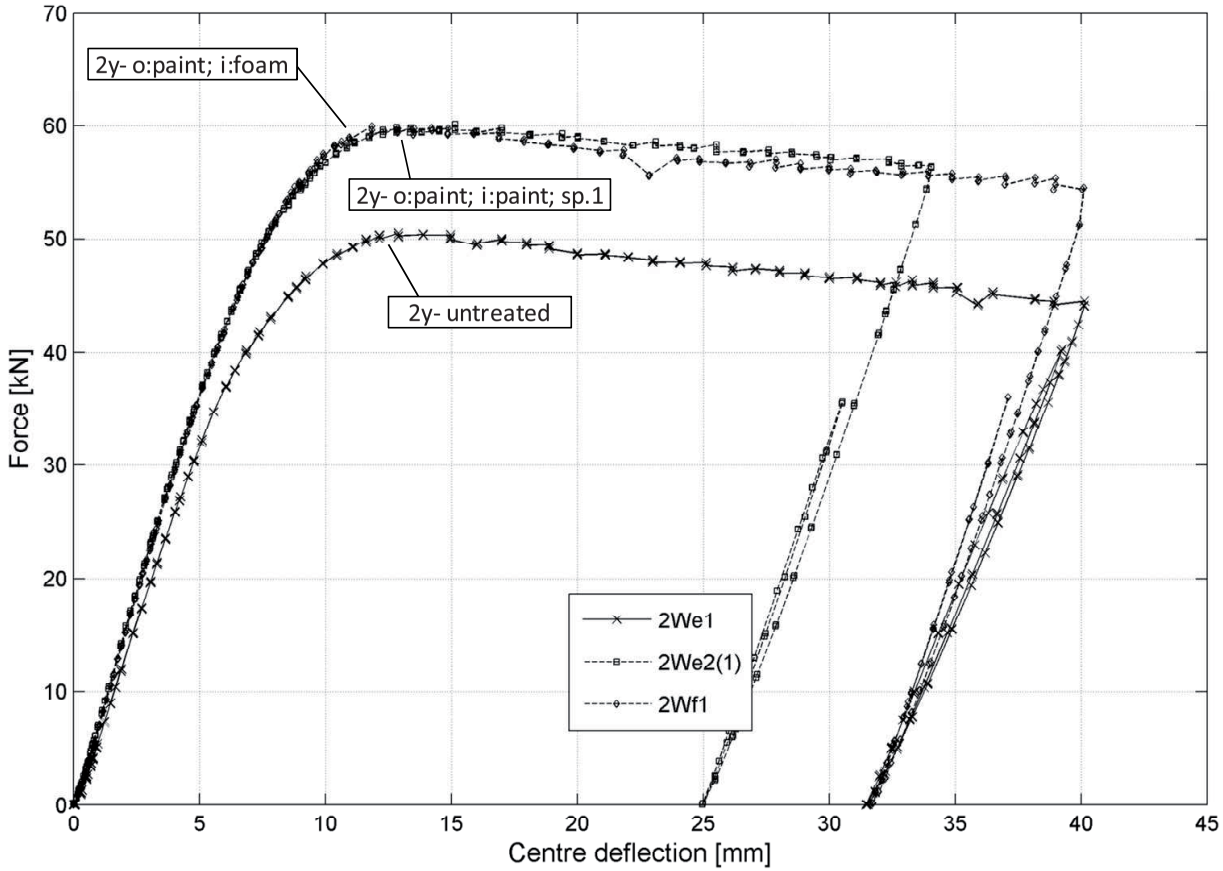

Figure 15-5. Strength results of the web-core beams.

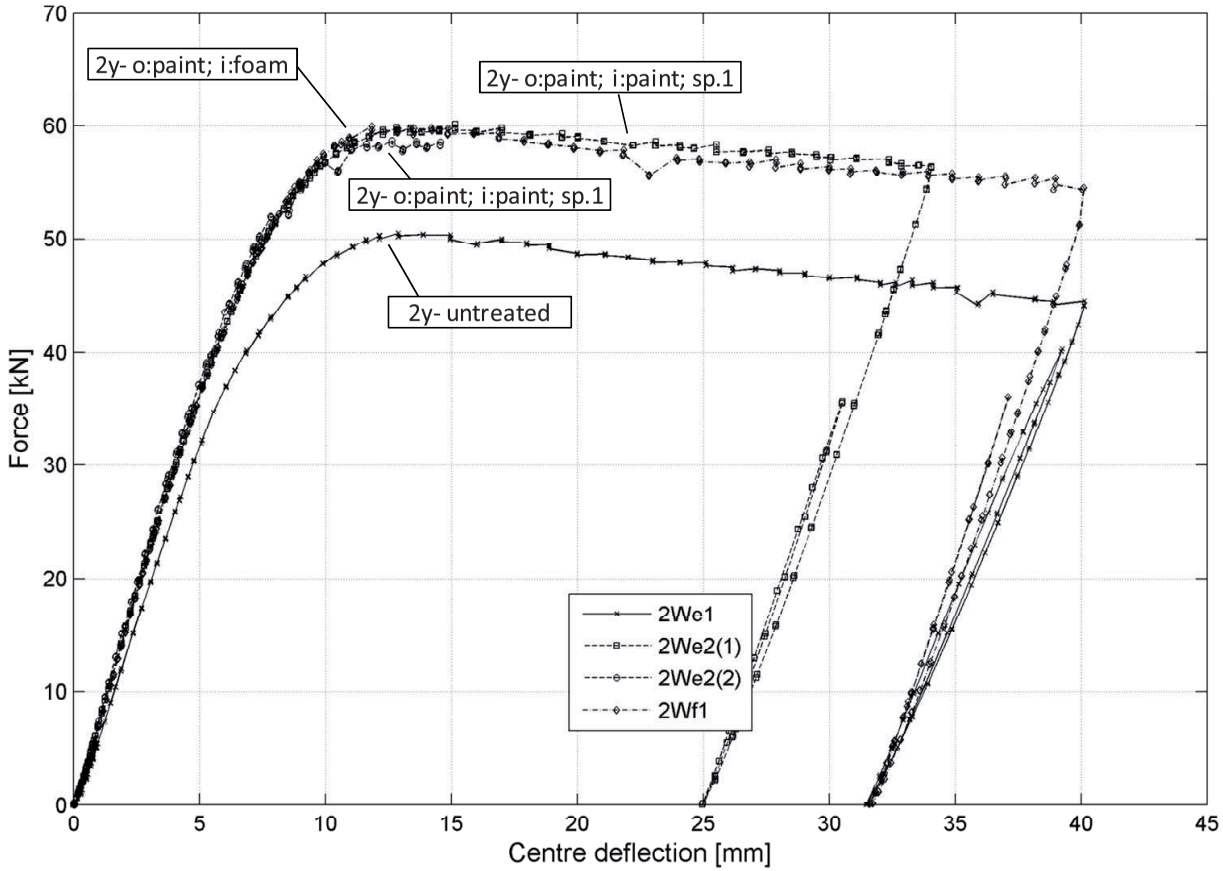

Figure 15-6. Strength results of the web-core beams.

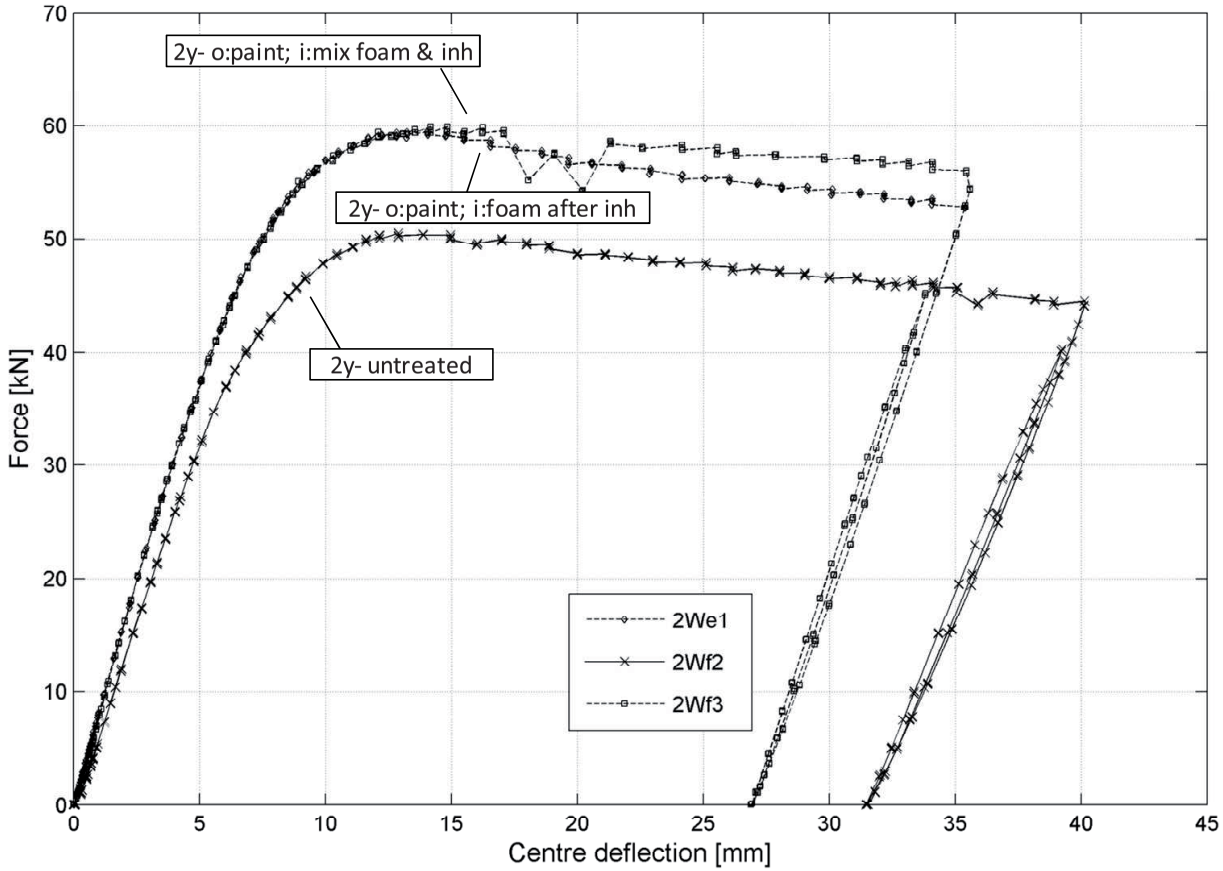

Figure 15-7. Strength results of the web-core beams.

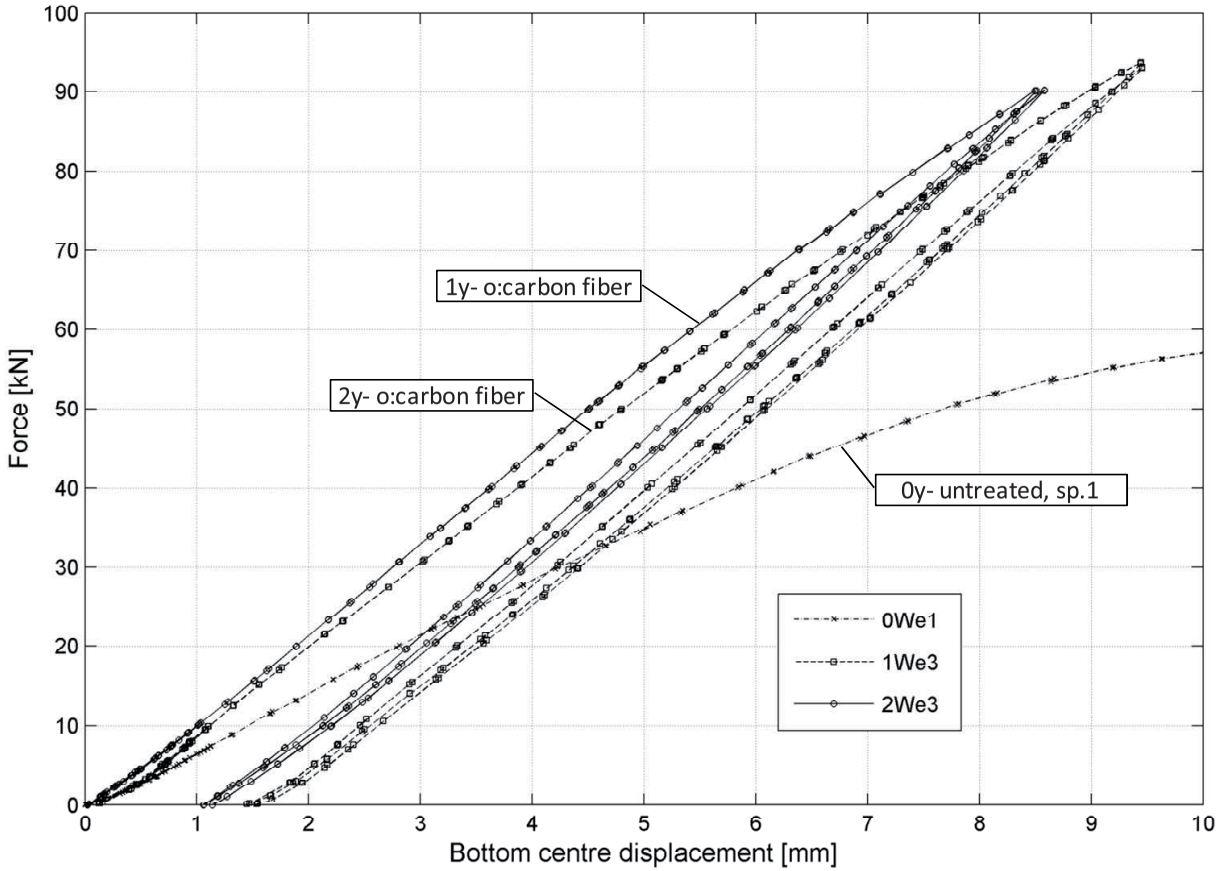

Figure 15-8. Strength results of the web-core beams.

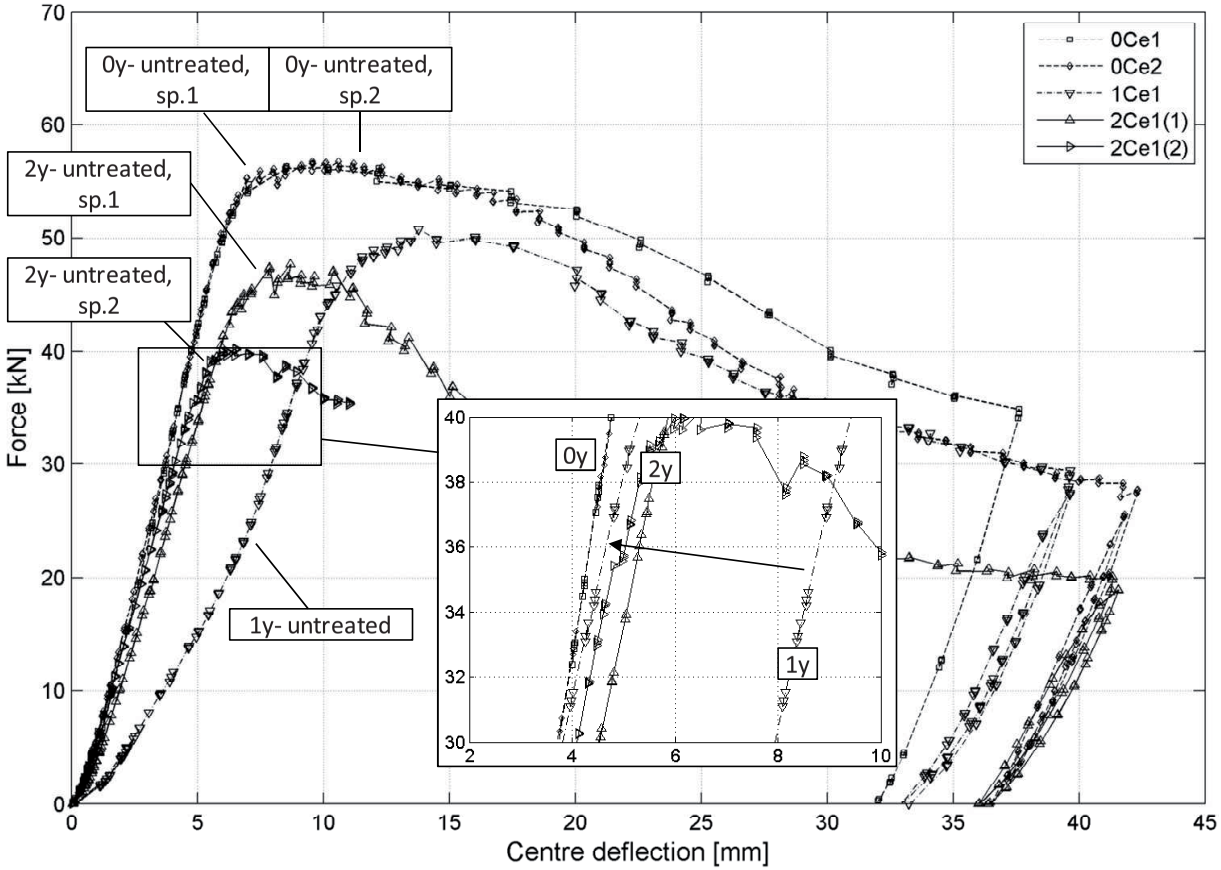

Figure 15-9. Strength results of the corrugated-core beams.

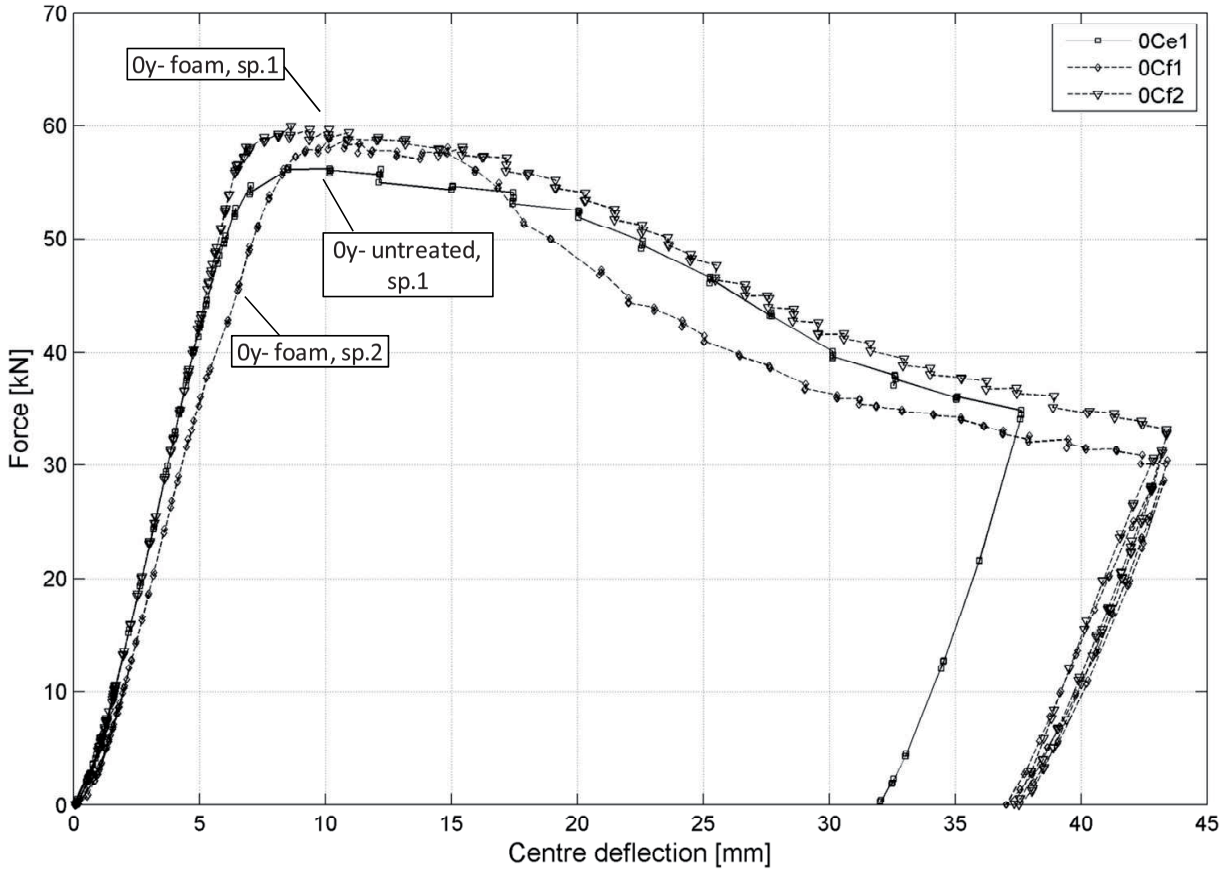

Figure 15-10. Strength results of the corrugated-core beams.

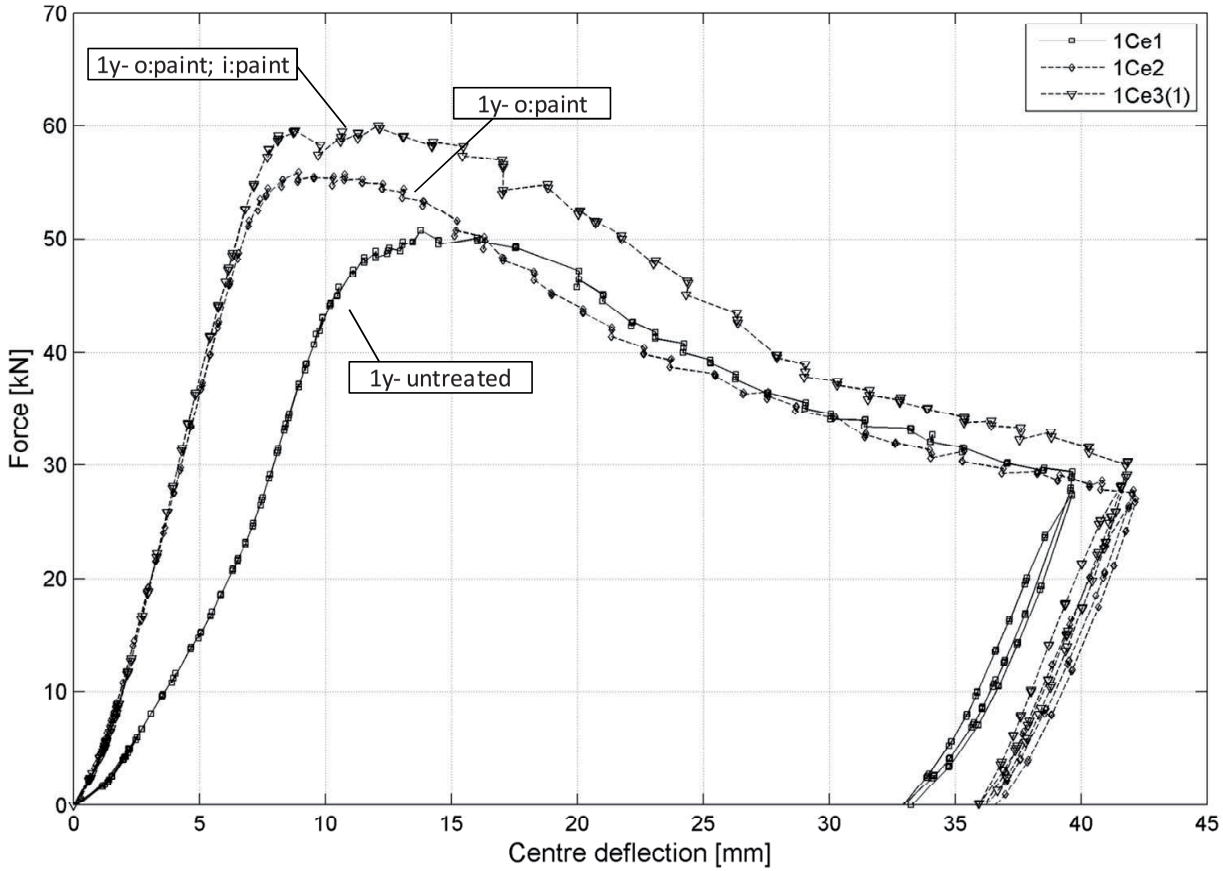

Figure 15-11. Strength results of the corrugated-core beams.

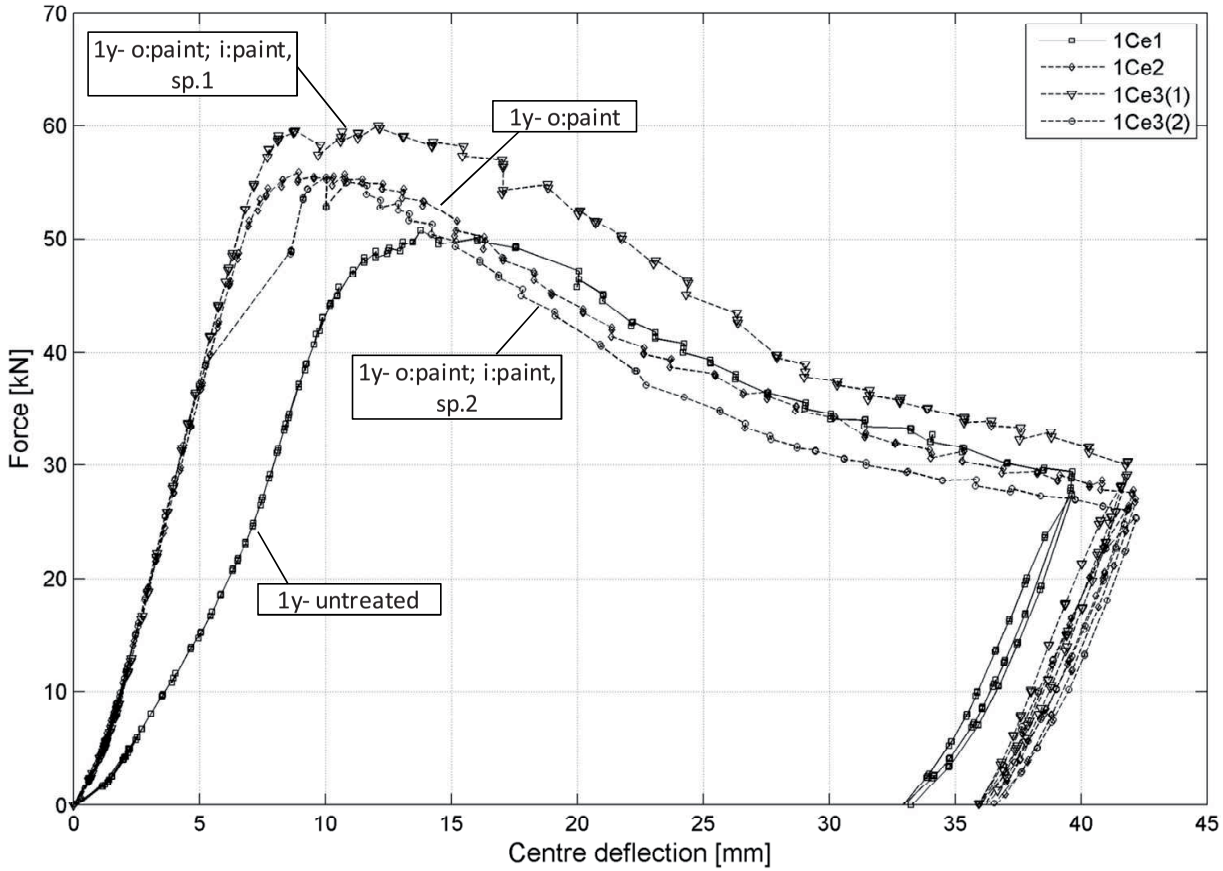

Figure 15-12. Strength results of the corrugated-core beams.

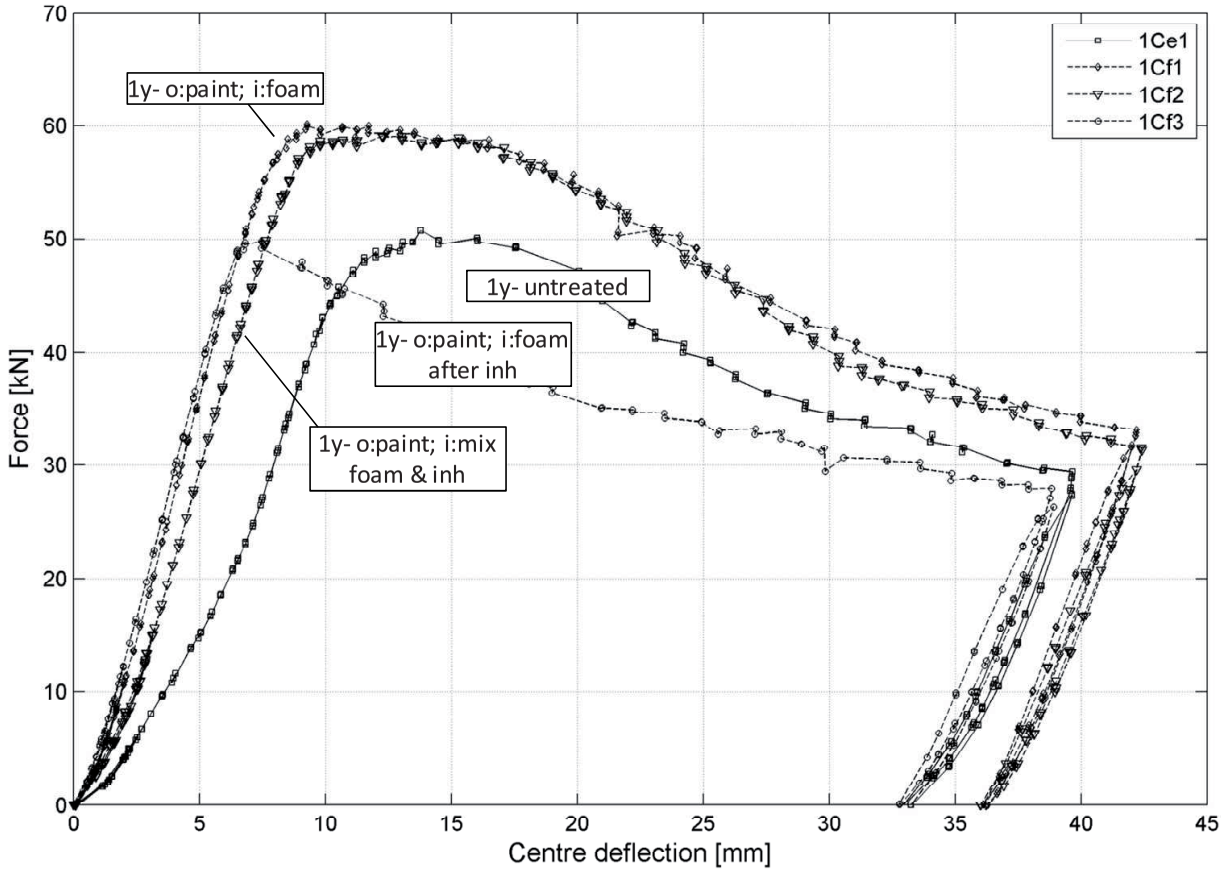

Figure 15-13. Strength results of the corrugated-core beams.

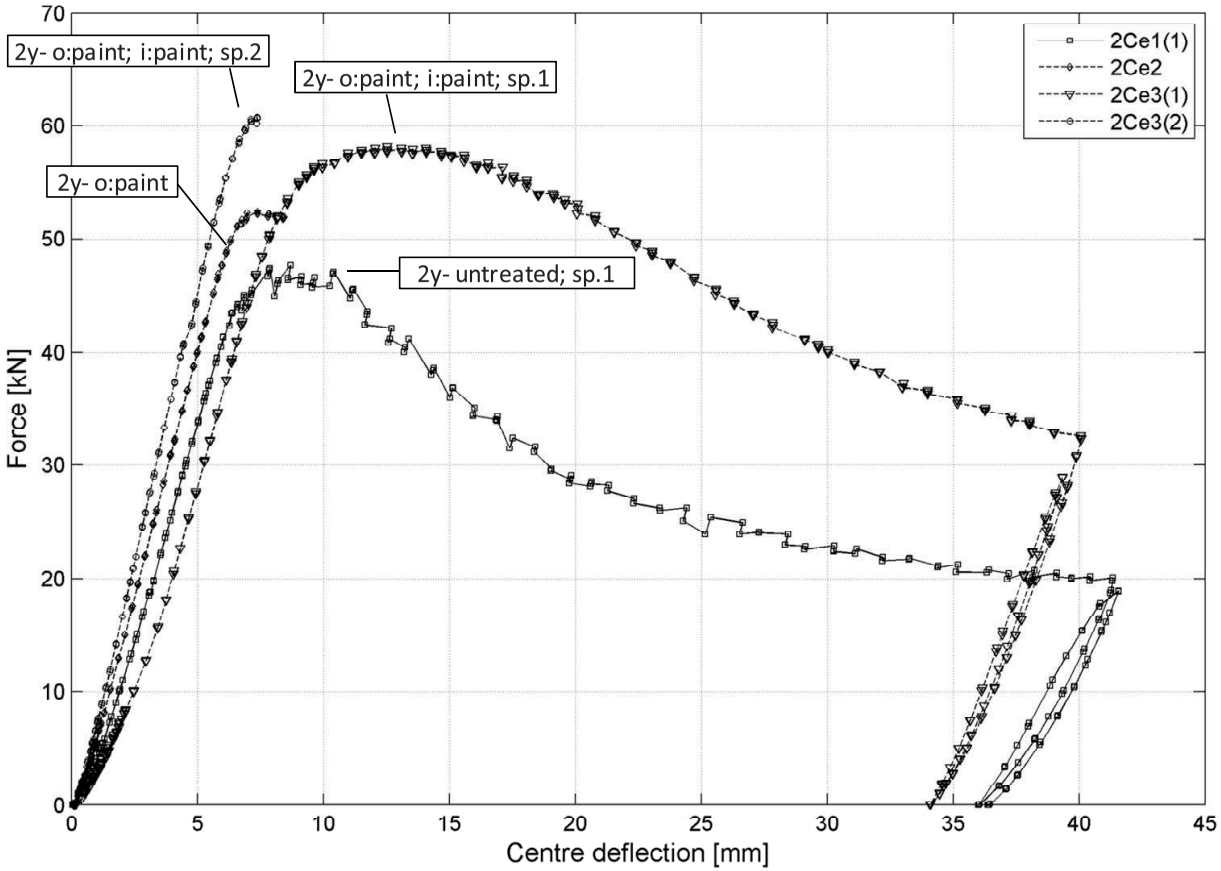

Figure 15-14. Strength results of the corrugated-core beams.

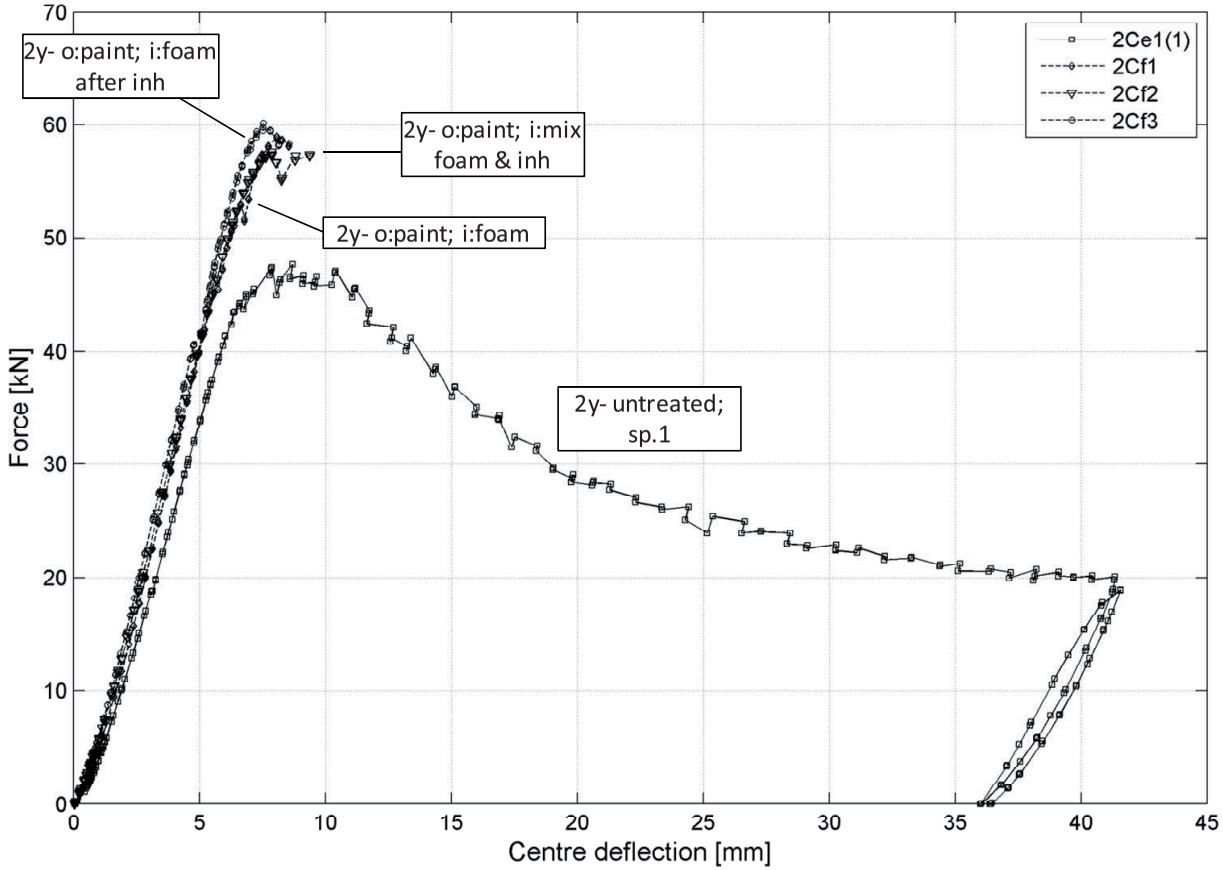

Figure 15-15. Strength results of the corrugated-core beams.

This report describes the ultimate strength experiments carried out on the web-core and corrugated-core laser-welded steel sandwich beams. The beams were differing by the extent of corrosion: they were exposed to the sea-water for one and two years. Uncorroded beams were also tested for comparison, making in total 41 tested specimens. Few different corrosion protection schemes were used: painting, filling the core with poly-urethane (PU) foam and using the corrosion inhibitor. Material stress-strain behaviour was determined with standard tensile tests. Thickness of the plates was measured on the tensile specimens to assess the extent of thickness reduction due to corrosion. The study was part of the research project Closed, Filled Steel Structures (SUTERA) funded by the Centennial Foundation of Federation of Finnish Technology industries during 01.01.2008-31.05.2011.

ISBN 978-952-60-4434-7 (pdf)
ISSN-L 1799-4896
ISSN 1799-490X (pdf)

Aalto University
School of Engineering
Department of Applied Mechanics
www.aalto.fi

BUSINESS + ECONOMY

ART + DESIGN + ARCHITECTURE

SCIENCE + TECHNOLOGY

CROSSOVER

DOCTORAL DISSERTATIONS

Aalto-ST 28/2011